

*Rec'd from Kellwell
3/5/93
1211*

USGS-OFR-84-788

USGS-OFR-84-788

NNA.870519.0104

UNITED STATES
DEPARTMENT OF THE INTERIOR
GEOLOGICAL SURVEY

PRELIMINARY REPORT ON LATE CENOZOIC FAULTING
AND STRATIGRAPHY IN THE VICINITY OF
YUCCA MOUNTAIN, NYE COUNTY, NEVADA

By

W C Swadley, D. L. Hoover, and J. N. Rosholt

9303110414 930305
PDR WASTE PDR
WT-11

102-5

CONTENTS

	Page
Abstract.....	1
Introduction.....	1
Geologic Setting.....	1
Methods.....	3
Late Cenozoic Stratigraphy.....	6
Late Pliocene and Pleistocene Deposits.....	8
Early Pleistocene and Pliocene(?) Deposits.....	8
Middle and Late Pleistocene Deposits.....	11
Holocene Deposits.....	12
Late Cenozoic Faulting.....	12
Summary and Discussion.....	19
References Cited.....	22
Appendix.....	23

ILLUSTRATIONS

Plate	1. Map showing the surficial deposits and late Cenozoic faulting in the area of Yucca Mountain.....(in pocket)	
Figure	1. Map of Nevada Test Site area showing location of Yucca Mountain and site of potential waste repository.....	2
	2. Generalized geologic map of the Yucca Mountain area.....	4
	3. Surficial units present in the NTS region.....	9
A1.	Diagram of south wall of trench 2.....	24
A2.	Diagram of south wall of trench 4.....	25
A3.	Diagram of south wall of trench 6.....	26
A4.	Diagram of north wall of trench 8.....	27
A5.	Diagram of south wall of trench 9.....	28
A6.	Diagram of south wall of trench 10A.....	29
A7.	Diagram of south wall of trench 10B.....	30
A8.	Diagram of south wall of trench 11.....	31
A9.	Diagram of north wall of trench 12.....	32
A10.	Diagram of south wall of trench 13.....	33
A11.	Diagram of south wall of trench 14.....	34
A12.	Diagram of north wall of trench 16.....	35
A13.	Diagram of north wall of trench 16B.....	36
A14.	Diagram of north wall of trench 17.....	37
A15.	Diagram of north wall of trench A1.....	38
A16.	Diagram of south wall of trench A2.....	39
A17.	Diagram of north wall of trench CF1.....	40
A18.	Diagram of south wall of trench CF2.....	41
A19.	Diagram of south wall of trench CF3.....	42

TABLES

Table 1.	Data from trenches across faults in the Yucca Mountain area....	5
Table 2.	Radiometric age data for fault-related secondary deposits exposed in trenches in the Yucca Mountain area.....	7
Table 3.	Radiometric age data for stratigraphic units of the NTS region.....	10
Table 4.	Summary of Quaternary faulting in the Yucca Mountain area.....	21

ABSTRACT

Mapping of surficial deposits and examination of faults in natural and trenched exposures in a 1100 km² area around the site of a potential repository for radioactive waste at Yucca Mountain have identified 32 faults that offset or fracture Quaternary deposits. Where the amount of Quaternary offset can be estimated, dip-slip movement is on the order of 3 m or less on faults in and near Yucca Mountain. Maximum Quaternary offset within the study area may be as much as 30 m. No strike-slip movement was demonstrated nor can it be ruled out.

Based on radiometric ages, correlations of stratigraphic units, and field observations, Quaternary faults are divided into three broad age groups: five faults moved between about 270,000 and 40,000 years ago; four faults moved about 1 m.y. ago; and 23 faults moved probably between 2 m.y. and more than 1.2 m.y. ago. Offset of Holocene deposits has not been demonstrated.

INTRODUCTION

Geological and hydrological investigations to evaluate Yucca Mountain in southern Nye County, Nevada (fig. 1), as the possible site for an underground radioactive waste repository were begun by the U.S. Geological Survey in 1978. These studies are being conducted in cooperation with the U.S. Department of Energy Nevada Nuclear Waste Storage Investigations. This report summarizes a reconnaissance study of late Cenozoic faulting in the vicinity of Yucca Mountain. Detailed investigations of faults in the Yucca Mountain area are continuing, but data and preliminary conclusions are presented at this time for use by the U.S. Department of Energy and others involved in evaluating the Yucca Mountain site.

The purposes of this fault study were to determine the location and extent of faults in the Yucca Mountain area that displace late Pliocene and Quaternary deposits and to make a preliminary assessment of the amount and age of fault displacements on which to base more detailed investigations.

This report is based on published and unpublished surficial maps of the Yucca Mountain area by Swadley and Hoover. Uranium-trend isotopic dates were determined by Rosholt. Preliminary analysis of trenches excavated across faults in the study area were by Swadley and Hoover unless noted otherwise.

GEOLOGIC SETTING

Yucca Mountain is in the southern Great Basin, an area chiefly characterized by north-trending linear mountain ranges that are flanked by extensive alluvial fans and separated by broad alluvial basins. Most ranges are deeply incised by narrow stream valleys. The climate is arid and vegetation is limited to sparse desert plants.

30817 (1665

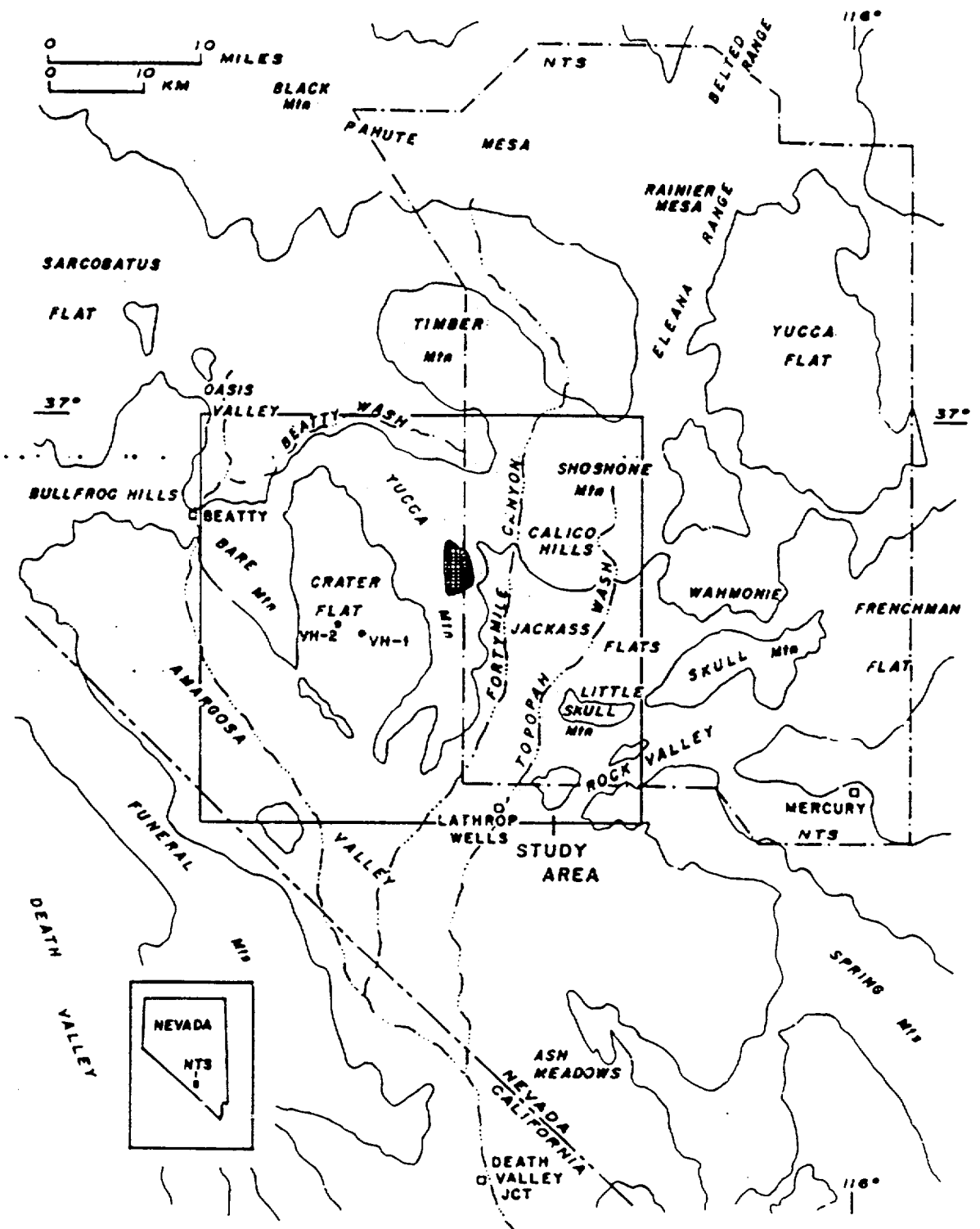


Figure 1.--Map of Nevada Test Site area showing location of Yucca Mountain and site of potential waste repository (shaded area).

The exposed bedrock in the vicinity of Yucca Mountain consists of Precambrian and Paleozoic quartzite, shale, and carbonate rocks and Tertiary volcanic rocks (fig. 2) (Stewart and Carlson, 1978). These rocks locally are overlain by late Tertiary and Quaternary surficial deposits. The area lies within a major Miocene volcanic field and contains several calderas, which produced voluminous pyroclastic deposits including the tuffs that underlie Yucca Mountain (Byers and others, 1976). Small basalt lava flows and cinder cones erupted in the Crater Flat area during the late Pliocene and Pleistocene.

Yucca Mountain consists of a series of subparallel ridges that are formed by blocks of resistant Tertiary volcanic rocks, mainly densely welded tuffs, which dip gently eastward and are bounded by north-trending faults. The areas bordering Yucca Mountain and the valleys between the ridges making up Yucca Mountain are underlain by alluvial gravels and, locally, by eolian deposits. The bedrock geology of Yucca Mountain is shown on maps by Christiansen and Lipman (1965), Lipman and McKay (1965), and Scott and Bonk (1984). The geology of the Bare Mountain quadrangle, west of Yucca Mountain, was mapped and described by Cornwall and Kleinhampl (1961). The volcano-tectonic history of Crater Flat (fig. 1) is discussed by Carr (1932).

METHODS

Late Cenozoic surficial deposits in the vicinity of Yucca Mountain were mapped on the basis of stratigraphy described by Hoover and others (1981). Mapping in the field was supplemented by the interpretation of conventional aerial photography. The locations of faults that offset the surficial deposits are shown on plate 1 along with the areal distribution of generalized time-stratigraphic surficial units.

Twenty-three trenches (pl. 1) were excavated in the Yucca Mountain area to evaluate Quaternary fault movement. Fourteen trenches are on Yucca Mountain or in valleys that border it; six trenches are on adjacent ridges that parallel Yucca Mountain; and the remaining three trenches are in the eastern part of Crater Flat, southwest of Yucca Mountain. Some trenches were excavated across recognized fault scarps, and others were placed in surficial deposits across the projection of a known bedrock fault.

Trenches were excavated using bulldozers to depths of 2 to 4 m and lengths of 20 to 40 m. The trenches were mapped by establishing a level line and a 2-m reference grid from which readily recognized stratigraphic units, sedimentary features, soil horizons, faults, and fractures were plotted. (The term fracture, as used in this report, refers to planar breaks in the deposits along which there is no demonstrable offset.) Diagrams of one wall of each trench illustrating these features are included in an appendix. More detailed logging of fault trenches is in progress.

Data obtained from the study of the trenches are summarized in table 1. Trenches 1, 15, GA1A, and GA1B exposed faulted Tertiary bedrock at shallow depths and Quaternary deposits were thin or absent; these trenches were abandoned and are not reported in table 1. Nineteen trenches exposed surficial deposits that are believed to range in age from 7,000-9,000 years old (unit Q1c) to as much as 2 m.y. old (unit QTa) (Hoover and others, 1981). Six of these trenches also exposed Tertiary volcanic rocks.

0317 (667)

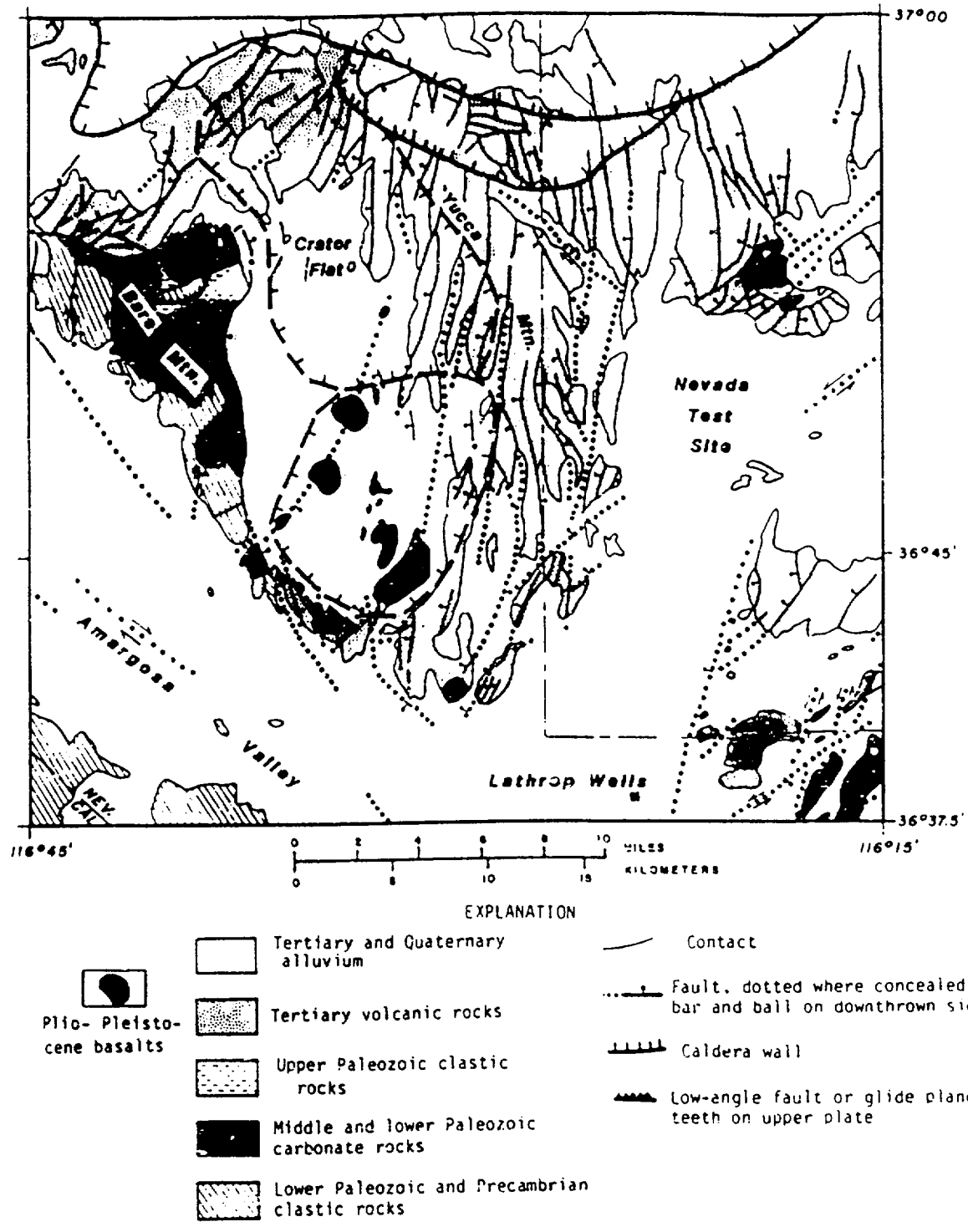


Figure 2.--Generalized geologic map of the Yucca Mountain area. Modified from Snyder and Carr, 1982.

Table 1.--Data from trenches across faults in the Yucca Mountain area

Trench no.	Fault	Trench location	Surficial units exposed in trench	Bedrock exposed in trench	Tectonic features that affect surficial deposits	Inferred age of tectonic feature	Remarks
2	G	On projection of bedrock fault	Q1c, Q2a, Q2b, Q2c	No	None		Indicates no fault movement after 270,000 yr
4	F	do.	Q1c	No	do.	None	Indicates no fault movement after 7,000 yr
6	F	do.	Q1c	In trench floor	do.	None	Do.
8	Solitario Canyon	On QTa - bedrock contact	Q1c, QTa	In upthrown block	Faults cut QTa; fractures cut QTa and QTa soil	1.2 m.y.	Fault movement dated by basaltic ash in fault zone
9	F	On projection of bedrock fault	Q1c, Q2c	In upthrown(?) block	None	None	Indicates no fault movement after 270,000 yr
10A	Solitario Canyon	do.	QTa	No	do.	None	Probably not located on fault
10B	Solitario Canyon	On QTa - bedrock contact	Q2c, QTa	In upthrown block	QTa faulted against T _v ; QTa soil and Q2c not faulted	<2 m.y.; >270,000 yr	-----
11	D	On projection of bedrock fault	Q2b, Q2c, QTa	No	None	None	Indicates no fault movement after 270,000 yr
12	E	On trace of bedrock fault	Q2 soil	In upthrown and downthrown block	Q2 soil buries fault scarp in bedrock	<40,000 yr	Indicates no fault movement after 40,000 yr
13	H	On projection of bedrock fault	Q2b, Q2c	No	None	None	Indicates no fault movement after 270,000 yr
14	C	On Q2 - bedrock contact	Q2a, Q2s	In upthrown block	Fractures cut Q2s and Q2s soil; do not cut Q2a	<70 ± 90 × 10 ³ yr, >30 ± 10 × 10 ³ yr	Ages of Q2s and Q2a by uranium-trend method
16	Paintbrush Canyon	On projection of bedrock fault	Q2e	No	None	None	Probably not located on fault
16B	Paintbrush Canyon	do.	Q2e, Q2s	In upthrown block	Fractures cut Q2e; do not cut Q2s	<700,000 yr, >270,000 yr	-----
17	Paintbrush Canyon	do.	Q2e	do.	None	None	Indicates no fault movement after 700,000 yr
A1	Paintbrush Canyon	do.	Q2e, Q2b	No	Fractures cut Q2e and Q2e soil; do not cut Q2b	about 700,000 yr, >160,000 yr	-----
A2	Paintbrush Canyon	do.	Q2b, Q2c	No	Fractures cut Q2c, not Q2c soil or Q2b	<800,000 yr, >270,000 yr	-----
CF1	M	On scarp in QTa	Q2, QTa	No	Faults cut QTa; do not cut some QTa soil horizons of Q2	1.2 m.y.	Fault movement dated by basaltic ash in fault zone
CF2	Q	do.	Q2, QTa	No	3 faults cut QTa and lower part of QTa soil, 1 fault cuts entire QTa soil; Q2 not cut	<2 m.y., >40,000 yr	Two periods of faulting likely
CF3	Q	On projection of scarp in QTa	Q2a, Q2c	No	Faults cut Q2c and Q2c soil; not Q2a	<270 ± 30 × 10 ³ yr, >40 ± 10 × 10 ³ yr	Ages of Q2c and Q2a by uranium-trend method

0653

17317

5

Five trenches (8, 10B, CF1, CF2, and CF3) exposed evidence of Quaternary offset and four other trenches (14, 16B, A1, and A2) exposed fractures in Quaternary units. These fractures parallel the faults on which the trenches are located, and are interpreted as fault related. The remaining 10 trenches showed no indication of Quaternary faulting. The evidence for Quaternary faulting derived from the trench studies is discussed in more detail below.

Where the trace of a fault plane was exposed in a trench wall, it was excavated by hand to search for slickensides and other directional features. None, however, were found. Neither the poorly consolidated Quaternary units nor the secondary carbonate deposits that commonly occur along the faults appeared to preserve such features. Slickensides associated with Quaternary faulting were observed only in an abandoned prospect pit along the Bare Mountain fault zone.

Stratigraphic units and post-fault carbonate and silica deposits were sampled in six trenches for isotopic age determinations. Sample locations are shown on trench diagrams in the appendix. Surficial deposits were dated by the uranium-trend method (Rosholt, 1980). This method is experimental but was used because materials needed for more conventional radiometric dating methods are sparse in the Yucca Mountain area. Dates determined by the uranium-trend method theoretically indicate the minimum age for deposition of surficial deposits (Rosholt, 1980). The technique is considered to be applicable for deposits that range in age from 5,000 to 900,000 years and has a potential estimated accuracy of about ± 10 percent. Uranium-trend dates have been used in an attempt to determine minimum ages for deposits that structurally and stratigraphically bracket the age of fault related features in trenches 2, 13, 14, and CF3. Approximate limits on the absolute age of faulting are inferred on the basis of these dates. The accuracy of the absolute ages derived by this method is not known, but ages determined for some stratigraphic units are reasonably consistent over the study area and are consistent with the broad limits on the ages of stratigraphic units in the study area inferred on the basis of correlations with better dated sequences from the surrounding region.

The uranium-series method (Szabo and others, 1981) was used to date deposits of carbonate or silica in trenches 14, CF1, and GA1A, interpreted as post-fault deposits. Uranium-series dates theoretically indicate the minimum age for the dated deposit, but the method only is considered to be accurate if the chemical system is closed. Most samples dated by this method yielded dates that appear to be inordinately young, but which can be considered as minimum ages (Szabo and others, 1981, p. 32). The dated samples from Yucca Mountain may not be from chemically closed systems, and the effect of this on the age determinations is not known. Dates determined by the uranium-series method are summarized in table 2.

Topographic profiles were measured across a number of fault scarps in the Crater Flat area, west of Yucca Mountain, to help characterize the scarps and possibly to provide a relative indicator of scarp age. Terms used in scarp descriptions are as defined by Bucknam and Anderson (1979).

LATE CENOZOIC STRATIGRAPHY

The late Tertiary and Quaternary deposits of the study area consist of alluvium, eolian sands, colluvium, lake sediments, and volcanic deposits.

Table 2.--Radiometric age data for fault-related secondary deposits
exposed in trenches in the Yucca Mountain area

[Age determination by uranium-series method by P. O'Malley and B. Szabo,
U.S. Geological Survey, written commun., 1982.]

Trench no.	Sample no.	Type of deposit	Age (in 10^3 yr)
14	TSV-412-1	Carbonate from K horizon Q2s soil	>400
		Opal from K horizon of Q2s soil	>350
	TSV-412-3	Opal from K horizon of Q2s soil	>550
	TSV-412-7	Opal from K horizon of Q2s soil	>400
CF1	TSV-386	Secondary carbonate along fault	27 ± 3
	TSV-387	K horizon of QTa	33 ± 4
GA-1A	TSV-395	Undisturbed carbonate deposit above fault	>32

These range in age from greater than 3 m.y. old for some of the lake sediments to less than about 150 years old for the youngest alluvial unit (Hoover and others, 1981). Hoover and others (1981) described the stratigraphy of these deposits (fig. 4) and defined characteristics by which they can be mapped and correlated across the region on the basis of age, lithology, and depositional environment. The following brief descriptions of the map units are based mainly on their work. More recently determined isotopic ages used to refine the stratigraphy reported by Hoover and others (1981) are summarized in table 3. The deposits are grouped herein into four major units: (1) late Pliocene and Pleistocene, (2) early Pleistocene and Pliocene(?), (3) middle and late Pleistocene, and (4) Holocene. The distribution of these units over the study area is shown on a generalized surficial map (pl. 1, in pocket).

Late Pliocene and Pleistocene Deposits

The oldest surficial deposits of the study are predominantly of late Pliocene age and consist of lacustrine sediments (fig. 4). These lacustrine deposits (unit QT1d) are mainly unconsolidated to moderately indurated marl and silt that locally contain beds of limestone, sand, and fine-grained volcanic ash. They were deposited in Lake Amargosa, which occupied much of what is now the Amargosa Valley (fig. 1) during the late Pliocene; remnants of the lake probably persisted into the early Quaternary.

The age of unit QT1d is not precisely known; however, an ash bed near the middle of the unit yielded radiometric ages that ranged from about 3 m.y. (fission-track method; C. W. Naeser, U.S. Geological Survey, written commun., 1980) to 3.8 m.y. (K-Ar method on biotite; R. L. Hay, University of California, Berkeley, written commun., 1979). A second ash bed near the top of the unit was dated at 2.1 ± 0.4 m.y. by the fission-track method (C. W. Naeser, written commun., 1982). A slightly younger age is suggested for the upper part of unit QT1d by mammoth remains that are considered to be less than 2 m.y. old (C. A. Repenning, U.S. Geological Survey, written commun., 1982).

Early Pleistocene and Pliocene(?) Deposits

These deposits consist of alluvium that mainly is early Pleistocene but in some areas may be as old as latest Pliocene. The alluvium (unit QTa, fig. 3) consists of debris flows with sparse bedded fluvial sediments; it occurs as dissected fans and fan remnants that are adjacent to bedrock ranges and, less commonly, as isolated outcrops several kilometers from the ranges. Unit QTa typically is moderately indurated, coarse, angular, unsorted gravel with minor amounts of sand- to clay-size material. In most exposures, QTa is partly cemented with calcium carbonate.

The approximate age of unit QTa is limited by the ages of enclosing units; there are no dated materials within the unit. QTa unconformably overlies QT1d at several localities in the Lathrop Wells quadrangle (Swadley, 1983), indicating that QTa deposits are less than 2 m.y. old in that area. Unit QTa is overlain by unit Q2e, that locally contains lenses of volcanic ash correlated with the Bishop ash by Izett (1982) on the basis of their similar chemistry. Radiometric dates for samples from the Bishop ash indicate that it is 0.74 m.y. old (Izett, 1982). The lower part of unit Q2e is considered approximately 0.74 m.y. old on the basis of the correlation with the Bishop ash. A period of erosion and weathering occurred following the deposition of QTa but prior to deposition of Q2e (Hoover and others, 1981), suggesting that

0 0 8 1 7 0 6 7 2

6

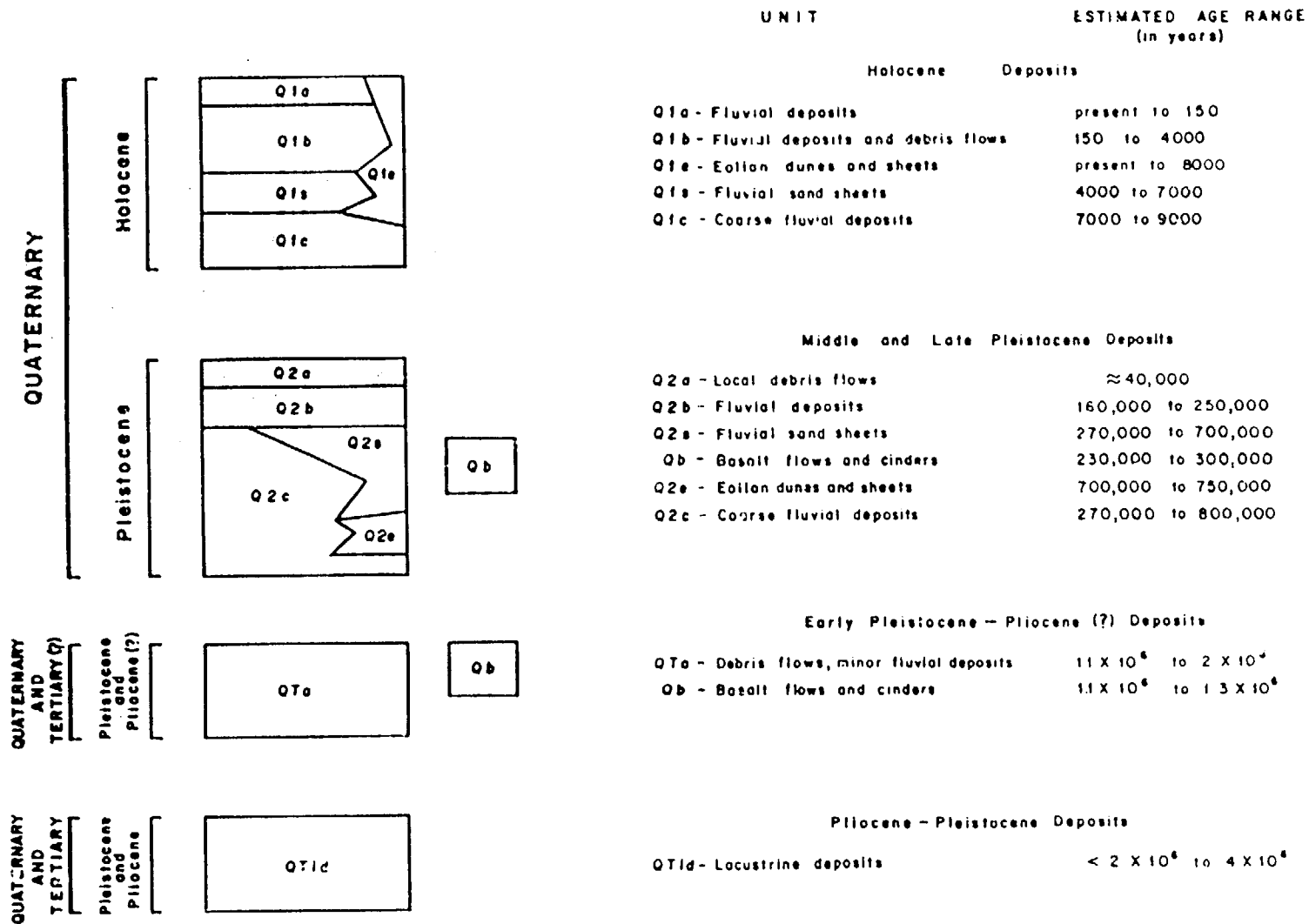


Figure 3.--Surficial units present in the NTS region. Modified from Hoover and others (1981). Estimated age ranges are based in part on radiometric data. Where data are not available, age limits have been estimated based on field relations, reconstruction of the depositional history, and correlations with dated units outside the NTS area.

Table 3.--Radiometric age data for stratigraphic units of the MTS region

[Ages shown are \pm one standard deviation. Determinations by uranium-trend method by J. M. Rosholt except where otherwise indicated.]

Stratigraphic unit	Material	Sample location	Age (in 10^3 yr)
¹ Q1c	Charcoal in fluvial gravel	Amargosa River bank, 2 km SE of Beatty, NV	8.3 \pm .075
Q	Clayey silt of eolian A horizon of Q2 soil	SW Frenchman Flat	30 \pm 30
² Q2	Loess	Basalt cinder cone, 11 km NW of Lathrop Wells, NV	25 \pm 10
Q2a(7)	Slope wash sand	Trench 14	38 \pm 10
	Slope wash below fault scarp	Trench CF3	40 \pm 10
	Slope wash	Trench 13	41 \pm 10
	Fluvial gravel	Trench 2	47 \pm 20
	Slope wash sand	Trench 14	90 \pm 50
Q2b	Fluvial gravel	Trench 2	145 \pm 25
	Fluvial gravel	Gravel pit near Shoshone, CA	160 \pm 18
Q2s	Fluvial sand	Jackass Flats	160 \pm 90
	Fluvial sand	Trench 14	270 \pm 90
	Fluvial sand	Trench 14	420 \pm 50
	Fluvial sand	Trench 14	480 \pm 90
Q2c (younger soil)	Fluvial gravel	Trench 13	240 \pm 50
	Fluvial gravel	Trench CF3	270 \pm 30
	Fluvial gravel	South Crater Flat	260 \pm 140
	Fluvial gravel	Jackass Divide	270 \pm 35
	Fluvial gravel	Rock Valley	310 \pm 30
Q2c (older soil)	Fluvial gravel	Jackass Divide	430 \pm 40
	Fluvial gravel	South Crater Flat	430 \pm 60
³ Q2e	Eolian sand containing volcanic ash	Striped Hills	730
⁴ Q11d	Volcanic ash bed near top of lake beds	Carson Slough, south Amargosa Desert	2.1 \pm 0.4 m.y.

¹ ¹⁴C analysis by S. W. Robinson, U.S. Geological Survey.

² Uranium-series analysis by B. J. Szabo, U.S. Geological Survey.

³ Correlation on basis of trace element chemistry to Bishop ash; analysis by G. A. Izett, U.S. Geological Survey.

⁴ Fission-track analysis by C. W. Meeser, U.S. Geological Survey.

Q1a deposits may be substantially older than the 0.74 m.y. old limit implied by its stratigraphic position below Q2e deposits. Basalt ash deposits in fractures within unit Q1a exposed in two fault trenches in eastern Crater Flat are inferred to be approximately 1.2 m.y. old on the basis of complex geological relationships discussed below, possibly restricting further the upper limit for the age of unit Q1a (see discussion of trenches 8 and CF1).

Middle and Late Pleistocene Deposits

Middle and late Pleistocene deposits (unit Q2, fig. 3) consist of fan alluvium, fluvial and eolian sands, and volcanic deposits. These deposits have been subdivided into five mappable units on the basis of relative age and lithology: three alluvial units, Q2c, Q2b, and Q2a (in order of decreasing age); eolian dunes and sand sheets, Q2e, and fluvial sand sheets, Q2s (fig. 4). The lithologies, stratigraphic relations, and soil development of these units are described in more detail by Hoover and others (1981, p. 15).

Unit Q2c consists of fluvial fan deposits and some debris flows. These deposits typically are unconsolidated, poorly to well-sorted, nonbedded to well-bedded, angular to rounded gravel with sand and silt in the matrix. Interbeds of silty sand are locally common. Alluvial fans of Q2c are generally deposited on unit Q1a on the middle and upper valley slopes; Q2c also occurs as terrace deposits in larger stream valleys.

Eolian deposits of unit Q2e occur as dunes and sand sheets in and adjacent to the Amargosa Valley. Ramps of fine, well-sorted sand as much as 50 m thick flank many of the hills bordering the Amargosa on the north. Unit Q2e is locally interbedded with the lower part of Q2c and is clearly older than Q2b.

Fluvial sand sheets of unit Q2s occur along major streams and along drainages downstream from dunes. The sheets consist of water-laid fine to medium gravelly sand or stream-reworked windblown sand and commonly rest on Q2c fans.

Unit Q2b is similar to Q2c in depositional environment and lithology. It occurs as terrace deposits that are inset in Q2c and underlies lower slope fans. These Q2b fans commonly merge upslope with Q2c fan deposits.

The youngest Q2 fluvial unit, Q2a, consists of debris flow deposits that are large enough to be mapped at only three localities. Q2a is poorly sorted, unconsolidated sand- to clay-size material that contains some gravel.

The inferred age of 0.74 m.y. old for lenses of volcanic ash in the lower part of unit Q2e discussed above is considered the approximate lower age limit for both units Q2e and Q2c. Younger Q2c gravels locally overlie and contain reworked cinders from a small basaltic volcano 11 km northwest of Lathrop Wells (fig. 1), which has yielded K-Ar dates ranging from 230,000 to 300,000 years old (Vaniman and others, 1982), indicating the approximate age for the younger part of Q2c deposition. A uranium-trend date of $270 \pm 30 \times 10^3$ years old was determined for a sample of Q2c from a soil horizon developed in the upper part of the unit. This date, which theoretically indicates the minimum age of Q2c deposition is consistent with the approximate age for the younger part of Q2c indicated by the relationship with the volcanic center near Lathrop Wells.

0 5 7 1 7

Uranium-trend dates determined for samples of Q2s in the Yucca Mountain area range from $480 \pm 90 \times 10^3$ years to $270 \pm 90 \times 10^3$ years. Stratigraphic relationships demonstrate that unit Q2s is equivalent in age to upper Q2c, in part equivalent to Q2e, and is older than Q2b. The minimum ages inferred from the uranium-trend dates are generally consistent with these stratigraphic relationships.

Samples of Q2b from the Yucca Mountain area have yielded uranium-trend dates that range from $145 \pm 25 \times 10^3$ years to $160 \pm 18 \times 10^3$ years (table 3). A minimum age of about 160,000 years for Q2b is preferred on the basis of the reliability of laboratory results. Samples from four exposures of slope-wash and fluvial deposits that have been correlated with Q2a yielded uranium-trend dates that range from $38 \pm 10 \times 10^3$ to $47 \pm 20 \times 10^3$ years (table 3).

Holocene Deposits

Holocene deposits in the study area consist of fluvial sands and gravels and eolian sand. These deposits have been subdivided on the basis of relative age and lithology into five mapping units: three units of fluvial gravel, Q1c, Q1b, and Q1a (in order of decreasing age); fluvial sand sheets, Q1s; and dunes and eolian sand sheets, Q1e (fig. 4).

Unit Q1c consists of unconsolidated fluvial gravel and minor debris flows that typically are poorly to well-bedded, moderately well-sorted gravel having a sandy matrix; Q1c locally contains numerous thin beds of sand. Q1c occurs as thin, broad fans on Q2c downstream from the incised parts of stream channels on valley slopes and underlies terrace remnants along larger drainages. Charcoal fragments from Q1c fluvial sand and gravel near Beatty, Nevada (fig. 1), yielded a ^{14}C age of $8,300 \pm 75$ years (S. Robinson, U.S. Geological Survey, written commun., 1981).

Q1e consists of well-sorted fine sand that occurs as small dunes and irregularly shaped sheets over much of the Amargosa Valley. It has been observed overlying all other units. Unit Q1s consists of thin sheets of fine moderately well-sorted gravelly sand and commonly overlies Q1c. Q1b and Q1a consist of unconsolidated fluvial gravel and sand and are confined to the channels of active washes. The subunits of Q1 are described in more detail by Hoover and others (1981, p. 20).

LATE CENOZOIC FAULTING

Thirty-two faults with associated offsets or fractures in late Cenozoic deposits were identified in the Yucca Mountain area on the basis of mapping and trench studies. The traces of faults that involve Quaternary deposits and their extensions in bedrock are shown on plate 1, along with several fault traces across which trenches were excavated but no disturbance of Quaternary deposits was recognized. The length of fault segments that have Quaternary offset cannot be determined in most cases, because materials necessary to demonstrate Quaternary offset are not present where faults extend into bedrock. The faults are described from east to west across the area; they are referred to by fault names where such names exist, otherwise a letter designation has been used to identify each fault or group of adjacent faults.

In the Calico Hills, in the northeastern part of the study area, four probable faults, collectively designated A on plate 1, form distinct linear features on aerial photographs and appear to offset unit QTa in outcrop. Three of these faults trend northeast and one trends eastward. The lineaments can be traced on aerial photographs across deposits of Q2c in some places, but do not cross Q1c deposits. No definite scarps were observed and offset of QTa is probably a half meter or less. It was not determined whether the lineaments in Q2c reflect vegetation growth controlled by fractures in QTa beneath undisturbed Q2c or offset of Q2c. None of the faults at this location were trenched.

Fault B, also in the Calico Hills, trends northeast and is exposed for less than 0.2 km in Paleozoic sedimentary rocks. It locally offsets deposits of QTa and Q2c, which are too small to show on plate 1. Offset, down to the southeast, is 2 m in QTa at the northeast end of the fault and about 0.5 m in Q2c at the southwest end. Fault B was not trenched, and it is not known whether the difference in the amount of offset is because of recurrent movement or a decrease in throw to the southwest.

The Paintbrush Canyon fault trends northward for 18 km in the eastern part of Yucca Mountain and continues to the north beyond the study area. Where it offsets Miocene volcanic rocks, the displacement is normal and down to the west. Although surficial mapping did not indicate Quaternary offset, evidence for disturbance of Pleistocene deposits was discovered in three trenches excavated across the fault (pl. 1). Trench A1 (fig. A15) exposed fractures in unit Q2e. These fractures do not appear to offset unit Q2b. In trench A2 (fig. A16), similar fractures cut unit Q2c but not the soil developed in Q2c or the overlying Q2b deposits. Because bedding features are scarce in these unconsolidated units, offset along the fractures was difficult to assess, but the lack of apparent disturbance adjacent to the fracture suggests any offset was minor, less than a few centimeters. Trenches 16 and 16B were cut near the southern end of the fault zone (north end of the Bow Ridge fault of Scott and Bonk, 1984) in deposits of unit Q2e. Trench 16 (fig. A12) showed no faults or fractures, but 16B (fig. A13) exposed carbonate-coated west-dipping fractures that cut Q2e but not overlying deposits of Q2s(?). The fracturing is interpreted as indicating minor offset on the fault in the underlying bedrock that produced fractures with no visible offset in the unconsolidated sand of unit Q2e.

Fault C (Bow Ridge fault of Scott and Bonk, 1984) parallels the Paintbrush Canyon fault (pl. 1) and also offsets Tertiary rocks down to the west. The fault trends northward for at least 6 km from the trench 15 site. It does not appear to cross Yucca Wash to the north, and its extent south of trench 15 is not known. No indication of Quaternary offset was detected by mapping of surficial deposits, but trench 14 exposed a fault in Tertiary volcanic rocks and fractures that cut across but do not appear to offset unit Q2s and the K horizon of the soil developed in it. These fractures do not cut the overlying Q2a (fig. A11). Uranium-trend dates determined for samples from units Q2s and Q2a in this trench are $270 \pm 90 \times 10^3$ years and $38 \pm 10 \times 10^3$ years respectively (table 3). Minor offset on fault C that produced the fractures in unit Q2s is inferred during the time interval between these dates. Uranium-series dates ranging from 350×10^3 to 550×10^3 years were determined for samples of carbonate and opal deposits (table 2) that extend across the faulted volcanic rocks without offset.

Along the northeast side of Yucca Mountain, four faults, D, E, F, and G, cut Tertiary volcanic rocks but, no offset of Quaternary deposits was observed. Each fault was investigated by one or more trenches (pl. 1). No evidence of Quaternary faulting was found. Data from these trenches are summarized in table 1 and trench wall diagrams appear in the appendix.

Fault I, near the south end of Yucca Mountain, cuts QTa and locally faults it against older Tertiary rocks. The fault strikes northeast and is down to the west; it was not trenched, and the amount of displacement is unknown. The fault is exposed for a distance of 2.4 km and appears to be covered by younger Q2 deposits to the north and south. A low northwest-facing scarp is exposed along part of the fault, but for most of its length, the downthrown block and the scarp are masked by windblown sand (Q2e) that locally extends across the fault without demonstrable offset.

The Solitario Canyon fault zone is one of the major structures of the Yucca Mountain area and marks the west boundary of the potential repository. The fault zone strikes northerly and extends for at least 12 km. Although the fault zone is complex, the net offset is normal and down to the west. Mapping of surficial deposits indicated several fault segments where QTa is faulted against Tertiary volcanic rocks for a total distance of 4.5 km (pl. 1).

Three trenches (8, 10A, and 10B) were cut in Quaternary deposits across the Solitario Canyon fault zone. Trench 8 exposed unit QTa displaced downward on the west against Tertiary volcanic rocks (fig. A4). The amount of offset is unknown. Reworked basaltic ash occurs in a fracture zone in unit QTa on the south wall of trench 8. Known late Cenozoic basaltic centers in the Crater Flat area, which are potential sources for the basaltic ash in trench 8, fall into three age groups on the basis of K-Ar dates. Basalt centers of the oldest group, approximately 3.75 m.y. old (Carr, 1982), are older than the maximum age for QTa interpreted from stratigraphic relations and isopic dates from the Amargosa Desert and are not considered a possible source for the reworked ash. Differences between phenocryst compositions determined by microprobe analyses of samples of the 3.75 m.y.-old basalt and ash from trench 8 and a similar ash from trench CF1, 2 km to the west (pl. 1), also suggest that the 3.75 m.y.-old basalt eruptions were not the source of the ash in the trenches (Wolfsberg and Vaniman, 1984). The younger basalt centers in Crater Flat, approximately 1.2 and 0.24 m.y. old (B. M. Crowe, Los Alamos National Laboratory, written commun., 1984), cannot be distinguished by their phenocryst compositions, which are similar to compositions of reworked ash samples from both trenches (B.M. Crowe, Los Alamos National Laboratory, written commun., 1984). The reworked ash deposits in the fault trenches, therefore, cannot be uniquely correlated with either the 1.2- or 0.24 m.y.-old basalt sources on the basis of their phenocryst compositions.

The faulting and emplacement of the basaltic ash in trench 8 seem to have preceded the development of the K horizon of the QTa soil because the fault at the west edge of the fault zone does not offset the K horizon and the fracture that contains the ash appears to be sealed by carbonate where the fracture intersects the overlying K horizon. Fractures within the fault zone that cut across the K horizon without visible offset are probably related to later minor offset on the fault in the underlying bedrock. No deposits exposed establish a minimum age for these fractures.

Trench 10B, 3.3 km north of trench 8, exposes QTa faulted against Tertiary volcanic rocks (fig. A7). The amount of displacement of unit QTa is unknown. The K horizon of the QTa soil and the overlying Q2c deposit extend across the fault without offset. No displaced or fractured Quaternary deposits were exposed in trench 10A (fig. A6).

Uranium-series dates for unfractured calcrete deposits from the Solitario Canyon fault zone, where QTa is faulted against Tertiary volcanic rocks (sample localities 113 and 115, plate 1), were reported by Szabo and others (1981, p. 21-22), who interpreted the ages of the calcrete as greater than 5,000 years for locality 113 and greater than 20,000 and 70,000 years for two samples from locality 115). If this interpretation is correct, these dates could also represent minimum ages for latest movements along parts of the fault zone because the calcrete was not fractured.

A fault designated H that is aligned with the Solitario Canyon fault zone, but is downthrown to the east, was investigated at the north edge of Yucca Mountain by trenches 13, GA1A and GA1B (pl. 1). Deposits of Q2c in trench 13 are not faulted (table 1). Carbonate deposits from an unfaulted soil overlying faulted Tertiary volcanic rocks in trench GA1A yielded a minimum uranium-series age of 32,000 years (table 2). No evidence confirming Quaternary movement was found.

Near the southern end of the Solitario Canyon fault zone, a possible fault, J, forms a northeast-trending 0.5-km-long lineament between QTa and Tertiary volcanic rocks. No offset could be demonstrated and no scarp is present where the lineament crosses QTa.

West of the Solitario Canyon fault zone, two parallel faults, K and N, trend generally north-northeast and are 7.5 and 6 km long, respectively. Both fault QTa down to the west against Tertiary volcanic rocks and are overlain locally by unfaulted deposits of Q1c. These faults were not trenched, and no data are available on the amount of Quaternary offset.

Fault L is exposed for less than 0.5 km in QTa along the east side of Crater Flat. The fault is marked by a north-northwest-trending brush line but does not display a scarp; it was not trenched and the direction and amount of offset are unknown.

Fault M consists of two segments that are not continuous on aerial photographs but are considered to be one fault because of alignment and similarities in the scarps. The northern segment trends north-northwest and is about 1 km long. It displaces QTa down to the west. The scarp is 1.5 m high and has a maximum slope angle of 7°. The southern segment cuts unit QTa for a distance of 1.5 km, trends north and northwest and is marked by a west-facing scarp 1.5 m high. The scarp has a slope of 9° and a surface offset of 1 m. Trench CF1, excavated across the scarp, exposed three faults that offset a QTa soil horizon about 2.5 m down to the west adjacent to the fault zone (fig. A17).

Sasaltic ash occurs along one of the faults in trench CF1 and appears to have been emplaced in an open fracture that formed at the time of faulting. Because near-surface open fractures in poorly consolidated alluvial deposits are assumed to be short-lived features, it is probable that faulting of unit

Q_{Ta}, the eruption of the basalt ash, and deposition of the ash in the open fracture essentially were contemporaneous. As discussed above, this ash is similar in composition to both the 1.2- and 0.24-m.y.-old basalts in the Crater Flat area. Although it was not possible to correlate uniquely the basaltic ash from the trench with basalt sources of either age on the basis of their composition, stratigraphic and structural relations suggest that the ash present in the fault zone is from the 1.2-m.y. old eruptions. A 1- to 2-m-thick K horizon (K₁ on fig. A17) interpreted by Swadley and Hoover (1983, p. 7-8) as post-dating the offset along the fault zone in trench CF1 contains stage III to stage IV carbonate development. A 1-m-thick pedogenic carbonate horizon developed on unit Q_{2c} gravel exposed in nearby trench CF3 (fault Q, 2.5 km south of CF1) contains only stage II carbonate. The stage III to IV carbonate developed across the fault zone in trench CF1 is considered to be significantly older than the stage II carbonate on Q_{2c} in trench CF3. A date of 0.27 ± 0.03 m.y. determined by the uranium-trend method for samples from the carbonate horizon developed on Q_{2c} in trench CF3 theoretically indicates the minimum age for the deposition of the Q_{2c} deposit (Swadley and Hoover, 1983). The K horizon thought to post-date the fault in trench CF1 is interpreted as older than the Q_{2c} deposit in trench CF3 and, therefore, older than the 0.24 m.y.-old basalts. It is concluded on the basis of these relationships that the ash in the fault zone in trench CF1 was erupted during the 1.2 m.y.-old basalt cycle and faulting in trench CF1 is coeval with these eruptions. It can be concluded through a similar line of reasoning that the unfaulted K horizon exposed in trench 8 on the Solitario Canyon fault also is older than the 0.24 m.y.-old basalt, and the ash and fault zone exposed in that trench are also approximately 1.2 m.y. old.

To the west the short, poorly defined fault O cuts Q_{Ta} and can be traced across an adjoining area of Q_{Ta} that is thinly covered with Q_{2c} gravel. The fault is indicated by a 0.5-km-long north-northwest-trending brush line, but does not form a scarp. No stratigraphic data are available on the amount of offset because the fault was not trenched.

Approximately 2 km southwest of fault M, two intersecting faults, designated P and Q occur chiefly in unit Q_{Ta}. Fault Q, to the west, extends for 0.9 km in a north-northeast direction. It is marked by a scarp 1 to 4 m high where it crosses Q_{Ta}. Two trenches, CF2 and CF3, were excavated across this fault. Trench CF2 (fig. A18), cut across the scarp, exposed the main fault and three minor faults. The amount of offset on these faults could not be determined because of a lack of bedding features in Q_{Ta}. Three faults offset Q_{Ta} but do not offset the upper part of the K horizon developed in Q_{Ta}. A minor fault, 1 m east of the main fault, cuts the upper part of the K horizon and indicates a period of faulting younger than that of the main fault. A topographic profile measured near trench CF2 gave a maximum scarp slope angle of 12° , a scarp height of 4 m, and a surface offset of 1.5 m. Trench CF3 was excavated 300 m south of CF2 in Q₂ deposits where no scarp is present but the fault is marked by a poorly developed brush line. CF3 revealed three small faults that offset Q_{2c} less than 1 m down to the west but do not offset an overlying Q_{2a} deposit (fig. A19). Uranium-trend dates determined for samples from this trench are $270 \pm 30 \times 10^3$ years for unit Q_{2c} and $40 \pm 10 \times 10^3$ for Q_{2a}, suggesting that movement occurred during the time interval between these two dates.

Fault P, to the east, trends northwest across QTa for 0.35 km and is recognized by the presence of a subtle brush line; no fault scarp was found. The fault trace is concealed by Q2 deposits to the north and south, and fault P may be somewhat longer than indicated by surface expressions. The fault was not trenched and the amount of offset is unknown.

At the southwest end of Yucca Mountain, fault R offsets QTa against Tertiary volcanic rocks for a distance of 1.3 km. The fault continues to the south for about 2.5 km where it offsets Tertiary volcanic rocks or is concealed by Q2 deposits. The segment that offsets Quaternary deposits strikes north-northeast and is downthrown to the west. The fault was not trenched.

Fault segment S probably connects with a fault that extends for 11 km to the north through Tertiary volcanic rocks. The segment that cuts Quaternary deposits is 1.1 km long and offsets only unit QTa. This segment is marked by a poorly developed brush line. Although no definite scarp was found where the fault trace crosses QTa, deposits of Q2c, which are too small to show on page 1, appear to have been deposited along the east side of the fault against an east-facing scarp. If this interpretation is correct, it suggests that the Quaternary offset on this segment of the fault is down to the east, which is the opposite of the offset demonstrated by Tertiary volcanic rocks exposed along the fault to the north (pl. 1). The fault was not trenched, and the amount of offset is unknown.

Northeast of fault S, a north-northeast-trending fault, designated T, faults QTa and also displaces QTa against Tertiary volcanic rocks. It is 7 km long and is downthrown to the west. The fault was not trenched, and the amount of offset is unknown. A profile measured where the fault offsets QTa gave a maximum scarp slope angle of 11° , scarp height of 1 m, and a surface offset of 0.7 m.

A short northeast-trending fault segment, designated U, near the southwest end of Yucca Mountain appears to displace QTa down to the west against Tertiary volcanic rocks although actual displacement of QTa could not be determined. The scarp is exposed for only 0.2 km but the fault can be traced on areal photographs for another 0.3 km to the southwest where it is partly obscured by Q1c deposits (pl. 1). The fault was not trenched; and no data are available on the amount of throw.

Fault V, located 1.5 km northeast of Black Cone in Crater Flat, has a north-northwest trend and extends for 1 km across an area of QTa. A very low east-facing scarp that is present only along part of the fault suggests that offset is down to the east. Where the fault trace crosses thin terrace deposits of subunit Q2c (pl. 1) the trace is visible on aerial photographs. It is not known whether this lineament reflects plant growth controlled by fractures in the underlying QTa or faulting in Q2c. The fault was not trenched, and the amount of Quaternary offset is unknown.

Near the north end of Bare Mountain there is a group of seven short, subparallel faults with a north-northeast trend. These faults collectively designated W on page 1, cut QTa or offset QTa against an older Tertiary gravel unit. They range in length from 0.2 to 1.0 km, and several can be traced on aerial photographs across areas where QTa is covered by thin

deposits of Q2c that do not appear to be offset. These faults were not trenched, and there are no data on the amount of offset; for most the sense of motion is unknown.

Northwest of location W an arcuate fault, designated X, is exposed chiefly in an area underlain by Tertiary gravel but locally cuts a narrow deposit of QTa. The fault is 2.5 km long. The southern part trends east-west and swings sharply to a north-northeast trend. No scarp was observed where the fault cuts QTa.

Fault Y, near the western edge of Crater Flat, is exposed for only 0.2 km in unit QTa. The fault trends north-northeast and is recognized by a brush line. No scarp is present but a cutbank exposure indicates that the offset is down to the east. The fault trace is concealed to the south by deposits of Q2c.

The Bare Mountain fault zone is a major structural feature of the area and marks the western edge of Crater Flat. It trends generally north and is about 20 km long. Although the fault is concealed for much of its length, evidence of Quaternary offset is exposed at several locations. Along the northern segment of the zone (BM-1, plate 1) QTa is faulted down against Paleozoic rocks. Locally Q2c fan deposits appear to cross the fault without offset. A prospect pit in dense secondary carbonate and opal deposits along the fault zone exposed a number of subparallel fault planes that dip 50° to 60° east. Slickensides on one of these planes showed only dip-slip movement. A scarp profile measured near the southern end of this segment where the fault trace crosses an area of QTa, gave a slope angle of 10° , a height of 1 m, and a surface offset of 0.8 m.

To the south (segment BM-2) the fault trace can be identified only where it crosses two small areas of QTa. The fault is recognized by a brush line but no scarp is present. A cut bank exposure in QTa revealed that the fault plane dips 75° to the east.

The southern segment, BM-3, exposes faulted QTa at two locations and also exhibits geomorphic evidence of Quaternary movement. At the southern location the fault has formed a well-defined scarp in QTa. A scarp profile measured here gave a slope angle of 20° , a height of 4 m, and a surface offset of 1.7 m. At the second location, an area of QTa is truncated by the fault but the downthrown block is covered by Q1 age deposits and no scarp was observed.

Along the southern segment of the fault zone, fans composed of Q1c fluvial gravel at several locations occur adjacent to but 10 to 30 m above small remnants of Q2c fans that appear to be faulted against Paleozoic bedrock. Commonly Q1c overlies Q2c or is inset into Q2c fans. The juxtaposition of Q1c deposits well above Q2c fans is interpreted as indicating uplift along this segment of the fault zone after Q2c deposition. The uplift elevated the bedrock valleys that were the source of the Q1c gravels and resulted in deposition of fans at elevations above the older Q2c deposits. These Q1c fans extend into the bedrock valleys on the upthrown side of the fault and cross the fault without offset. The fault has not been trenched, but the relative positions of Q1c and Q2c deposits indicate Quaternary uplift could be in the range of 10 to 30 m along the southern part of the Bare Mountain fault zone.

SUMMARY AND DISCUSSION

Offset or fracturing of Quaternary deposits was demonstrated for 32 faults within the Yucca Mountain study area. The fault segments for which Quaternary offset can be demonstrated range in length from 16 km, the Bare Mountain fault zone, to less than 0.5 km. The longest continuously exposed scarp in Quaternary deposits is a 4-km segment located near the south end of the Solitario Canyon fault zone.

For most faults the amount of Quaternary offset has not been determined. Where offset can be measured or where fault scarps are preserved, dip-slip movement on the order of 3 m or less is indicated. The one exception is the southern segment of the Bare Mountain fault zone where geomorphic evidence suggests Quaternary offset may be in the range of 10 to 30 m.

Strike-slip movement could not be demonstrated nor could such movement be ruled out. The poorly consolidated surficial deposits exposed in the trenches and the secondary carbonate deposits along the trace of faults are poor mediums for the preservation of slickensides and other small-scale directional features. Strike-slip offset on the order of tens of meters would probably be detected by geomorphic evidence such as offset of streams or other linear features, whereas offset of a few meters or less probably could not be detected.

Although absolute age data are limited, faults with Quaternary displacement can be divided into three broad age groups. The youngest group consists of faults B, C, Q, the Paintbrush Canyon fault, and the Bare Mountain fault zone; these faults offset or produced fracturing in deposits of Q2 age. Based on uranium-trend age determinations as discussed above, age brackets of less than $270,000 \pm 90,000$ yr and greater than $39,000 \pm 10,000$ yr and less than $270,000 \pm 30,000$ yr and greater than $40,000 \pm 10,000$ yr have been inferred for faults C and Q, respectively. Offset on the Paintbrush Canyon fault after about 700,000 yr and before 270,000 yr is suggested by correlation of stratigraphic units where fracturing is exposed in trenches A1 and A2. Quaternary offset on the southern part of the Bare Mountain fault zone is inferred during the interval between 270,000 and 9,000 yr ago based on geomorphic evidence and stratigraphic correlations. Movement on fault B after 270,000 yr is inferred from the minimum age of the youngest offset unit, Q2c; no minimum age of offset has been determined for this fault.

Faults of the intermediate age group offset only QTa and older units; where these faults are exposed in areas of QTa, a distinct scarp is commonly observed. Only general age constraints can be inferred for Quaternary offset along faults of this group. Quaternary movement of the Solitario Canyon fault zone and fault M has been tentatively dated at about 1.2 m.y. ago based on occurrences of basaltic ash in the fault zones as discussed above. Inferred age brackets for Quaternary offset on fault I are less than 2 m.y., based on the maximum age inferred for unit QTa and greater than about 700,000 yr, the approximate minimum age inferred for Q2e deposits that appear to extend across the fault scarp without offset. Fault T is included in the intermediate group because the height and slope angle of the scarps of faults T and M are similar. Based on preliminary scarp measurements, faults in Crater Flat have been classified as significantly older than 1.2 m.y. where no scarp is preserved or about 1 m.y. old or younger for faults that exhibit scarps

similar in height and slope angle to fault M, tentatively dated at 1.2 m.y. old. In this preliminary study, comparisons have been limited to scarps of similar height (1-2 m) and scarps formed in the same rock type (unit QTa). For these comparisons it is assumed that the fault offset included some scarp-forming component.

The 23 faults of the oldest group offset QTa and older units, but no scarps are preserved. General age limits for Quaternary offset on faults of this group are younger than 2 m.y., the maximum age inferred for unit QTa, and older than about 1.2 m.y., inferred from the lack of preserved scarps. Minimum age constraints are demonstrated for some faults of the oldest group where stratigraphic units younger than QTa overlie a fault without offset. Faults S, V, and Y and faults P and R are locally overlain by apparently unfaulted deposits of Q2c and Q2b, respectively. Minimum age limits for Quaternary offset of greater than 270,000 yr and greater than 160,000 yr are inferred for these two groups of faults from the minimum ages of the overlying stratigraphic units. Fault group A and faults K, N and U are overlain in places by unfaulted Q1c deposits and a minimum age limit for Quaternary offset of greater than 7,000 yr is inferred. No minimum age limit can be demonstrated by this method for faults J, L, X, and fault group W. Table 4 summarizes the data on each fault and the inferred ages of offset.

Where age constraints have been inferred from radiometric dating and from stratigraphic correlations of faulted and unfaulted deposits at a trenched site, no offset younger than about 40,000 yr has been demonstrated. Holocene offset has not been demonstrated in the study area nor can it be ruled out.

Table 4.--Summary of Quaternary faulting in the Escaz Mountains area.

Fault or fault group ¹	Trench number	Youngest unit faulted or fractured	Oldest unit not faulted or fractured	Inferred age of last movement	Method of dating	Remarks
A (4)	not trenched	Q1a	Q1c	$<2 \times 10^6$ >7,000	Correlation of stratigraphic units	-----
B	do.	Q2c	Unknown	<270,000	do.	No minimum age determined
Paintbrush Canyon fault	A1, A2, 16, 16b	Q2e (fractures in trench A2)	Q2c soil (in trench A1)	<700,000 >270,000	do.	-----
C	14	Q2s (fractures in trench 14)	Q2a	$<270 \pm 90 \times 10^3$ > $18 \pm 10 \times 10^3$	Uranium-trend	-----
D	11	No Quaternary offset found	Q1a	-----	-----	No evidence of Quaternary offset
E	12	do.	Q2 soil	-----	-----	No.
F	4, 6, 9	do.	Q2c	-----	-----	No.
G	2	do.	Q2c	-----	-----	Do.
Solitario Canyon fault zone	8, 10, 10b	Q1a	Q1a soil	1.2×10^6	Petrographic correlation of basalts ash; correlation of stratigraphic units	-----
H	13, GALL, GALL	No Quaternary offset found	Q2c	-----	-----	-----
I	Not trenched	Q1a	Q2e	$<2 \times 10^6$ >700,000	Correlation of stratigraphic units	-----
J	do.	Q1a	Unknown	$<2 \times 10^6$	do.	>1.2 m.y. age inferred from lack of scarp
K	do.	Q1a	Q1c	$<2 \times 10^6$ >7,000	do.	Do.
L	do.	Q1a	Unknown	$<2 \times 10^6$	do.	>1.2 m.y. age inferred from lack of scarp
M	CF1	Q1a	Q2 soil	1.2×10^6	Petrographic correlation of basalts ash; correlation of stratigraphic units	-----
N	Not trenched	Q1a	Q1c	$<2 \times 10^6$ >7,000	Correlation of stratigraphic units	>1.2 m.y. age inferred from lack of scarp
O	do.	Q1a	Q2c(?)	$<2 \times 10^6$ >270,000(?)	do.	No.
P	do.	Q1a	Q2b(?)	$<2 \times 10^6$ >160,000(?)	do.	Do.
Q	CF2, CF3	Q2c	Q2a	$<270 \pm 30 \times 10^3$ > $40 \pm 10 \times 10^3$	Uranium-trend	Two episodes of faulting; younger episodes dated in trench CF3
R	Not trenched	Q1a	Q2b(?)	$<2 \times 10^6$ >160,000(?)	Correlation of stratigraphic units	-----
S	no.	Q1a	Q2c	$<2 \times 10^6$ >270,000	do.	-----
T	do.	Q1a	Unknown	$<2 \times 10^6$	do.	1 m.y. or younger age inferred from scarp
U	do.	Q1a	Q1c	$<2 \times 10^6$ >7,000	do.	>1.2 m.y. age inferred from lack of scarp
V	do.	Q1a	Q2c(?)	$<2 \times 10^6$ >270,000(?)	do.	Do.
W (?)	no.	Q1a	Unknown	$<2 \times 10^6$	do.	Do.
X	do.	Q1a	Unknown	$<2 \times 10^6$	do.	No.
Y	do.	Q1a	Q2c	$<2 \times 10^6$ >270,000	do.	Do.
Here Mountain fault zone	no.	Q2c	Q1c	<270,000 >9,000	Correlation of stratigraphic units and geomorphic evidence	-----

¹Number of faults in group shown in parenthesis.

²Unit shown is faulted except where fractures are indicated.

REFERENCES CITED

- Bucknam, R. C., and Anderson, R. E., 1979, Estimation of fault-scarp ages from a scarp-height--slope-angle relationship: *Geology*, v. 7, no. 1, p. 11-14
- Byers, F. M., Jr., Carr, W. J., Orkild, P. P., Quinlivan, W. D., and Sargent, K. A., 1976, Volcanic suites and related cauldrons of Timber Mountain-Oasis Valley caldera complex, southern Nevada: U.S. Geological Survey Professional Paper 919, 70 p.
- Carr, W. J., 1982, Volcano-tectonic history of Crater Flat, southwestern Nevada as suggested by new evidence from drill hole USW-VH-1 and vicinity: U.S. Geological Survey Open-File Report 82-457, 23 p.
- Christiansen, R. L., and Lipman, P. W., 1965, Geologic map of the Topopah Spring NW quadrangle, Nye County, Nevada: U.S. Geological Survey Geologic Quadrangle Map GQ-444, scale 1:24,000.
- Cornwall, H. R., and Kleinhampl, F. J., 1961, Geology of the Bare Mountain quadrangle, Nevada: U.S. Geological Survey Geologic Quadrangle Map GQ-157, scale 1:62,500.
- Hoover, D. L., Swadley, W C, and Gordon, A. J., 1981, Correlation characteristics of surficial deposits with a description of surficial stratigraphy in the Nevada Test Site region: U.S. Geological Survey Open-File Report 81-512, 27 p.
- Izett, G. A., 1982, The Bishop ash bed and some older compositionally similar ash beds in California, Nevada, and Utah: U.S. Geological Survey Open-File Report 82-582, 44 p.
- Lipman, P. W., and McKay, E. J., 1965, Geologic map of Topopah Spring SW quadrangle, Nye County, Nevada: U.S. Geological Survey Geologic Quadrangle Map GQ-439, scale 1:24,000.
- Rosholt, J. N., 1980, Uranium-trend dating of Quaternary sediments: U.S. Geological Survey Open-File Report 80-1087, 65 p.
- Scott, R. B. and Bonk, Jerry, 1984, Preliminary geologic map of Yucca Mountain with geologic sections, Nye County, Nevada: U.S. Geological Survey Open-File Report 84-494.
- Snyder, D. B., and Carr, W. J., 1982, Preliminary results of gravity investigations at Yucca Mountain and vicinity, southern Nye County, Nevada: U.S. Geological Survey Open-File Report 82-701, 36 p.
- Stewart, J. H., and Carlson, J. E., 1978, Geologic map of Nevada: U.S. Geological Survey, scale 1:500,000.
- Swadley, W C, 1983, Map showing surficial geology of the Lathrop Wells quadrangle, Nye County, Nevada: U.S. Geological Survey Miscellaneous Investigations Map I-1361, scale 1:48,000
- Swadley, W C, and Hoover, D. L., 1983, Geology of faults exposed in trenches in Crater Flat, Nye County, Nevada: U.S. Geological Survey Open-File Report 83-608, 15 p.
- Szabo, B. J., Carr, W. J., and Gottshall, W. C., 1981, Uranium-thorium dating of Quaternary carbonate accumulations in the Nevada Test Site region, southern Nevada: U.S. Geological Survey Open-File Report 81-119, 35 p.
- Vaniman, D. T., Crowe, B. M., and Gladney, E. S., 1982, Petrology and geochemistry of hawaiite lavas from Crater Flat, Nevada: *Contributions to Mineralogy and Petrology*, v. 80, p. 344-357.

00317 0535

APPENDIX

Preliminary diagrams of nineteen trenches excavated in the
Yucca Mountain area to evaluate Quaternary fault movement.

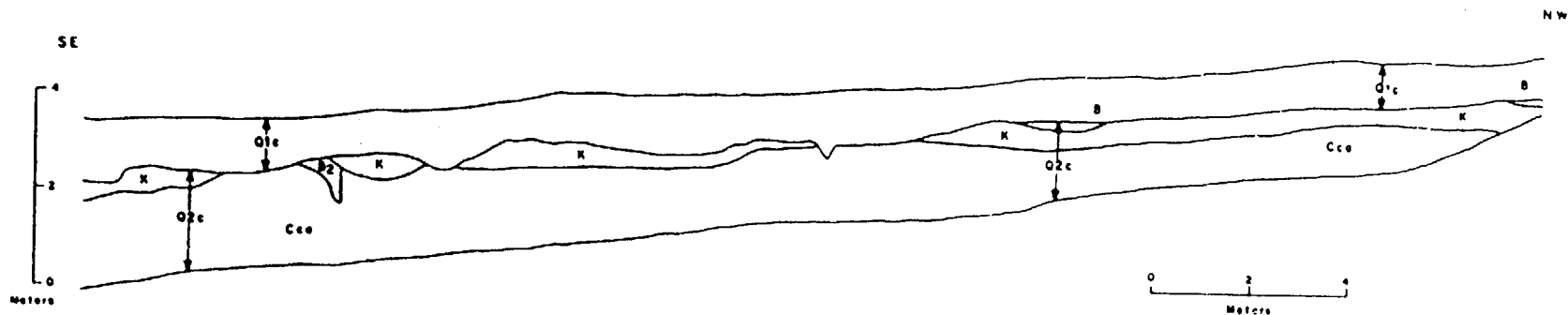


Figure A1.--Diagram of south wall of trench 2. Trench trends N. 60° W. across the projection of fault G. Mapped in May 1982 by Swadley, L. D. Parrish and H. E. Huckins, Fenix & Scisson (F&S). Samples of Q2a and Q2b dated by uranium-trend method (table 1) were collected from north wall from strata not preserved in south wall. Sample location is opposite southeast end of diagram.

<u>Unit</u>	<u>Description</u>
Q1c	Gravel, sandy, unconsolidated, mostly pebbles with scattered cobbles; poorly bedded to nonbedded
Q2c	Gravel, mostly pebbles and cobbles with scattered boulders, poorly sorted, poorly bedded. Soil developed in Q2c consists of B, B2, K, and Cca horizons
B	B horizon, light-brown, cambic, developed in poorly sorted gravel
B2	Similar to B with threads and filaments of carbonate minerals
K	K horizon--poorly sorted gravel with stage III carbonate development
Cca	Cca horizon--poorly sorted gravel with stage I carbonate development

7
1
3
0
0
25

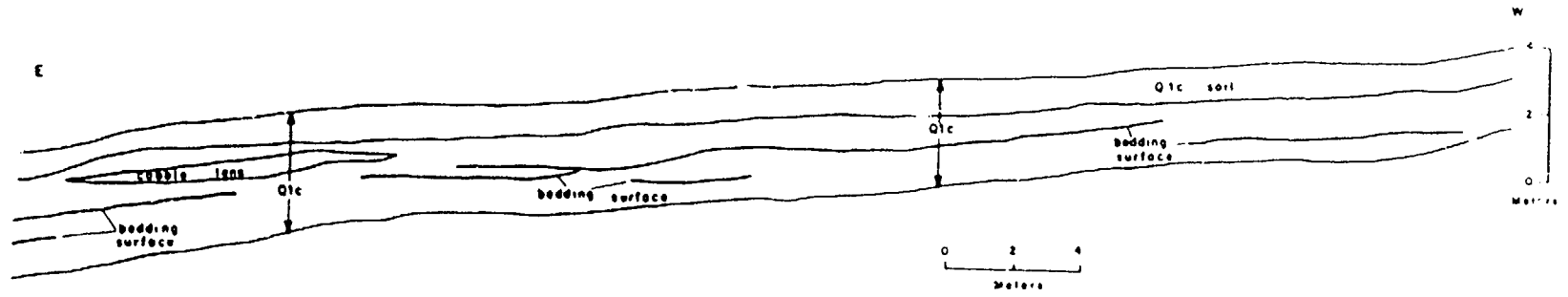


Figure A2.--Diagram of south wall of trench 4. Trench trends N. 85° W. across the projection of fault F. Mapped in June 1982 by Swadley.

<u>Unit</u>	<u>Description</u>
Q1c	Gravel, angular, poorly sorted, poorly bedded; sandy matrix and scattered sand lenses; mapped bedding surfaces are poorly defined and discontinuous, may be scour surfaces. Weak soil development in unit, lower contact of soil mapped at base of Cca horizon (stage I carbonate development)

A 8 9 0 7 1 8 0 2

26

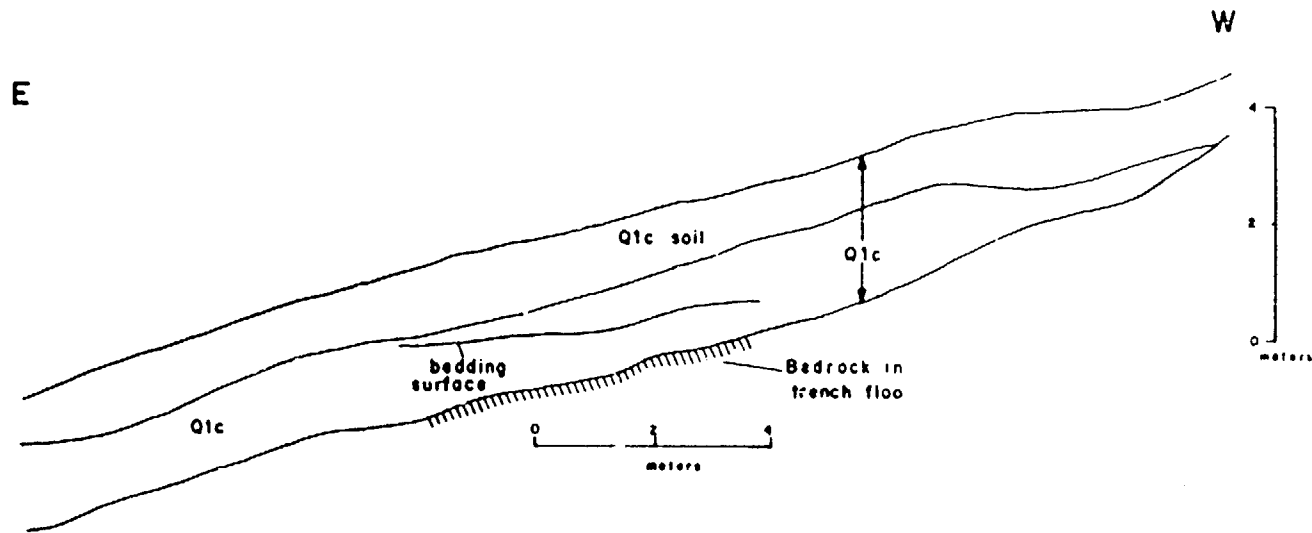


Figure A3.--Diagram of south wall of trench 6. Trench trends N. 70° W. across the projection of fault F. Mapped in June 1982 by Swadley and H. E. Huckins.

<u>Unit</u>	<u>Description</u>
Q1c	Gravel, sandy, angular, poorly sorted, poorly bedded; mostly pebbles and cobbles with scattered boulders. Weakly developed soil; lower contact mapped at base of Cca horizon (stage I carbonate development.)

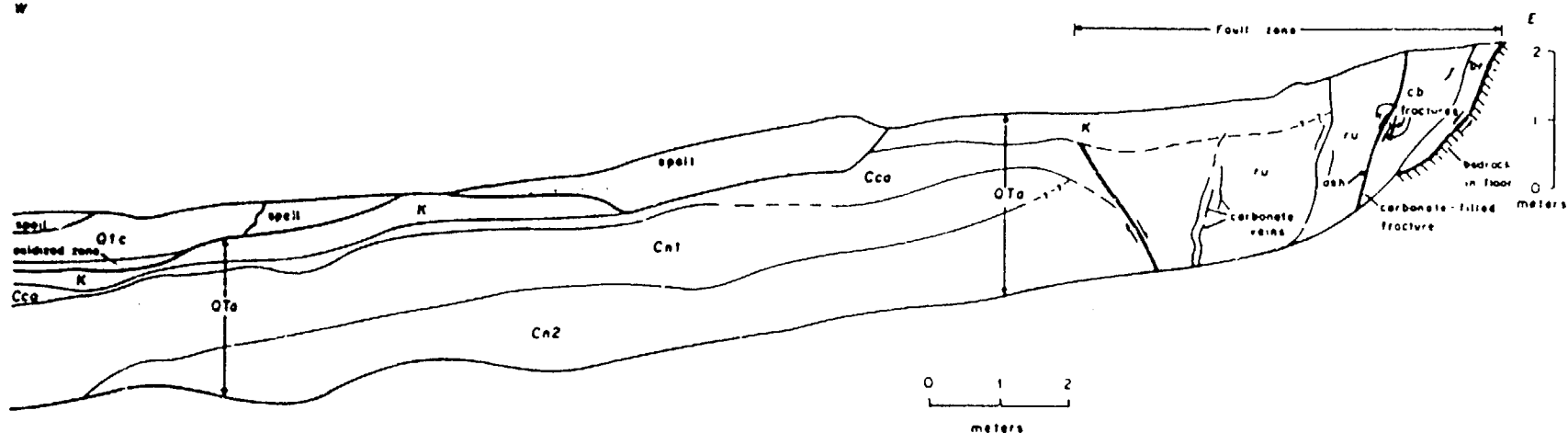


Figure A4.--Diagram of north wall of trench 8. Trench trends N. 80° E. across the Solitario Canyon fault zone. Mapped in November 1982 by Swadley and H. E. Huckins. QTa is displaced against Tertiary volcanic rocks by main fault at east end of trench. Minor fault at west edge of fault zone cuts QTa but not the K horizon developed in QTa. Later fracturing extends into and through the K horizon.

<u>Unit</u>	<u>Description</u>
Q1c	Gravel, sandy, unconsolidated, angular, poorly sorted
QTa	Gravel, coarse, angular, poorly sorted, soil developed in QTa consists of K, Cca, Cn1 and Cn2 horizons
K	K horizon--poorly sorted angular gravel with stage IV carbonate development; thin laminated zone at top. Oxidized zone at west end of trench consists of weathered fragments of K horizon in a matrix of reddish-brown sand
Cca	Cca horizon--angular poorly sorted gravel with stage III to II carbonate development
Cn1	Gravel, angular, moderately well sorted, mostly pebbles and small cobbles
Cn2	Gravel, coarse, angular, poorly sorted
br	Breccia, with abundant laminated opaline carbonate along main fault.
cb	Carbonate, porous and some fault breccia with scattered plates of laminated carbonate and brown opal
ru	Rubble and unsorted gravel, cemented with porous, secondary carbonate. Carbonate increases to the east across fault zone, locally it obscures the K horizon in this unit
Ash	Location of loose 1.2 m.y.-old basaltic ash along fracture in opposite wall of trench

27 / 1 1 1 1

169071800

28

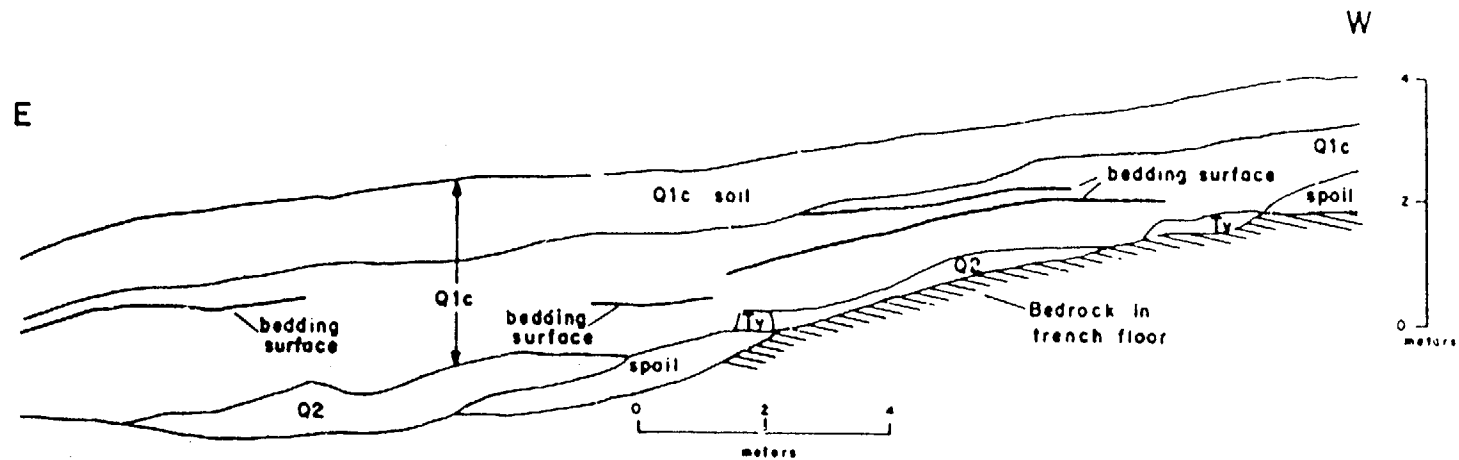


Figure A5.--Diagram of south wall of trench 9. Trench trends N. 65° W. across projection of fault F. Mapped in June 1982 by Swadley and H. E. Huckins.

<u>Unit</u>	<u>Description</u>
Q1c Soil	Soil--weakly developed in sandy poor sorted gravel. Lower contact marked by base of stage i carbonate development
Q1c	Gravel, angular, poorly sorted, poorly bedded; pebble-cobble gravel with scattered boulders; sandy, silty matrix. Bedding surfaces shown are poorly defined and discontinuous, may be scour surfaces
Q2c	Gravel, angular, poorly sorted, nonbedded
Tv	Tertiary volcanic rocks--welded tuff, also exposed in trench floor

269029

71800

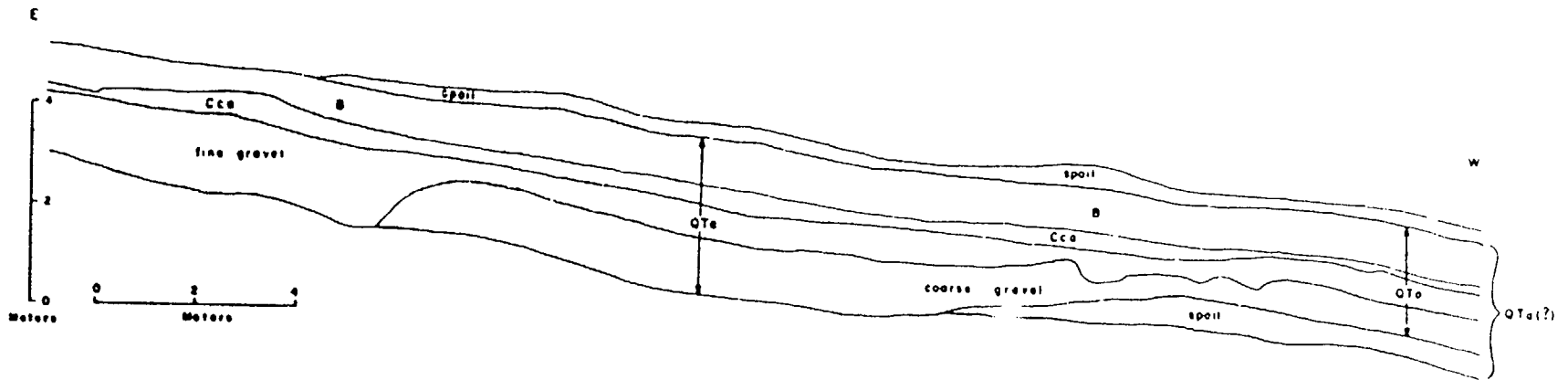


Figure A6.--Diagram of south wall of trench 10A. Trench trends N. 80° E. across a projection of the Solitario Canyon fault zone. Mapped in April 1983 by Swadley and H. E. Huckins.

<u>Unit</u>	<u>Description</u>
QTa(?)	Gravel--consists of a coarse cobble to boulder unit that is unsorted and nonbedded overlain by a sandy, angular pebble to cobble gravel that is poorly sorted and poorly to moderately well bedded. Soil developed in unit consists of B and Cca horizons
B	B horizon--cambic, light-brown; 0.2-0.3 m thick; may include younger slope wash unit at top
Cca	Cca horizon--developed in poorly sorted sandy gravel, stage I! to III carbonate development

0593
71917

30

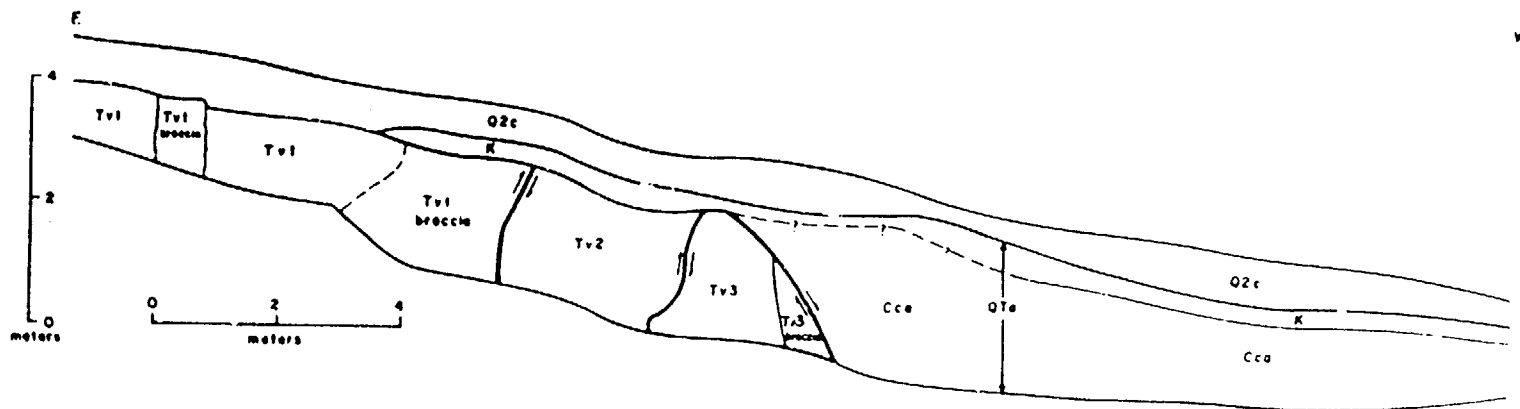


Figure A7.--Diagram of south wall of trench 10B, Solitario Canyon fault zone. Trench trends N. 80° W. Mapped in April 1983 by Swadley and H. E. Huckins. Fault at west edge of fault zone offsets QTa against Tertiary volcanic rocks. K horizon, developed in faulted QTa, and the overlying Q2c extend across the fault without offset.

<u>Unit</u>	<u>Description</u>
Q2c	Gravel, angular, poorly sorted, sandy matrix. Soil (not mapped separately) consists of light-brown cambic B horizon and a stage II Cca horizon
QTa	Gravel, coarse, poorly sorted, sandy matrix; cemented with stage III to IV carbonate development.
K	K horizon--gravel, angular, sandy matrix; cemented with stage III to IV carbonate development
Cca	CCa horizon--gravel, angular, poorly sorted; sandy, tuffaceous matrix; stage II carbonate development
Tv1	Tuff, welded, purplish-brown
Tv2	Vitrophyre, black
Tv3	Tuff, slightly welded, light-brown

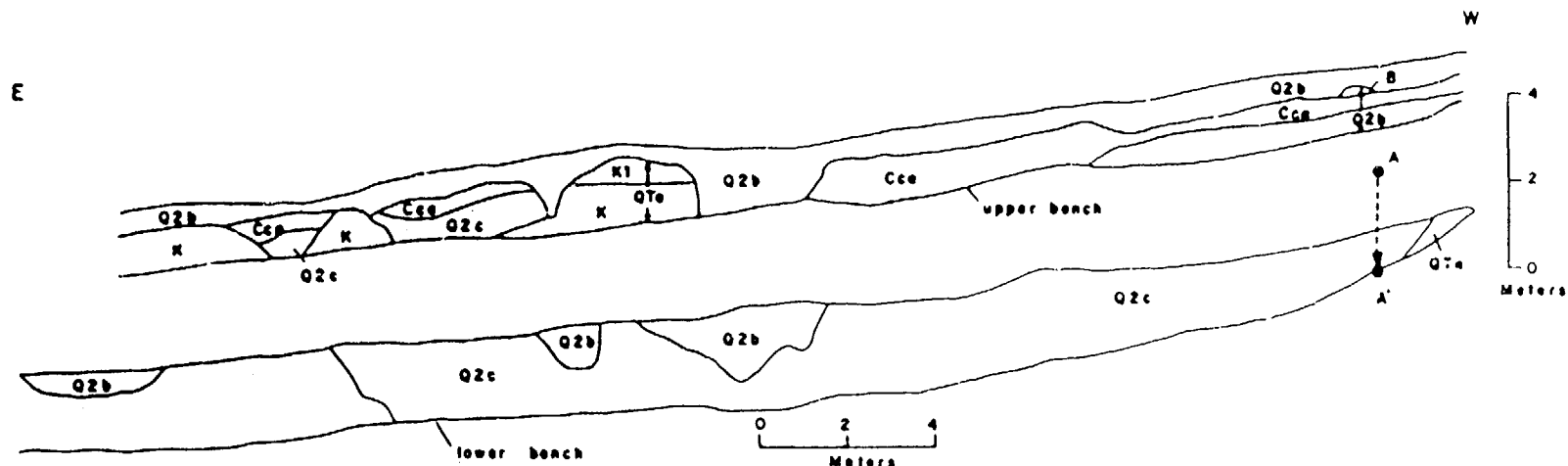


Figure A8.--Diagram of south wall of trench 11. Trench trends N. 75° E. across projection of fault D. Mapped in June 1982 by Swadley and H. E. Huckins. Trench cut on two levels, upper bench is 2-3 m wide. For clarity, lower level of cut has been displaced from A to A' in this figure.

<u>Unit</u>	<u>Description</u>
Q2b	Gravelly sand, gravel is mostly angular pebbles with scattered cobbles. Soil horizons (not mapped) consist of yellowish-brown cambic B horizon and thin stage I Cca horizon
Q2c	Gravel, angular, poorly sorted, non-bedded, sandy matrix; includes pebble- to boulder-size clasts. Soil horizons developed in Q2c consist of B and Cca horizons
B	B horizon--yellowish-brown, cambic; developed in sandy, poorly sorted gravel
Cca	Cca Cca horizon--stage I to II carbonate development in poorly sorted gravel
QTa	Gravel, angular, unsorted, nonbedded Soil developed in unit consists of K and Cca horizons
K	K horizon--stage III to IV carbonate development in unsorted gravel
K1	Laminated part of K horizon
Cca	CCa horizon--stage II carbonate development in unsorted gravel

0594
31
717

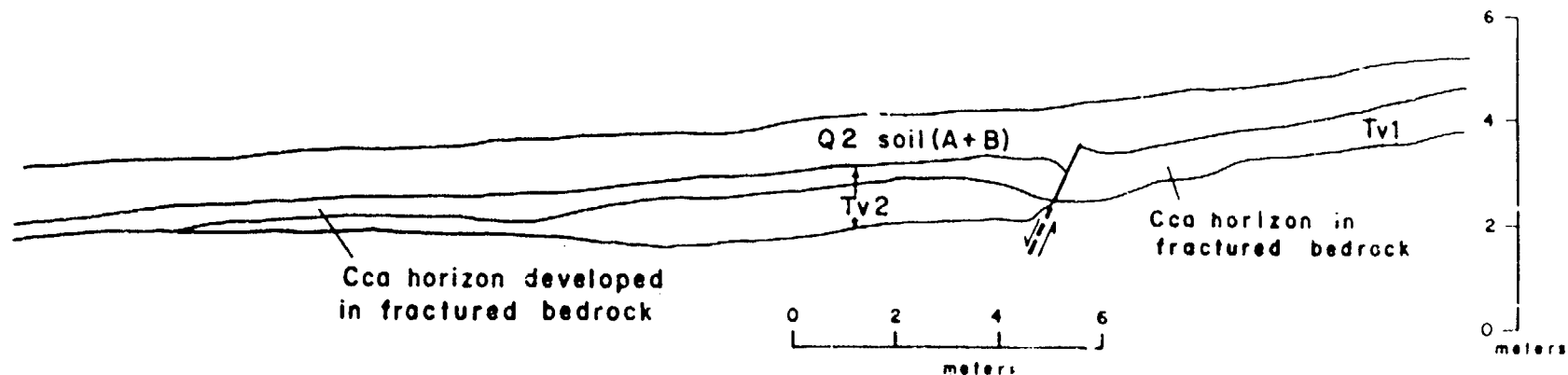


Figure A9.--Diagram of northwest wall of trench 12. Trench trends N. 45° E. across trace of fault E. Mapped in June 1982 by Swadley and H. E. Huckins.

<u>Unit</u>	<u>Description</u>
Q2 Soil	Soil developed across existing fault in bedrock, probably in eolian and slope wash deposits. No offset is apparent in soil. Soil development consists of thin A horizon and light-brown cambic B horizon (not mapped)
Tv1	Grayish-red welded tuff. Where exposed above trench floor includes common to abundant carbonate as coatings and fracture fillings.
Tv2	Dark-gray, platy-weathering welded tuff. Upper part of exposure in trench wall includes common to abundant carbonate as coatings and fracture fillings

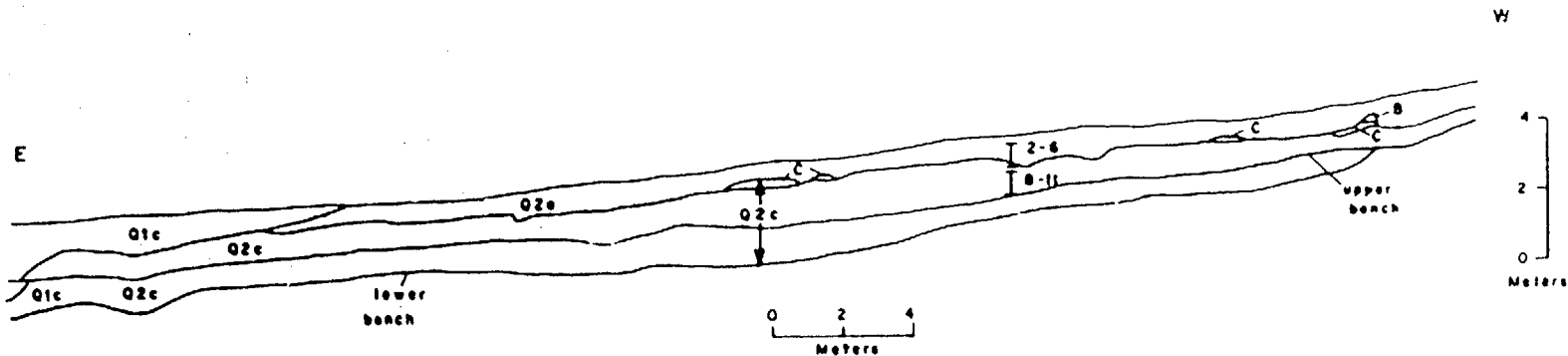


Figure A10.--Diagram of south wall of trench 13. Trench trends N. 50° E. across projection of fault H. Cut on two levels, upper bench is 1-1.5 m wide. Mapped in June 1982 by Swadley and H. E. Huckins. Sample locations for uranium-trend age determinations shown by bar

<u>Unit</u>	<u>Description</u>
Q1c	Gravel and sand, unconsolidated, poorly sorted non bedded
Q2b	Gravelly sand, poorly sorted; gravel chiefly pebbles with few cobbles. Soil development consists of yellowish-brown cambic B horizon and thin stage I Cca horizon (not mapped)
Q2c	Gravel, angular, poorly sorted, poorly bedded; sandy matrix; well consolidated. Exposed soil development in unit consists of B and Cca horizons
B	B horizon--light-brown, cambic. Single small remnant exposed
Cca	Cca horizon--poorly sorted sandy gravel with stage II carbonate development

<u>Sample No.</u>	<u>Radiometric Ages</u>	
	<u>Unit</u>	<u>Age (in 10³ yr)</u>
YM13-2 thru 6	Q2a	41±10
YM13-8 thru 11	Q2c	240±50

9650
 33
 7100

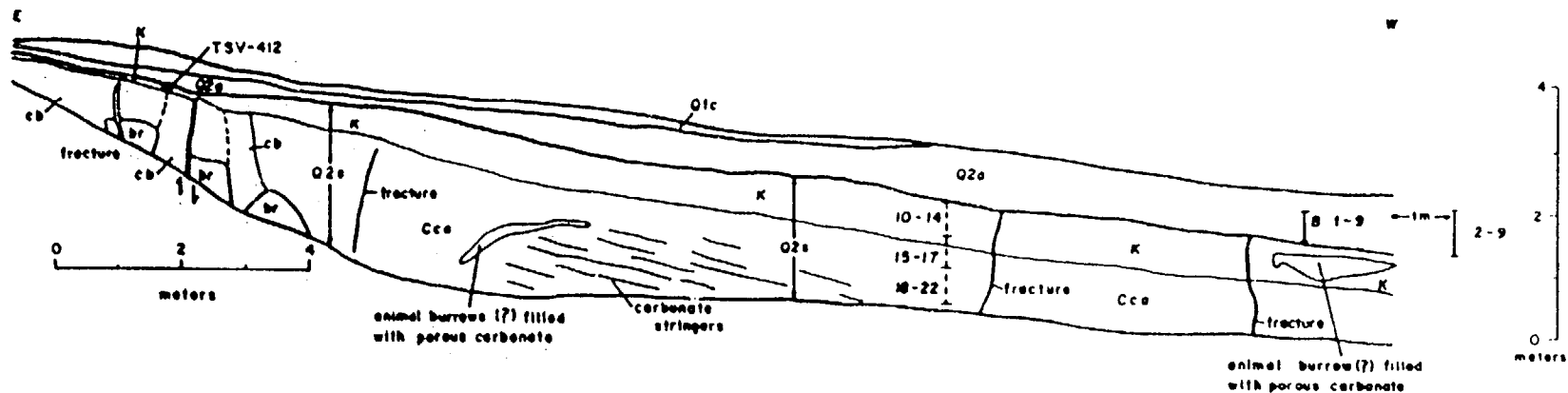


Figure A11.--Diagram of south wall of trench 14. Trench trends east-west across the trace at fault C. Mapped in May 1982 by Swadley, L. D. Parrish, and H. E. Huckins. Fault offsets blocks of Tertiary volcanic rocks. Fractures cut Q2s and its soil but not the overlying Q2a. The K horizon that developed in Q2s extends across the fault without offset but is fractured (fractures too small to show on this figure) and fracture surfaces are coated with secondary carbonate immediately above fault. Animal burrow 5 m west of the main fault may have been dug along a fracture in Q2s. Sample locations for uranium-trend age determinations shown by bar; bar is dashed where location is projected from north wall. Sample location for uranium-series age determinations (sample TSV-4.2) shown by cross.

Unit	Description
Q1c	Sand, gravelly, unconsolidated
Q2a	Sand, gravelly, slightly indurated with clay
Q2s	Sand, gravelly. Exposed soil horizons developed in unit consist of K and Cca horizons
K	K horizon--sand, gravelly, stage III to IV carbonate development
Cca	Cca horizon--sand, gravelly, stage I to II carbonate development; carbonate stringers along bedding(?) surfaces
cb	Colluvium and breccia with abundant laminar opaline carbonate Laminae parallel fractures, soil horizons, and surfaces of large blocks in underlying breccia
br	Breccia and blocks of Tertiary volcanic rocks

Radiometric Ages

Sample No.	Unit	Age (in 10^3 yr)
YM 14-2 thru 9	Q2a	90±50
YM 14-10 thru 14	Q2s	270±90
YM 14-15 thru 17	Q2s	420±50
YM 14-18 thru 22	Q2s	480±90
YM 14 B-1 thru 9	Q2a	38±10
TSV-412-1	Q2s K horizon	>400 and >350
TSV-412-3	Q2s K horizon	>550
TSV-412-7	Q2s K horizon	>400

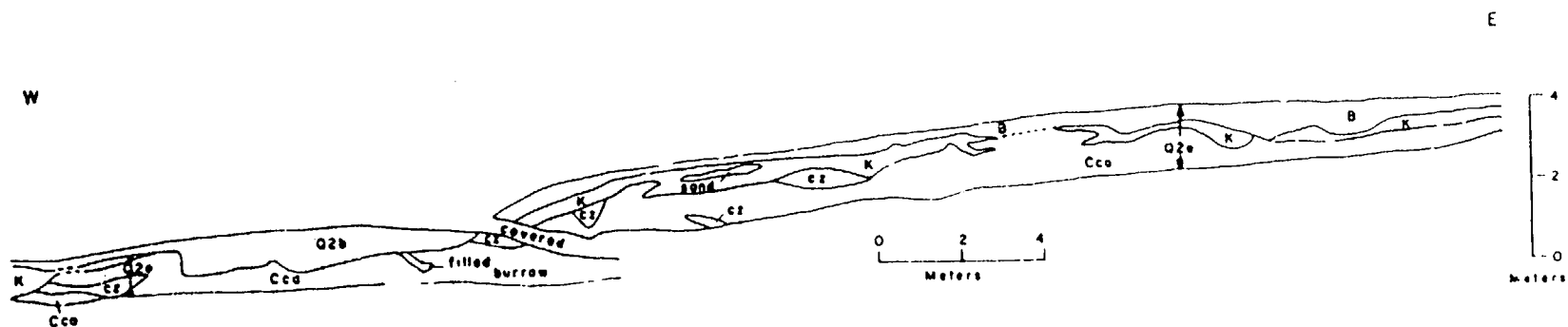


Figure A12.--Diagram of north wall of trench 16. Trench trends N. 75° W. cross a projection of the Paintbrush Canyon fault. Mapped in June 1982 by Swadley and H. E. Huckins.

<u>Unit</u>	<u>Description</u>
Q2b	Sand, poorly bedded, moderately well sorted; locally cemented with carbonate at base. Unit channels into underlying Q2e
Q2e	Eolian sand, fine, well sorted, nonbedded. Soil development consists of B, K, and Cca horizons
B	B horizon--light-brown, cambic, developed in well sorted fine sand
K	K horizon--stage III carbonate development in well sorted sand. Horizon is discontinuous, probably disrupted by burrows
Cca	Cca horizon--well sorted sand with stage I to II carbonate development. Root casts common to abundant. Includes local zones of carbonate enrichment (cz) that may be nonpedogenic

9 0 8 1 7 36

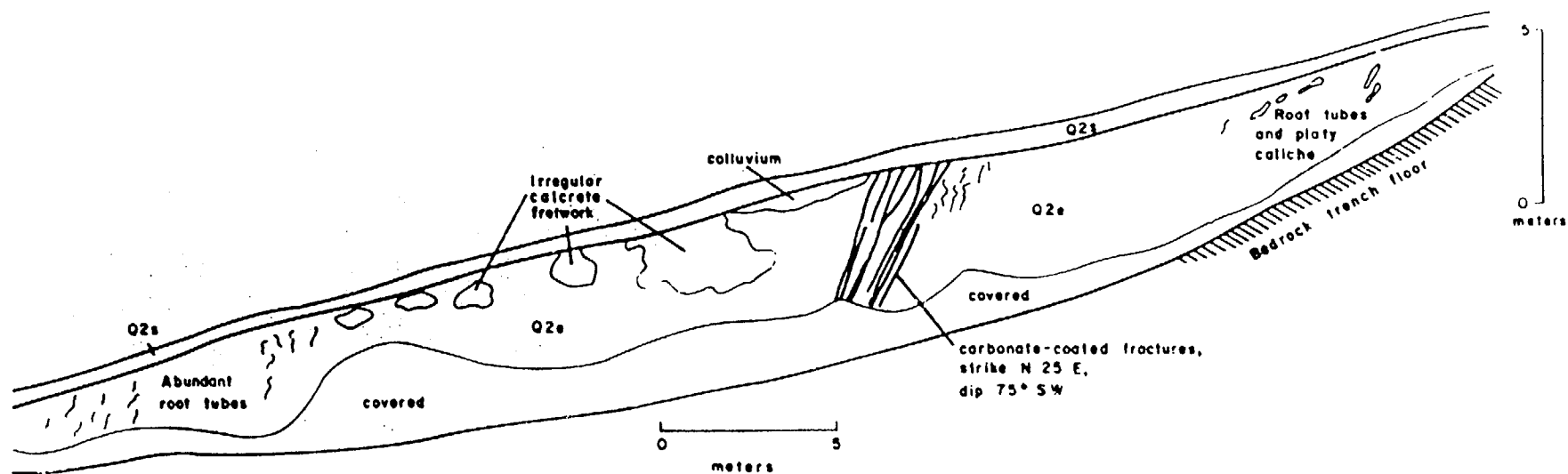


Figure A13.--Diagram of north wall of trench 16B, located near the southern end of the Paintbrush Canyon fault. Mapped in February 1983 by W. J. Carr (USGS). Fractures cut unit Q2e but not overlying Q2s.

<u>Unit</u>	<u>Description</u>
Q2s	Sand, light-grayish-brown, and angular gravel. Probably a mixture of slope wash and colluvium
Q2e	Sand, eolian, well sorted, nonbedded; includes scattered clasts and lenses of colluvial gravel; root tubes and secondary carbonate deposits common. Q2e soil not preserved

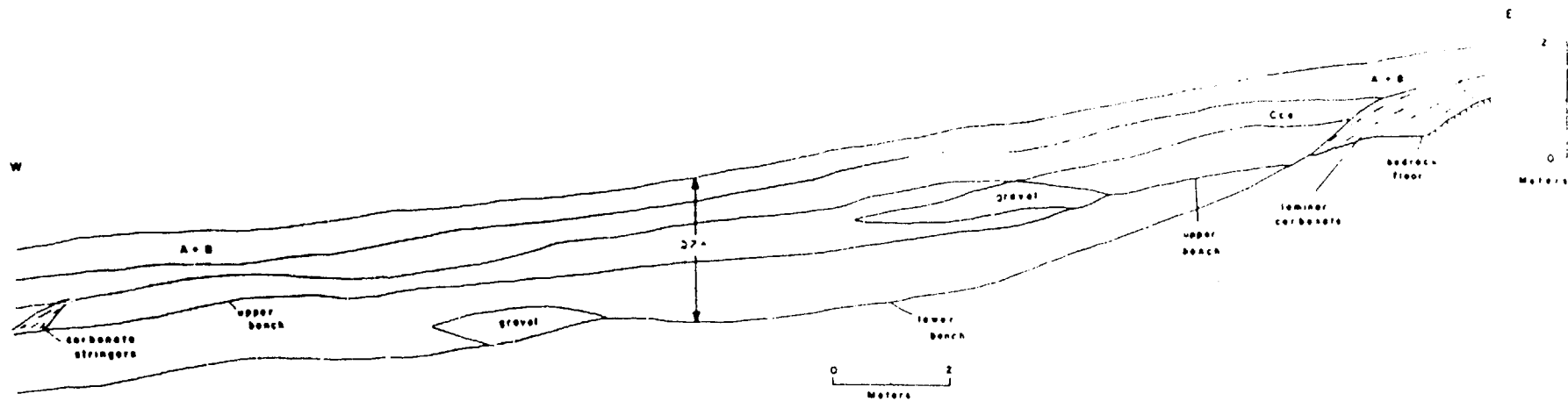


Figure A14.--Diagram of north wall of trench 17. Trench trends N. 55° W. & cross a projection of a branch of Paintbrush Canyon fault. Cut on two levels, upper bench is 1-2 m wide. Mapped in July 1983 by Swadley and L. D. Parrish.

<u>Unit</u>	<u>Description</u>
Q2e	Eolian sand, moderately well to well sorted, poorly consolidated, nonbedded; includes scattered clasts and lenses of colluvial gravel. Root casts locally common. Soil developed in unit consists of A, B, and Cca horizons
A+B	A and B horizons, undivided. A horizon is light-gray silt and clay; vesicular, preserved locally. B horizon is light brown, cambic
Cca	Cca horizon--stage II carbonate development in fine well-sorted sand

10701

88

10817

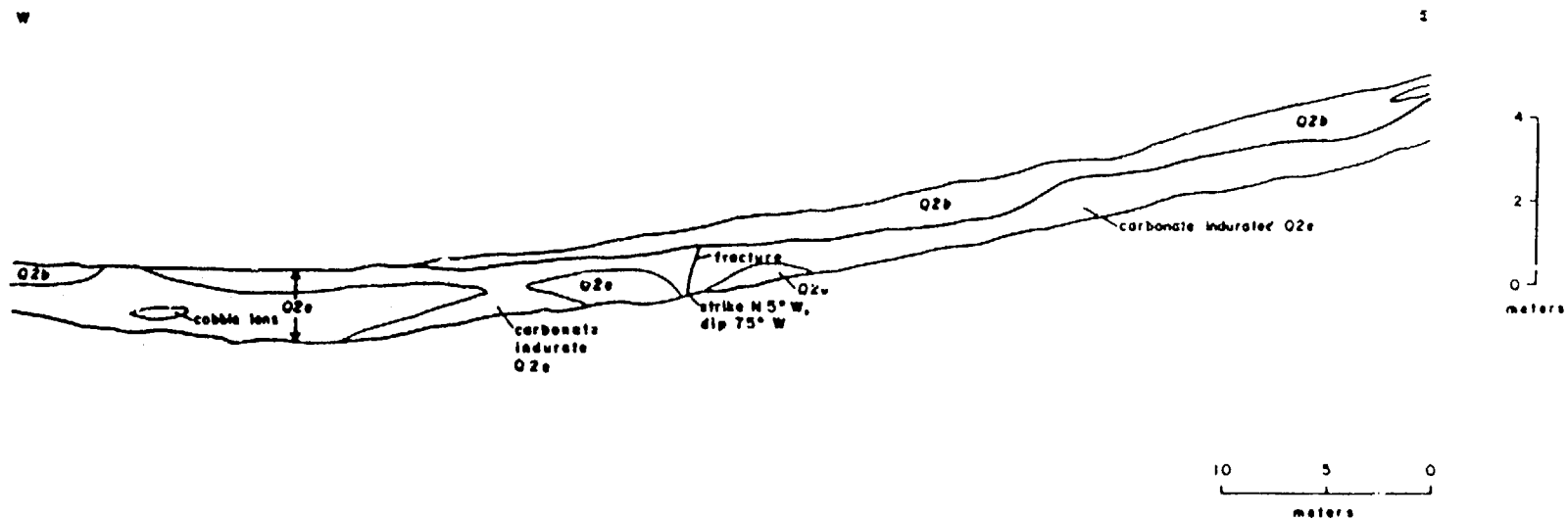


Figure A15.--Diagram of north wall of trench A1, Paintbrush fault. Trench trends east-west. Mapped in 1979 by A. J. Gordon (F&S) and L. D. Parrish (F&S). Fractures cut unit Q2e and its soil but not the overlying Q2b.

<u>Unit</u>	<u>Description</u>
Q2b	Gravelly sand, probably a mixture of colluvium and slope wash. Soil horizons (not mapped) consist of light-brown cambic B horizon and stage II Cca horizon
Q2e	Eolian sand, well sorted locally includes pebbles and cobbles (colluvium). Root casts common. Sand is commonly moderately indurated with patchy areas of nonpedogenic carbonate (shown by stipple pattern). Soil development consists of thin stage III K horizon (not mapped)

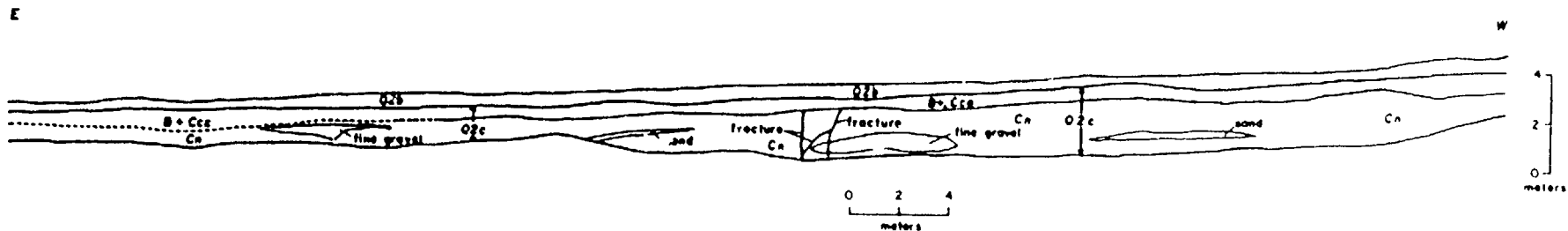


Figure A16.--Diagram of south wall of trench A2, Paintbrush Canyon fault. Trench trends N. 85° E. Mapped in July 1983 by Swadley and L. D. Parrish. Fractures cut unit Q2c but not its soil or the overlying Q2b.

<u>Unit</u>	<u>Description</u>
Q2b	Sandy gravel, probably a mixture of slope wash and colluvium Soil (not mapped) consists of a weak cambic B horizon and a stage I Cca horizon
Q2c	Gravel, sandy, poorly sorted, poorly bedded
B+Cca	B and Cca soil horizons undivided: B horizon is light brown, cambic; developed in sandy gravel; Cca horizon, stage II carbonate development in sandy gravel
Cn	Gravel, very sandy, poorly sorted, poorly bedded; coarse, with scattered boulders; well indurated; includes lenses of sand and fine gravel

7
 3
 1
 7

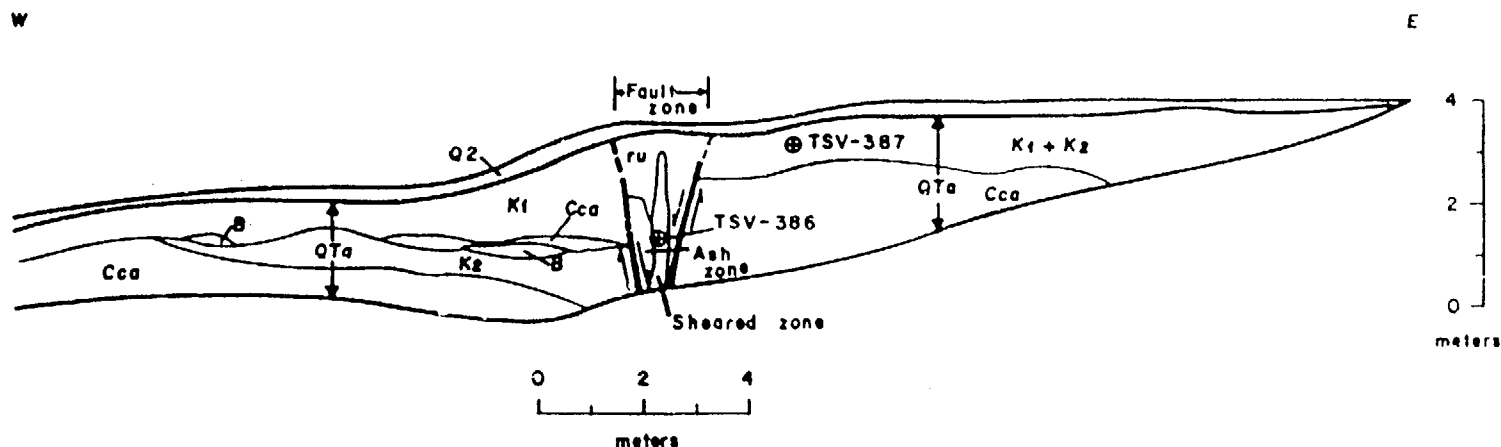


Figure A17.--Diagram of north wall of trench CF1, excavated across fault M. Trench trends east-west. Diagram modified from Swadley and Hoover (1983). Faults cut QTa and offset a pre-fault soil horizon (K2) down to the west. A post-fault soil horizon (K1) appears to overlie the fault without offset; however, the abundance of post-fault carbonate deposits in the fault zone partly obscures this horizon. Sample localities for TSV-386 and TSV-387 (table 2) are projected from the south wall of trench.

<u>Unit</u>	<u>Description</u>
Q2	Gravel, sandy, unsorted. Soil development consists of a clayey silt vesicular A horizon and a light-brown cambic B horizon (not mapped)
QTa	Gravel, coarse, angular, unsorted. Soil development in QTa includes four soil horizons described below
K1	K horizon--unsorted gravel, cemented with stage III to IV carbonate development; represents post-fault soil development. Anomalously thick K1 horizon shown west of fault zone is probably caused by nonpedogenic carbonate deposited in permeable material adjacent to the fault
Cca	Gravel, unsorted stage I carbonate development
B	B horizon--argillic, reddish-brown sand and gravel; remnant of pre-fault soil
K2	K horizon--gravel, unsorted; cemented with stage III to IV carbonate development. Represents pre-fault K horizon preserved in downthrown block; in upthrown block it merges upward with post-fault K1
Ash zone	Gravel containing stringers and pods of 1.2 m.y.-old basaltic ash
ru	Rubble and disturbed QTa gravel cemented with nonpedogenic(?) carbonate. Soil zones not recognized in fault zone because of abundant carbonate cement

3070 4130

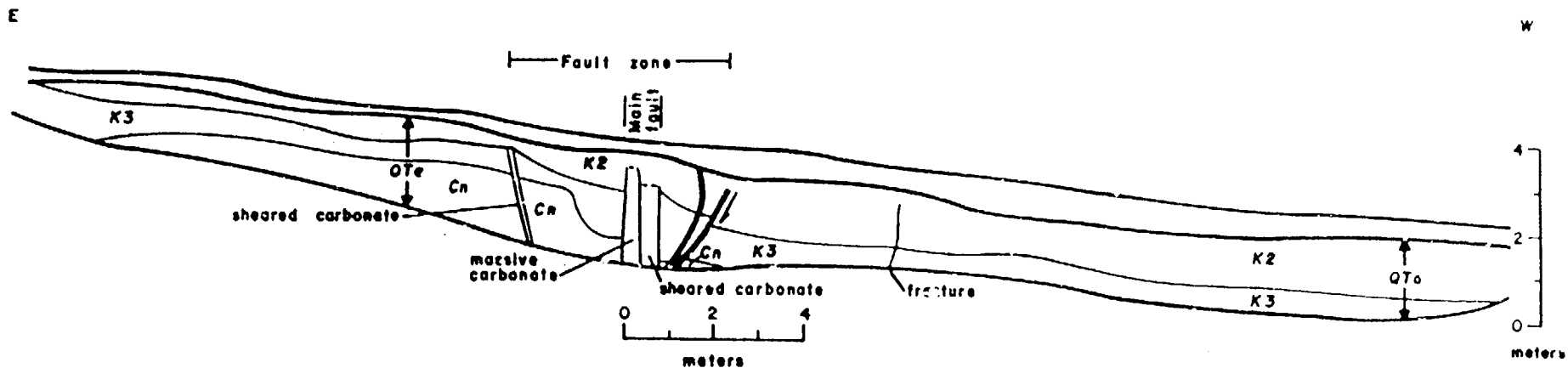


Figure A18.--Diagram of south wall of trench CF2, located across fault Q. Trench trends N. 88° W. Diagram modified from Swadley and Hoover (1983). Four faults cut QTa but not the overlying Q2. The main fault and two minor faults do not extend through the K2 horizon indicating some soil development after faulting. One fault does cut the K2 horizon which suggests a later episode of faulting. The apparent displacement of the lower contact of the K horizons may be due to post-fault deposition of carbonate in permeable zones near the faults.

<u>Unit</u>	<u>Description</u>
Q2	Sandy gravel; soil development consists of light-gray vesicular silt and clay A horizon 5-20 cm thick; and a pale-yellowish-brown to pale-brown cambic B horizon developed in sandy gravel; 5-70 cm thick (not mapped)
QTa	Gravel, coarse, nonbedded, poorly sorted. Soil horizons mapped separately
K2	Gravel, well cemented with massive to laminated stage IV carbonate; 0-1.5 m thick
K3	Gravel, moderately cemented with stage III carbonate; 0.5-1.5 m thick
Cn	Gravel, coarse, poorly sorted, nonbedded

41 21866
 71866
 41 21866

42

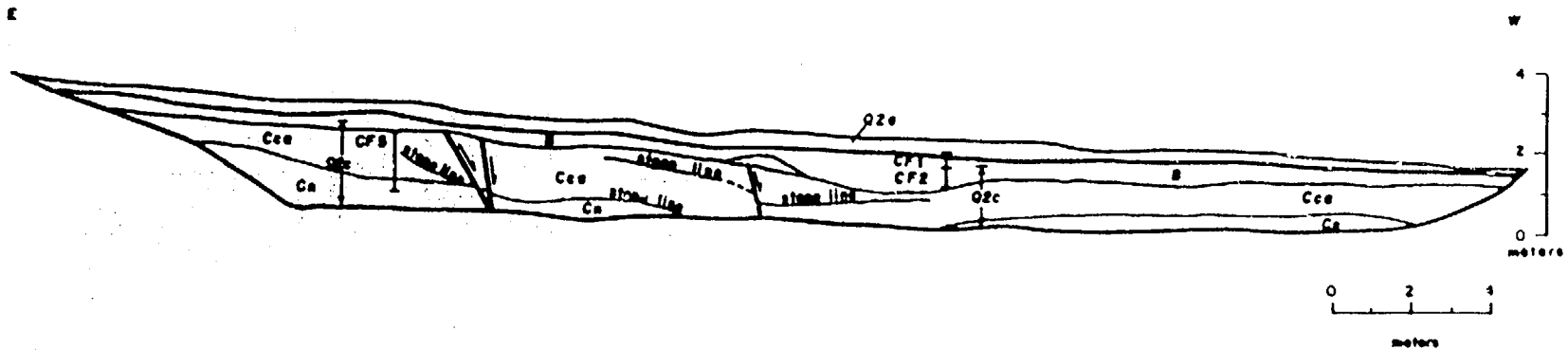


Figure A19.--Diagram of south wall of trench CF3. Trench trends N. 83° W. across fault Q. Diagram modified from Swadley and Hoover (1983). Three faults cut unit Q2c and its soil but not the overlying Q2a. Sample locations for uranium-trend age determinations shown by vertical bar.

<u>Unit</u>	<u>Description</u>
Q2a	Sand, silty, some gravel. Probably largely slope wash deposits
Q2c	Gravel, sandy, poorly sorted. Soil development consists of B, Cca, and Cn horizons
B	B horizon--cambic, light-brown, developed in sandy gravel. As mapped, upper part of unit includes the B horizon of the overlying Q2a (20-45 cm thick). Where B is thick, west of main fault, it probably includes some colluvial sand
Cca	Cca horizon--gravel, sandy, stage II carbonate development
Cn	Gravel, sandy, poorly sorted, fairly well bedded

Uranium-trend Age Determination

<u>Sample No.</u>	<u>Unit</u>	<u>Age (in 10³ yr)</u>
CF1	Q2a	40±10
CF2	Q2c	270±20
CF5	Q2c	260±140



**The Geology of North America
Volume K-2**

QE
D1
G48
1986
v. K-2

***Quaternary Nonglacial Geology:
Conterminous U.S.***

Edited by
Roger B. Morrison
Morrison and Associates
13150 West Ninth Avenue
Golden, Colorado 80401

#24009806



1991

UNIVERSITY OF NEVADA, LAS VEGAS
LIBRARY

Chapter 3

Dating methods applicable to the Quaternary

John N. Rosholt*

U.S. Geological Survey, MS 963, Box 25046, Denver Federal Center, Denver, Colorado 80225

Steven M. Colman

U.S. Geological Survey, Woods Hole, Massachusetts 02543

Minze Stuiver

Department of Geological Sciences and Quaternary Research Center, University of Washington, Seattle, Washington 98195

Paul E. Damon

Department of Geosciences, University of Arizona, Tucson, Arizona 85721

Charles W. Naeser, Nancy D. Naeser, Barney J. Szabo, and Daniel R. Muhs

U.S. Geological Survey, MS 424, Box 25046, Denver Federal Center, Denver, Colorado 80225

Joseph C. Liddicoat

University of California, Santa Cruz, California 95064

Steven L. Forman

Institute of Arctic and Alpine Research and Department of Geological Sciences, University of Colorado, Boulder, Colorado 80309

Michael N. Machette and Kenneth L. Pierce

U.S. Geological Survey, MS 913, Box 25046, Denver Federal Center, Denver, Colorado 80225

SUMMARY OF QUATERNARY DATING METHODS

Steven M. Colman and Kenneth L. Pierce

INTRODUCTION AND COMPILATION OF QUATERNARY DATING METHODS

A wide variety of dating methods are used in Quaternary research, and each method has many applications and limitations. Because of this variety, we cannot discuss the applications and limitations of all methods here. The more versatile and widely used methods, including ^{14}C , K/Ar, fission-track, U-series, paleomagnetism, thermoluminescence, and amino acid dating are treated more comprehensively in this chapter than other methods that are shown on the summary chart. The summary chart is provided here to give an overview of dating work and research for the Quaternary.

This summary consists mainly of a table (Plate 2) that is modified and updated from Colman and Pierce (1977, Plate 1, ref. 66). The table is intended as an overview and concise guide to Quaternary dating methods. It contains many subjective judg-

ments and should not be considered definitive; the entries for applicability, age range, and optimum resolution are particularly interpretive. Details concerning assumptions, analytical techniques, uncertainties, and interpretations should be obtained from specialized references using the key references in Plate 2 as a guide. The dating methods described range from well-known and established techniques to experimental procedures whose results are subject to considerable interpretation.

Key references included on Plate 2 are intended as an entry into the vast literature on dating methods; space prohibits a more complete listing. We have emphasized recent review papers and notable examples of applications as sources of additional references and information. Dating methods discussed in other sections of this chapter are indicated by asterisks in the summary table. The first five references are reviews or edited volumes that discuss Quaternary dating methods in general; references 6-11 are edited volumes that focus on individual methods or closely related methods. In the interest of brevity and clarity, we have not cited individual papers in these edited volumes. Some dating methods are based on fundamental geological principles, such as stratigraphy, for which references are deemed unnecessary here.

For the purpose of our discussion and summary table, it is useful to classify dating methods, which can be done in a variety of ways. Perhaps the simplest classification is one that groups methods that share similar assumptions, procedures, or applica-

*Deceased.

Rosholt, J. N., Colman, S. M., Stuiver, M., Damon, P. E., Naeser, C. W., Naeser, N. D., Szabo, B. J., Muhs, D. R., Liddicoat, J. C., Forman, S. L., Machette, M. N., and Pierce, K. L., 1991. Dating methods applicable to the Quaternary, in Morrison, R. B., ed., Quaternary nonglacial geology: Conterminous U.S.: Boulder, Colorado, Geological Society of America, The Geology of North America, v. K-2.

TABLE 1. CLASSIFICATION OF QUATERNARY DATING METHODS*

----- Numerical-age -----					
..... Calibrated Age -----					
..... Relative-age -----					
----- Correlated-age -----					
Sidereal	Isotopic	Radiogenic	Chemical and Biochemical	Geomorphic	Correlation
Historical records	¹⁴ C	Uranium-trend	Amino acid racemization	Soil profile development	Stratigraphy
Dendrochronology	K-Ar and ³⁹ Ar- ⁴⁰ Ar	Thermoluminescence	Obsidian hydration	Rock and mineral weathering	Tephrochronology
Varve Chronology	Uranium-series†	Electron-spin resonance†	Tephra hydration	Rock varnish	Paleomagnetism
	Fission track	²¹⁰ Pb	Lichenometry	Progressive land-form modification	Fossils and artifacts
		Other cosmogenic isotopes	Soil chemistry	Rate of deposition	Stable isotopes
				Rate of deformation	Astronomical correlation
				Geomorphic position	Tectites and microtectites

*Dashed line indicates the type of result most commonly produced by the methods below it; dotted line indicates the type of result less commonly produced by the methods below it.

†Methods above this line routinely produce numerical ages; methods below the line are more experimental and involve nonradioactive processes or processes whose effects on age estimates are not well established.

tions. Accordingly, we have grouped dating methods into six categories (Plate 2; Table 1, lower part of header): sidereal (annual), isotopic, radiogenic, chemical and biological, geomorphic, and correlation methods. Dating methods may also be classified by the type of result they produce (Plate 2; Table 1, upper header); numerical-age (quantitative estimate on a ratio scale), calibrated-rate (numerical-age based on the rate of a process rate that has been calibrated by another dating method), relative-age (chronologic order, in some cases including some measure of magnitudes of age differences), and correlated-age (correlated to independently dated deposits or to standard stratigraphic sections).

RADIOCARBON DATING

Minze Stuiver

INTRODUCTION

An early interest in radiocarbon dating of geological samples was expressed by Richard Foster Flint when attending a lecture given by W. F. Libby at the 1948 Viking Fund Supper Conference in New York. At the conclusion of Libby's remarks, the audience remained mute until Flint commented, "Well, if you people are not interested in this, I am. . . . If you don't want anything dated, I am for it, and would like to send some material"

(quote from Taylor [1987] which also contains other relevant references). The relatively large sample size (one pound of carbon) needed at that time may explain the reluctance of the archeologists present at the meeting to commit themselves to the combustion of precious museum materials. The 40 years of progress in radiocarbon dating technology is best illustrated by comparing the above required sample size to the 0.05-mg C sample (Nelson and others, 1986) recently used for a radiocarbon age determination by accelerator mass spectrometry.

During the last decade, two major improvements were made. A major breakthrough has been the above-mentioned direct detection of ¹⁴C in mg samples through accelerator mass spectrometry. In addition, the conventional decay counting technique can now deliver an enhanced level of exactness (Stuiver, 1978) that has resulted in a high precision radiocarbon age terminology. It is especially the latter improvement that is important for radiocarbon timescale calibration.

The cosmic ray-produced ¹⁴C isotope is used for a wide array of scientific investigations. The technique is used in many disciplines, and requires of the radiocarbon "expert" a truly interdisciplinary mode of thinking. Applications can be found in cosmic ray and solar physics (paleochanges in cosmic ray flux and solar surface conditions [Stuiver and Quay, 1980]), oceanography (the mixing and circulation of water masses [Stuiver and

others, 1983b)), climatology (long-term changes in carbon reservoir properties related to the Holocene-Wisconsin climate change [Andree and others, 1986b]), environmental chemistry (fossil fuel dilution of atmospheric ^{14}C [Stuiver and Quay, 1981] and particulate carbon and methane in the atmosphere [Currie and others, 1983; Levin, 1985]), glaciology (ice core stratigraphy [Andree and others, 1986a]), archeology (chronometry), geology (geochronometry as, for instance applied to earthquake frequency research [Sieh, 1984]), hydrology (groundwater dating [Mook, 1980]), and geophysics (earth geomagnetic field change deduced from long-term atmospheric ^{14}C change [Sternberg and Damon, 1983]).

The majority of geological applications is directed toward the determination of time. Because ^{14}C disappears fairly rapidly from the geological scene through radioactive decay, the applicable timespan is relatively short. With a half life of 5,570 yr, the amount of ^{14}C in a sample is reduced by a factor 2 every 5,570 yr. For 10 half lives, or 55,700 yr, the reduction is a factor $2^{10} = 1024$. For the maximum ages of about 75,000 yr determined so far, the amount of ^{14}C in a sample is only 1/10,000 of its original level. Clearly the timespan limitations of the radiocarbon method result from the obvious statistical truth that measurement error becomes infinitely large when the activity to be measured approaches zero.

As with all measuring devices, there are technical factors that limit the precision and accuracy with which an age can be determined. Major limitations are also imposed by the degree to which the basic assumptions of the ^{14}C dating method are correct. Whereas improvement of the technique can still lead to further progress, the limitations imposed by the basic assumptions provide much greater obstacles. For instance, with high-precision dating it is now possible to date a sample with a radiocarbon age error of ± 15 yr. After converting the radiocarbon age to a calendar year age, however, there can occasionally be an uncertainty of centuries in the calibrated age.

A conventional radiocarbon age can be calculated from the measured ^{14}C activity by using the conventional radiocarbon half life (5,568 yr) and by assuming constancy of atmospheric ^{14}C level in the past (Stuiver and Polach, 1977). The calculation also corrects for isotope fractionation by using the ^{13}C isotope as an indicator of possible enrichment or depletion of sample ^{14}C during its formation. The primary function of the laboratory is to measure the remaining ^{14}C activity of the sample and to determine the uncertainty (standard deviation) in the measurement. This information is then converted into a conventional radiocarbon age \pm a standard age error.

CONTAMINATION

Given the age supplied by the laboratory, the user has to decide whether the number given provides relevant information. A major concern will be adherence to another assumption: The remaining sample ^{14}C should be representative of its original activity, which implies a closed system with respect to carbon

exchange with its environment. In other words, samples should not receive, between the moment of formation and the moment of sampling, an admixture of carbonaceous material having a specific ^{14}C content different from that of the original sample.

The user can reduce the influence of contamination by selective sampling; for instance, collect samples far below the surface where root contamination is usually less. Remaining rootlets should be removed before drying the sample. Part of the laboratory procedure is oriented toward reducing the influence of contaminants. Organic materials are acidified to remove carbonates, and an alkali treatment is given to appropriate samples for the removal of humic materials.

In addition to the above in situ contamination, foreign materials can also be introduced during sampling and transport, or during storage and handling of the sample in the laboratory. These additions can usually be entirely avoided by following proper procedures. However, for in situ contamination, the best possible procedures, although minimizing the effects, do not necessarily remove all contaminants.

The influence of specific levels of modern contamination is largest for the older samples. As mentioned, a sample in the mid-50,000-yr range contains only 1/1,000 of its original activity. The addition of a similar minute amount of modern contamination will double its ^{14}C content, and reduce the sample age by one half life or 5,570 yr. For the 75,000-yr sample, contamination levels of only one part in 10,000 will have a similar impact. This should be a warning against attaching too much significance to very old dates. But even the forewarned user should realize that the existence of samples with 75,000-yr-old radiocarbon ages implies an upper limit of ^{14}C contamination of 1 part in 10,000. Thus it must be possible to collect "similar" samples (samples containing less than 1 part in 10,000 ^{14}C contamination) in the 50,000 to 60,000 yr range. These samples would then yield reliable ages because the low level of ^{14}C contamination would be negligible.

Contamination with older materials (e.g., graphite) is usually of lesser import than contamination with younger materials because the relative change in ^{14}C activity induced by the contaminants is often greater for the younger additions. For instance, a 10-mg-C-old (lacking ^{14}C) addition to a 1-g-C sample reduces the sample ^{14}C activity by 1 percent for all samples of any age. This one percent ^{14}C dilution results in an 80-yr-older radiocarbon age, because ^{14}C decays with a constant rate of approximately 1 percent per 80 yr. A 10-mg addition of younger material to a large sample also has relatively little influence when the sample is very young (after all, adding material of the same age would not change the age of the contaminated sample), but usually has drastic consequences for the age of an old sample. For instance, a 37,000-yr-old sample retains about 1 percent of its original ^{14}C activity. Doubling this activity by adding to a 1-g C sample another 10 mg C of modern material (defined as material of zero age or 100 percent ^{14}C activity) reduces the age of the contaminated material to 31,400 yr.

A detailed discussion of the contamination-induced change

in radiocarbon ages is given by Grootes (1983) and Bradley (1985).

Given the amount and activity of the contamination, the "new" radiocarbon age can be very precisely calculated. In actual practice, however, the influence of contamination can often only be evaluated in general terms such as, "the charcoal sample was very well preserved and a visual inspection indicated an absence of rootlets;" therefore, the chances of retaining contaminants after pretreatment are small.

The nonhomogenous dispersal of contaminating material has become important now that mg C samples are measured. For instance, consider a lake core with 5 percent graphite contamination. Combustion of a large sample would produce an age 400 yr too old. But a mg C sample selected randomly could well be a graphite particle and result in an infinite age. However, here the small-sample approach can also be used to eliminate the influence of graphite (or coal) contamination by selecting macrofossils (e.g., leaves) that were originally in ^{14}C equilibrium with the atmosphere.

RESERVOIR EFFECTS

A radiocarbon age is calculated with the aid of an equation in which the ratio of the measured sample ^{14}C activity to presumed initial ^{14}C activity is the important parameter. The initial activity used in the equation is that measured for the laboratory oxalic acid standard. The oxalic acid ^{14}C has been calibrated against the ^{14}C activity of a 19-century wood sample. Thus the initial activity used for the calculation of a conventional radiocarbon age is tied to atmospheric ^{14}C activity because, after correction for isotope fractionation, the wood reflects atmospheric ^{14}C level.

The ^{14}C content of nonatmospheric carbon reservoirs (e.g., oceans or lakes) may differ from the atmospheric value. Thus, a so-called reservoir correction has to be applied to account for the age differences between reservoirs. As these reservoirs usually have a lower specific ^{14}C activity (activity per gram C) than that of atmospheric carbon dioxide, the conventional radiocarbon ages have to be reduced.

The reservoir correction for the surface mixed layer of the midlatitude ocean is approximately 300 radiocarbon yr. A conventional radiocarbon age would therefore be 300 yr too old for samples properly corrected for isotope fractionation (for details, see Stuiver and Polach, 1977). For oceanic regions where upwelling of older waters reduces surface water ^{14}C activities even more, the reservoir correction is still larger. The largest correction is for Antarctic coastal regions, where shells of the last century may have conventional radiocarbon ages of 1,000 to 1,300 yr (Stuiver and others, 1983a).

The ages of the top of the sediment (or, to be more precise, a few cm below the top to avoid the influence of nuclear bomb ^{14}C) of lake cores reflect the reservoir deficiency of those lakes. These may range from a few hundred years for lakes approaching equi-

librium with the atmosphere to 2,500 yr for lakes with important groundwater bicarbonate contributions (Stuiver, 1975).

A weakness in the above approach is the assumption of a constant past reservoir deficiency. Variable lake levels and bicarbonate concentrations may well cause a variable reservoir deficiency. Here again, accelerator mass spectrometry provides a breakthrough because it is now possible to measure at various depths the age differences between plant macrofossils (in equilibrium with the atmosphere), lake carbonate, and gyttja. The first study of this kind has been made for the sediments of a small closed basin of the Lobsingensee, Switzerland (Andree and others, 1986c).

THE RADIOCARBON AGE ERROR

Most analytical facilities outside the radiocarbon community estimate an error (one standard deviation) in a measurement by assessing the data obtained for repeat analyses of identical samples. The histogram of repeat analyses gives the precision of measurement. Repeat analyses are only made for a limited number of samples because it is not cost effective to make multiple measurements of each sample. Thus the precision obtained for a limited number of analyses is used for an error estimate of all sample measurements.

The error in precision is not the only error in a measurement. A laboratory can be quite reproducible in its repeat measurements, yet be off in accuracy through a systematic deviation from the true value. Systematic errors are usually evaluated through interlaboratory comparisons of results obtained for the same sample.

Contributing to the radiocarbon age error is the statistical uncertainty in a radioactivity measurement. Radioactive disintegration varies randomly about a mean value, and measured count rates of the same sample form a Poisson probability curve. Even the laboratory with the most sophisticated instrumentation cannot escape the realities of Poisson counting statistics. Thus the Poisson error in the count rates, when converted into radiocarbon years, provides a minimum age error.

Unfortunately, the radiocarbon community has traditionally been satisfied with reporting age errors based on counting statistics alone. It is now clear that this was an unwise choice. Interlaboratory comparisons of results obtained for the same samples show substantial underreporting of the radiocarbon age errors (The International Study Group, 1982; Stuiver, 1982). In order to arrive at a realistic estimate of the precision error, as well as possible systematic errors, the recipient of a radiocarbon age should request from the supplier information on interlaboratory comparison and reproducibility measurements.

TIME-SCALE CALIBRATION

As previously mentioned, a radiocarbon age is derived from a comparison of present-day remaining ^{14}C activity to an atmospheric ^{14}C level which is assumed to have been constant during

the past. As atmospheric ^{14}C levels, however, did change, it is evident that a radiocarbon age is only an approximation of the actual age in calendar years. For a conversion of a radiocarbon age to a more realistic calendar date, a calibration curve is needed where radiocarbon ages of wood samples are plotted versus age in calendar years. Such calibration curves are obtained by determining the radiocarbon ages of wood samples dated independently by dendrochronological means.

The construction of a calibration curve from radiocarbon ages with limited precision is not a simple matter. Not only should the standard error in the determination be as small as possible, but the calculation of this error has to be realistic in that it should account for all variability encountered in the laboratory procedures. Proof of accuracy has to come from a comparison of results obtained in two or more laboratories.

High-precision calibration curves covering the last 4,500 yr are now available. The internationally recommended 4,500-yr curve (Stuiver and Kra, 1986) was obtained by combining the data of the Seattle and Belfast radiocarbon laboratories (Stuiver and Pearson, 1986; Pearson and Stuiver, 1986). The comparison of the Seattle and Belfast data demonstrate systematic differences of only a few radiocarbon years and age differences for contemporaneous samples that can be fully explained by the precisions quoted by the Belfast and Seattle laboratory. The above high-precision curve has, on average, a radiocarbon-age error of ± 12 yr (Stuiver and Pearson, 1986) for bi-decadal wood samples.

Additional calibration curves are given in the special 1986 issue of *Radiocarbon* on age calibration. Dendrochronologically dated wood currently available covers nearly the last 10,000 yr, and an extension by a few thousand years is possible using varve chronologies (Stuiver and others, 1986). Detailed age calibration further back in time is not yet possible.

Although the availability of a precise calibration curve reduces the margin of error in calibrated AD/BC dates, a substantial uncertainty remains, because a given radiocarbon age may correspond to several AD/BC dates. A continuous spectrum is even possible when ^{14}C levels in the atmosphere decline at the same rate as ^{14}C declines through radioactive decay. All samples formed during such an interval will have the same radiocarbon content at the end of the interval, and thus yield identical radiocarbon ages. Such a major disaster area for radiocarbon calibration occurs between 420 BC and 750 BC where radiocarbon ages are nearly all in a narrow 2,430 to 2,470-yr-BP band.

The wiggly nature of the calibration curve causes a radiocarbon date to be converted in a range (or ranges) of calibrated (cal) AD/BC (or cal BP where 0 BP equals 1950 AD ages), even if the radiocarbon-age determination could be made without error. Figure 1 is the graphic representation of these ranges encountered when converting ideal (zero error) radiocarbon ages into calibrated ages. The baseline ranges of up to a few decades are due to the uncertainty in the calibration curve, whereas the larger deviations are obtained when the conversion process is influenced by the wiggles. A large vertical Figure 1 spike represents a radiocarbon age that, after conversion, gives a wide range

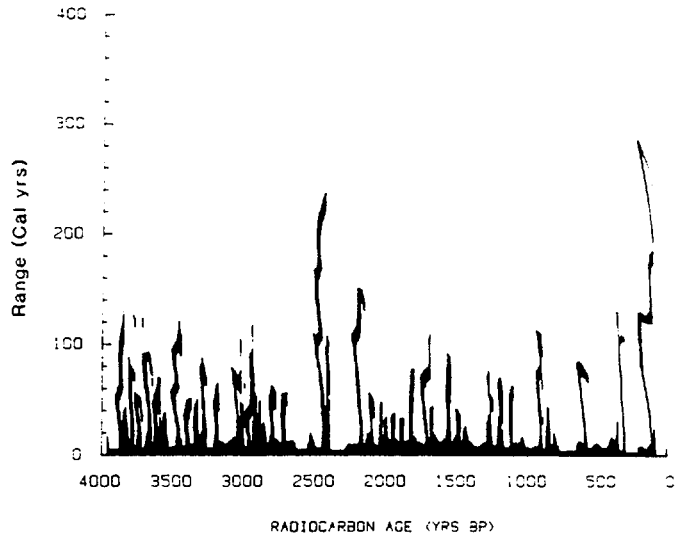


Figure 1. The ranges, in calendar years, obtained from the calibration of radiocarbon ages up to 4,000 yr B.P.

of cal years. Multiple intercepts are responsible for the wiggly nature of the individual cal age uncertainty.

For the above example (zero error in the sample ^{14}C determination), 50 percent of the ages show an age range larger than expected from the uncertainty in the calibration curve alone. This increases to 72 percent for an age determination with an 80-yr error (i.e., the oldest and youngest cal ages derived from a specific radiocarbon age differ by more than 160 yr in 72 percent of the cases). Unfortunately, the benefits of high-precision dating (with radiocarbon-age error circa 15 yr for 6-g C samples) appear to be partly, but not always, negated by the conversion process.

K-AR DATING OF QUATERNARY VOLCANIC ROCKS

Paul E. Damon

INTRODUCTION

There are two basic methods of isotopic dating that make use of the radioactive decay of ^{40}K to ^{40}Ar . These are the conventional K-Ar method and the $^{40}\text{Ar}/^{39}\text{Ar}$ method. In the conventional method, the K content of the sample is usually measured by flame photometry or atomic absorption spectrometry, and the radiogenic ^{40}Ar by mass spectrometric isotope dilution. In the $^{40}\text{Ar}/^{39}\text{Ar}$ method, ^{39}K is first converted to ^{39}Ar by an n, p reaction in a nuclear reactor, and the argon isotope ratios are determined by mass spectrometry. The $^{40}\text{Ar}/^{39}\text{Ar}$ method has the advantage of allowing both isotopes to be released from similar K sites in minerals by incremental heating. This yields a

TABLE 2. EFFECT OF CONTAMINATION BY 70 MICROGRAMS OF A PRECAMBRIAN FELDSPAR (1.5 Ga) CONTAINING 4.00×10^{-6} MOLES/GRAM RADIOGENIC ^{40}Ar ON A 30-ka FELDSPAR

	Weight (g)	K (%)	^{40}Ar Radiogenic -12 x 10 mole	^{40}Ar Atmospheric -12 x 10 mole	^{40}Ar Atmospheric (%)	K-Ar Date (ka)
Uncontaminated	12.600	9.48	6.36	20.6	76.4	30.7 ± 1.6
Contaminated	12.600	9.48	9.16	20.6	69.2	44.2 ± 1.8

spectrum of $^{40}\text{Ar}/^{39}\text{Ar}$ ratios as a function of the temperature of incremental release. Even though argon may have been lost from mineral sites in which argon was less tightly held, plateaus are frequently obtained at higher temperatures for tightly held argon, and the plateau data yields a better value of the time since the sample began retaining argon by correcting partial argon loss. The $^{40}\text{Ar}/^{39}\text{Ar}$ method is particularly useful for dating geologically old samples where there is a high probability of resetting of the K-Ar clock by argon loss during subsequent thermal events. Thermal resetting is much less probable and relatively easily recognized in Quaternary volcanic rocks, but other problems must be overcome. Several books and many papers have been written on the subject of K-Ar dating. A summary of both methods with many references is available in Faure (1986).

Three major problems are encountered in the dating of Quaternary volcanic rocks: (1) The correction for the atmospheric argon is very large and subject to error due to isotope fractionation resulting from incomplete equilibration (Krummenacher, 1970), (2) samples are more easily biased by extraneous older materials (e.g., see Fig. 8-7 of Dalrymple and Lanphere, 1969), (3) amounts of excess radiogenic argon that would be negligible for older samples may seriously affect the apparent age of Quaternary volcanic rocks (for review see Chapter 8 of Dalrymple and Lanphere, 1969).

Argon has three stable isotopes, which compose nearly 1 percent by volume of the Earth's atmosphere. The isotopic abundance of the three isotopes according to Nier (1950) is: ^{36}Ar (0.337%), ^{38}Ar (0.063%), and ^{40}Ar (99.60%). In the conventional method, measurement of ^{40}Ar and ^{36}Ar is made by isotope dilution in which the diluent is very pure ^{38}Ar . The concentration of ^{40}Ar and ^{36}Ar is measured relative to the known amount of ^{38}Ar diluent. Atmospheric ^{40}Ar must be subtracted from the measured sample ^{40}Ar to obtain radiogenic ^{40}Ar . ^{36}Ar is used as a measure of the atmospheric component. The atomic ratio of ^{40}Ar to ^{36}Ar in air is 295.5 but, as a result of instrumental fractionation, the ratio measured when pure air argon is introduced into a mass spectrometer may not be exactly 295.5. A fractionation correction must be determined by repeated, precise measurement of air argon samples. As an example, consider a Quaternary sample argon measurement comprising 95 percent air and 5 percent radiogenic ^{40}Ar . If the fractionation correction is 1 percent, a

failure to apply the correction would result in a 19 percent error in the radiogenic ^{40}Ar measurement.

There will be an error in the atmospheric air correction if the atmospheric Ar has been fractionated prior to measurement. For example, atmospheric Ar entering a rapidly cooling volcanic rock may not fully equilibrate. As a result of equipartition of energy, the average velocity of ^{36}Ar is 5.4 percent greater than ^{40}Ar and will equilibrate faster. The effect of nonequilibration would be a reduction in apparent age as a result of over correction for atmospheric Ar. It will be shown later that this effect can be minimized by using ground-mass crystallites rather than phenocrysts in the K-Ar dating of Quaternary volcanic rocks.

The effect of contamination by extraneous older materials can be very severe, as shown in Table 2. Large xenocrysts that may contain inherited radiogenic ^{40}Ar must be removed and extreme care taken to avoid contamination during sample preparation.

Radiogenic ^{40}Ar is released from rocks heated by magma, and argon is soluble in the magma and minerals. At the low Ar pressures likely to occur in magma chambers of volcanic flows, Henry's Law will hold (Damon, 1970):

$$^{40}\text{Ar}_E = Sp \quad (1)$$

where $^{40}\text{Ar}_E$ = moles/g of dissolved radiogenic ^{40}Ar , S = moles/g dissolved at 1 bar, and p = the partial pressure of argon. For example, S for albite at 1000°C is 3.9×10^{-9} moles/g. If the partial pressure of ^{40}Ar in the magma reached .001 bar, the albite would dissolve 3.9×10^{-12} m/g of ^{40}Ar . This amount would prohibit a meaningful date for a Quaternary volcanic rock. Fortunately, upon extrusion, the excess ^{40}Ar will tend to escape, but the mineral will also tend to equilibrate with atmospheric argon. Again, as will be shown, the smaller the mineral, the more rapid the equilibration.

EQUILIBRATION OF ARGON AT ELEVATED TEMPERATURES

A good approximation to diffusion in minerals can be obtained by use of the concept of an escape constant, λ_d (Damon, 1970):

TABLE 3. TIME FOR 99 PERCENT LOSS OF EXCESS $^{40}\text{Ar}_E$ AT 1,050° C*

r_c (cm)	0.142	0.071	0.027	0.006	0.001
t	1 month	1 week	1 day	1 hour	2 minutes

* $D_0 = 1.18 \times 10^{-4} \text{cm}^2/\text{sec}$ and $E = 26 \text{Kcal/mole}$.

TABLE 4. TIME FOR 99 PERCENT LOSS OF EXCESS $^{40}\text{Ar}_E$ †

T	20° C	50° C	100° C	200° C	300° C	400° C
t (yr)	1.22×10^{11}	1.93×10^9	8.44×10^8	5.08×10^3	41	1.4
T	515° C	590° C	715° C	1,030° C	1,100° C	
t	1 month	1 week	1 day	1 hour	35 minutes	

† $r_c = 0.005 \text{cm}$; diffusion parameters are those of Table 2.

$$\lambda_d = \frac{gD}{X^2} \tag{2}$$

where g is a geometry factor, D is the diffusion coefficient, and X is the pertinent diffusion dimension, e.g., the radius of a sphere or the thickness of thin slab of large area. D is related to temperature by the Arrhenius equation:

$$D = D_0 \exp(-E/RT) \tag{3}$$

where E is the activation energy for diffusion, R is the Boltzmann constant, and T is the temperature in degrees Kelvin.

At magmatic temperatures in the magma chamber before eruption, argon will rapidly equilibrate, and the argon content of the mineral will be the excess ^{40}Ar supported by the partial pressure of ^{40}Ar in the magma chamber (Equation 1).

Upon extrusion, the lava with its contained minerals will tend to approach equilibrium with the atmosphere. The excess ^{40}Ar will escape and atmospheric Ar will enter. For the dating of Quaternary rocks, we require a close approximation to equilibrium, i.e., a $^{40}\text{Ar}/^{36}\text{Ar}$ ratio of 295.5. For example, consider a small plagioclase crystal in the melt with $D_0 = 1.18 \times 10^{-4} \text{cm}^2/\text{sec}$ and $E = 26 \text{Kcal/mole}$ (Laughlin, 1969), and approximate its geometry as that of a cylinder whose length is great compared to its radius r_c . According to Jost (1960), the escape of excess ^{40}Ar for losses greater than 30 percent closely approximates an exponential relationship.

$$^{40}\text{Ar}(t) = \frac{^{40}\text{Ar}_E(0)}{(2.405)^2} \exp(-\lambda_d t) \tag{4}$$

where $^{40}\text{Ar}_E(t)$ is the average concentration of $^{40}\text{Ar}_E$ after a time

t, $^{40}\text{Ar}_E(0)$ is the initial concentration before eruption, t is the time after eruption, and g in Equation 2 is $(2.405)^2$. Because the square of the radius (r_c^2) and temperature (T) enter into the exponential of Equation 4, the rate of loss is critically dependent upon crystal size (Table 3) and temperature (Table 4). At magmatic temperatures, ground mass plagioclase microlites would lose 99 percent of excess radiogenic argon within minutes, whereas phenocrysts would retain much of their excess radiogenic argon during the cooling process. This effect would tend to yield anomalously old ages. On the other hand, the phenocrysts will also not equilibrate completely, resulting in fractionation of atmospheric argon. The excess ^{36}Ar , when multiplied by the air ratio, will tend to produce anomalously young ages. Thus, ages which are too young or too old may result, depending on which effect is dominant in each particular case.

Groundmass plagioclase microlites lose their excess argon rapidly and equilibrate rapidly with air. Consequently, they tend to yield consistent ages if not reset by subsequent thermal events. It should be emphasized that a temperature of 100°C sustained for a sufficiently long time could cause a significant error in the age of plagioclase microlites. From Table 5, it can be seen that a temperature of 100°C sustained for 60,000 yr would result in a 15 percent loss of argon from the microlites.

COMPARISON OF THEORY WITH PRACTICE

Theory then suggests that for young samples that have not been deeply buried or otherwise thermally reset, plagioclase microlites are better K-Ar clocks than phenocrysts that may not have completely lost excess argon or equilibrated with air. Our

TABLE 5. PERCENT ^{40}Ar LOSS AT 100°C^*

Percent loss	15	30	45	60	75	90
t (yr)	6.0×10^4	1.7×10^5	4.5×10^5	1.1×10^6	2×10^6	3.9×10^6

*Diffusion parameters of Table 2, $r_c = 0.005$ cm.

TABLE 6. WORST CASE EXAMPLES FOR K-Ar DISCORDANCY BETWEEN PLAGIOCLASE MICROLITE CONCENTRATES AND PHENOCRYSTS

Sample No.	Type	K (%)	$^{40}\text{Ar}_{\text{rad}}$ (10^{-12} m/g)	$^{40}\text{Ar}_{\text{air}}$ (%)	K-Ar Date (Ma)
UAKA-6-65	Microlite	0.852	3.59	88.4	2.43 ± 0.32
UAKA-6-65	Phenocryst	0.190	3.14	39.2	9.52 ± 0.81
UAKA-85-365	Microlite	0.992	10.82	37.2	6.28 ± 0.15
UAKA-85-365	Phenocryst	0.318	1.88	89.3	3.41 ± 0.24
UAKA-85-367	Microlite	0.762	8.301	40.6	6.27 ± 0.16
UAKA-85-367	Phenocryst	0.135	0.962	79.6	4.10 ± 0.24
UAKA-85-378	Microlite	1.202	1.032	83.1	0.49 ± 0.035
UAKA-85-378	Phenocryst	0.162	0.271	95.6	0.967 ± 0.158

experience has confirmed theoretical expectations. Dates on microlite concentrates yield reasonable results consistent with stratigraphy, whereas K-Ar dates on phenocrysts are often discordant. This is true not only for plagioclase; biotite and hornblende phenocrysts also frequently yield discordant ages for Quaternary rocks. However, sanidine phenocrysts usually give concordant dates.

Table 6 shows the worst cases that we have observed during years of dating young rocks. Sample UAKA-6-65 was one of the earliest and the most extreme examples of the not infrequent discordance between K-Ar dates on plagioclase microlites and phenocrysts from the same rock and, fortunately, alerted us to the problem. Phenocrysts from this sample are very large, up to 2 cm, translucent and semiperfect. This sample had not completely equilibrated with air nor lost all of its excess ^{40}Ar . However, the dominant effect was the large amount of excess ^{40}Ar . This also occurred for sample UAKA-85-378. The dominant effect in samples UAKA-85-365 and UAKA-85-367 seems to be incomplete equilibration with air, leading to over correction.

An added factor in favor of dating the microlites is the much higher K content of the more sodic microlites compared to the more calcic phenocrysts. This results in a higher radiogenic ^{40}Ar content and, typically, a lower air correction. Sample UAKA-6-65 is atypical because of its extremely high excess ^{40}Ar content that results in a relatively low percent air correction.

It is important to sample the Quaternary rock to be dated in such a way as to minimize error. The quickly quenched parts of a flow may not have been purged of excess argon or equilibrated with air. The rubbly bottom of a flow may contain extraneous older material, and vuggy samples may contain exorbitant amounts of air. We prefer to sample the massive interior of the flow; it has few vesicles and has cooled relatively slowly, allowing time to purge excess ^{40}Ar . Typically, air corrections are usually also much lower for samples from the interior of the flow.

In preparing the Quaternary volcanic rock sample, phenocrysts, xenocrysts, and xenoliths should be removed before preparing the microlite concentrate. Glass, clay, and ferromagnesian should be removed from the sieve-classified fraction (e.g., $<100>150$) by the usual heavy-liquid and magnetic-separation methods. Carbonate, if present, and residual glass should be removed by washing in dilute acids.

CONCLUSIONS

The fundamental limitation in K-Ar dating of Quaternary volcanic rocks is not our inability to measure argon precisely. Rather, it is intrinsic to several basic assumptions of the method which are not always met. Specifically, the sample to be dated must have no excess ^{40}Ar or extraneous ^{40}Ar from contamination and it must have equilibrated with atmospheric argon. In addi-

tion, the atmospheric correction should not be prohibitively high. These limitations can be minimized by careful sampling, careful sample preparation, and by dating groundmass feldspar concentrates rather than phenocrysts. Because of their small size, micro-lites lose excess ^{40}Ar and equilibrate with atmospheric argon much more rapidly than phenocrysts. Guided by this strategy, we have had gratifying success in dating volcanic rocks even as young as Wisconsin. But, in the words of Bobby Burns, the Scottish bard, "The best laid plans of mice and men gang oft aglae."

FISSION-TRACK DATING

Charles W. Naeser and Nancy D. Naeser

INTRODUCTION

Fission-track dating has been applied to many problems in Quaternary geology. Most studies involve dating of volcanic ash layers or determining rates of landform development. Examples of such studies are given below. To a more limited extent, the method has been used in archaeological studies (for example, Fleischer and others, 1965b; Bigazzi and Bonadonna, 1973; Wagner, 1978; Gleadow, 1980).

THEORY AND METHODS

A fission track is a zone of intense damage formed when a fission fragment passes through a solid. When an atom of ^{238}U fissions, the nucleus breaks up into two lighter nuclei, one averaging about 90 atomic mass units and the other about 135 atomic mass units, with the liberation of about 200 MeV of energy. The two highly charged nuclei recoil in opposite directions and disrupt the electron balance of the atoms in the host mineral or glass along their path. This disruption of electron charge in turn causes the mutual repulsion of positively charged ions and the displacement of the ions from their normal crystallographic positions in the host. The result is a zone of damage defining the fission track (Fleischer and others, 1975). The new track is tens of angstroms in diameter and about 10 to 20 μm in length.

A track in its natural state can only be observed with a transmission electron microscope, but a suitable chemical etchant can enlarge the damage zone so that it can be observed with an optical microscope at intermediate magnifications ($\times 200$ – 500). Common etchants used to develop tracks include nitric acid (for apatite), hydrofluoric acid (mica and glass), concentrated basic solutions (sphene), and alkali fluxes (zircon) (Fleischer and others, 1975; Gleadow and others, 1976).

Because ^{238}U fissions spontaneously at a constant rate, the age of a mineral or glass can be calculated from the number of spontaneous fission tracks and the amount of uranium that it contains. The relative abundance of ^{238}U and ^{235}U is constant in nature, and thus the easiest and most accurate way to determine the amount of uranium is to create a new set of fission tracks by

irradiating the sample in a nuclear reactor to induce fission of ^{235}U with a known dose of thermal neutrons. Early development of the fission-track method is reviewed by Fleischer and others (1975) and Naeser (1979).

Two major factors determine whether or not a sample can be dated by the fission-track method. First, the sample must contain a mineral or glass of appropriate uranium content. In Quaternary samples, there must be enough uranium that a statistically significant number of tracks can be counted in a reasonable time. Second, tracks must completely retained once they are formed, or the calculated age will be anomalously young. Heating can cause partial to complete fading (annealing) of the spontaneous tracks. The fission track is stable in most non-opaque minerals at temperatures of 50°C or less, but fission tracks in natural glasses can be affected at much lower temperatures (Seward, 1979; Naeser and others, 1980). Several Quaternary studies have made use of track fading, for example, to determine rates of landform development (e.g., Zeitler and others, 1982; Naeser and others, 1983; Coates and Naeser, 1984).

In the Quaternary studies, only zircon and glass are routinely used for fission-track dating, and they require two different laboratory procedures. The external detector method (Naeser, 1976, 1979) is used to date single crystals of zircon because the uranium distribution is inhomogeneous in individual zircon grains. In contrast, glass is usually dated by the population method (Naeser, 1976, 1979); because all of the glass from a single source has a similar uranium concentration, it is possible to determine the spontaneous and induced track densities from different splits of the same sample. (The reader is referred to Naeser and Naeser [1984] for a more detailed discussion of the theory and methodology of fission-track dating.)

ADVANTAGES AND LIMITATIONS

One advantage that fission-track dating has over most other methods is that sample contamination often can be readily recognized and, therefore, minimized. In conventional radiocarbon and K-Ar dating, bulk samples must be analyzed. Contamination of a sample with older or younger carbon can result in an erroneous radiocarbon age, and a few older detrital grains can have a significant effect on a K-Ar age (Damon, this chapter; Naeser and others, 1981). Fission-track dating is a grain-specific method in which individual grains are scanned and counted. In the case of zircon dating, an age is obtained on each grain that is counted. Therefore, older detrital grains often can be recognized and discarded from the age calculation.

A major limitation of fission-track dating of Quaternary samples is that very young samples ($< 100,000$ yr) usually have a very low spontaneous track density. This requires tedious examination of large numbers of mineral grains or glass shards and produces ages with large analytical uncertainties. Naeser and others (1982) noted one glass sample in which they did not see any spontaneous tracks after scanning thousands of shards. However, even though the analytical uncertainty is large for very young

samples, some such results can solve significant geological problems.

Zircons, although preferable to glass, are not present in all samples. In tephra, their presence depends on the chemistry of the parent magma. Acidic tephra are more likely to yield usable zircons than basic tephra. Zircons that are extremely fine grained ($<75 \mu\text{m}$) cannot be dated by the fission-track method, and this is often the case in tephra sampled a long distance from the vent.

Natural glasses have been extensively dated because of the widespread occurrences of tephra and obsidian in Quaternary rocks. The dating of natural glasses presents special problems. The greatest of these is the ease with which glass can lose spontaneous tracks by annealing (Fleischer and others, 1965a; Storzer and Wagner, 1969; MacDougall, 1976; and Seward, 1979). Hydrated glass shards, which are found in most tephra beds, are particularly susceptible to annealing (Lakatos and Miller, 1972). Work by Naeser and others (1980) has shown that both hydrated and nonhydrated glass can lose tracks at ambient surface temperatures over periods of geologic time. In a study of 14 tephra from upper Cenozoic ($<30 \text{ Ma}$) deposits of the western United States, only one glass had a fission-track age that was concordant with the fission-track age of coexisting zircon. All other samples had ages that were significantly younger than the zircon ages. Seward (1979) showed that 60 percent of the glass fission-track ages of Quaternary tephra studied in New Zealand were significantly younger than the fission-track ages of the coexisting zircons.

APPLICATIONS

Tephrochronology

The major contribution of fission-track dating to Quaternary studies has been in the field of tephrochronology. Fission tracks have proved to be the most suitable method for dating tephra, particularly those older than the maximum limit of radiocarbon dating, which for most analyses is 40 to 50 ka.

The following two studies illustrate the use of fission-track dating in tephrochronology. Volcanic ash beds of the Pearlette family occur in Pleistocene deposits of western North America (Izett and others, 1970, 1972). Before 1970, the Pearlette ash was considered to be the product of a single eruption, and it was used as an isochronous time marker for many midcontinent Quaternary deposits. Izett and others (1970, 1972) reported consistent chemical differences among three subsets of the Pearlette ash samples. They suggested that the three subsets could be correlated geochemically with three major ash-flow deposits originating in the region of Yellowstone National Park, Wyoming. The three ash-flow deposits were dated at $2.02 \pm 0.08 \text{ Ma}$ (Huckleberry Ridge Tuff), $1.27 \pm 0.10 \text{ Ma}$ (Mesa Falls Tuff), and $0.616 \pm 0.008 \text{ Ma}$ (Lava Creek Tuff) by the K-Ar method (J. D. Obradovich, personal communication, 1973). Naeser and others (1973) dated zircons from two of the three subsets of Pearlette tephra and obtained ages of $1.9 \pm 0.1 \text{ Ma}$ for ash correlated with the Huckleberry Ridge Tuff and $0.6 \pm 0.1 \text{ Ma}$ for ash correlated

with the Lava Creek Tuff. These ages matched the ages in the source region and confirmed the geochemical evidence of Izett and others (1970, 1972) that there were three Pearlette ashes rather than just one.

In another study, fission-track dating has demonstrated that a tephra is considerably older than had been inferred from radiocarbon dating of associated organic matter. The Salmon Springs Drift at its type locality, at Salmon Springs, Washington, consists of two drift sheets separated by about 1.5 m of peat, silt, and volcanic ash (Lake Tapps tephra) (Crandell and others, 1958; Easterbrook and others, 1981). The peat grades downward with decreasing organic content into about one meter of silt, which in turn grades into the volcanic ash (D. J. Easterbrook, personal communication, 1980). The peat was radiocarbon dated at $71,500^{+1700}_{-1400} \text{ yr BP}$ by the enrichment method (Stuiver and others, 1978), and the drift sheets were thus considered early Wisconsin in age. Fission-track dating of this ash and a correlative ash at Auburn, Washington, along with paleomagnetic and tephrochronological evidence, shows that the Lake Tapps tephra is ca. 860,000 yr old, and thus the Salmon Springs Drift is an order of magnitude older than indicated by the radiocarbon date (Easterbrook and others, 1981).

Landscape evolution

Several studies have used fission-track dating to determine rates of landform development. An example is a study in the Powder River Basin, Wyoming, that involved dating of clinker formed by natural burning of coal beds.

The burning of the coal occurs when the coal beds are exposed to atmospheric oxygen. In the Rochelle Hills, coal beds are exposed as east-flowing streams cut headward through the west-dipping coal. This headward erosion lowers the water table in the coal, allowing it to burn. If the heat from the burning coal anneals the spontaneous tracks in the detrital zircons, then the zircons record the time when the clinker cooled after the burn.

Coates and Naeser (1984) dated zircons separated from the clinker capping the mesa north of Little Thunder Creek, Wyoming. This study showed that the ages of zircons in the clinker become progressively younger from east to west. Zircons from eastern end of the mesa give ages of ca. 700,000 yr, while zircons at the western edge of clinker development do not contain any spontaneous fission tracks, indicating an age of $<80,000 \text{ yr}$ for that burn. The results of this study show that during the last 700,000 yr, the burn front at Little Thunder Creek has migrated westward about 8 km, and that there has been about 200 m of downcutting of the eastern edge of the escarpment.

Another example of using fission-track dating to study landscape evolution is the use of apatite ages to determine the uplift and erosion (cooling) history of a mountain block. Apatite will not retain fission tracks if it is held at temperatures in excess of 105°C (for heating of 10^8 yr duration) to 150°C (10^5 yr). When a rock containing apatite cools during an uplift/erosion cycle, the apatite in that rock will begin to record fission tracks.

Therefore, apatite fission-track ages provide information on the uplift history of a mountain block.

Naeser and others (1983) used apatite ages to determine an uplift/erosion rate of the Wasatch Mountains northeast of Salt Lake City, Utah. They separated and dated apatite from the Precambrian rocks of the Farmington Canyon Complex. Apatite fission-track ages as young as 5 Ma were found at the base of the mountains near the Wasatch Fault, indicating that these rocks had been at a temperature in excess of $\approx 120^\circ\text{C}$ prior to 5 Ma. The data indicate further that the latest episode of uplift in this segment of the Wasatch Mountains began about 10 Ma and has continued to the present with an average uplift rate of 0.4 mm/yr, and that these rocks have been cooling at a rate of about $12^\circ\text{C}/\text{m.y.}$

SUMMARY

Fission-track dating has widespread application in Quaternary studies. The major contribution has been in the field of tephrochronology, where fission-track dating has been used to date tephra horizons in Quaternary deposits and thereby date Quaternary events. The method has also been used to study the rates of landform development and to determine rates of tectonic processes and how those rates relate to the overall development of the landscape.

CONVENTIONAL URANIUM-SERIES AND URANIUM-TREND DATING

B. J. Szabo and J. N. Rosholt

INTRODUCTION

Climatic fluctuation was the dominating condition during the Quaternary. It resulted in expansion and recession of pluvial lakes, glaciation and deglaciation, large glacio-eustatic sea-level changes affecting both stable and uplifting coastlines, and landscape evolution. The alternating periods of higher versus lower precipitation and temperature influenced rock weathering, alluviation, and soil evolution; also, climatic changes enhanced the mobility of elements in soil profiles and formation of associated secondary minerals. Many of these secondary deposits and some young volcanic rocks are potentially datable by conventional U-series dating, and the time of deposition of some Quaternary sediments can be estimated by uranium-trend dating; both techniques of dating provide the opportunity for deciphering the timing of some of the complex Quaternary events.

The natural radioactive series of ^{238}U , ^{235}U , and ^{232}Th produce numerous daughter products of varying chemical properties and half lives (Fig. 2). Both the parents and their daughter elements are common trace constituents in nearly all geologic materials. If any of these materials containing the parent isotopes remain undisturbed for a period of about 2 m.y., a state of secular equilibrium between parents and all of their respective radioac-

tive daughter nuclides will become established—that is, all measured parent-to-daughter activity ratios are unity. However, several geochemical processes can cause isotopic and elemental fractionation resulting in states of disequilibrium. Conventional uranium-series dating is based on the measurement of the extent to which the state of secular equilibrium is approached in a closed system after the initial disturbance. In contrast, uranium-trend dating is based on the measurement and modeling required to determine the extent and maintenance of disequilibrium in an open system after sedimentation.

CONVENTIONAL URANIUM-SERIES DATING

The conditions for reliable conventional U-series dating are that the material remained a closed system through geologic time with respect to the nuclides of interest, and that the material is pure, reasonably uniform, and was not subject to recrystallization or other processes that could produce subsequent mobilization of daughter products.

The most commonly utilized methods for Quaternary deposits rely on the measurements of disequilibrium between ^{230}Th and ^{234}U (^{230}Th deficiency method), between ^{231}Pa and ^{235}U (^{231}Pa deficiency method), and ^{234}U and ^{238}U (^{234}U excess method). Deficiencies of ^{230}Th and ^{231}Pa in secondary minerals are due to the marked difference between the aqueous mobility of uranium relative to thorium and protactinium. Uranium is readily leached from weathered source rocks, then transported and re-deposited, whereas ^{230}Th and ^{231}Pa are extremely insoluble, and trace amounts dissolved from source rocks are effectively removed from solution by adsorption during transport. Materials datable by the ^{230}Th and ^{231}Pa deficiency methods are either (1) geologically derived, such as various forms of carbonates, sulfates, phosphates, opal, and young volcanic rocks, or (2) biogenic in origin, such as corals, mollusks, bones, and peat deposits. The upper (oldest) limit of ^{230}Th deficiency dating is about 360 ka; the upper limit of ^{231}Pa deficiency dating (used mainly as a complementary method to ^{230}Th dating) is about 180 ka.

Natural waters and secondary minerals generally contain excess ^{234}U relative to ^{238}U because the alpha recoiling (Fleischer, 1980) associated with the process of ^{238}U radioactive decay to ^{234}U (Fig. 1) displaces the ^{234}U atoms to more leachable sites than those of ^{238}U atoms, which occupy the original crystal lattice positions. The excess ^{234}U is then the measure of the age of the material, provided that the initial $^{234}\text{U}/^{238}\text{U}$ activity ratio can be ascertained. The ^{234}U excess method has been used for dating corals, speleothems, and calcitic veins. The range for practical dating by this method is between about 100,000 and 1.5 m.y. Equations used for the age calculations and general chemical procedures are described by Ivanovich (1982) and Lally (1982).

Secondary carbonates

Inorganic (predominantly calcite) and organic (aragonite or calcite) carbonate deposits are common components in most

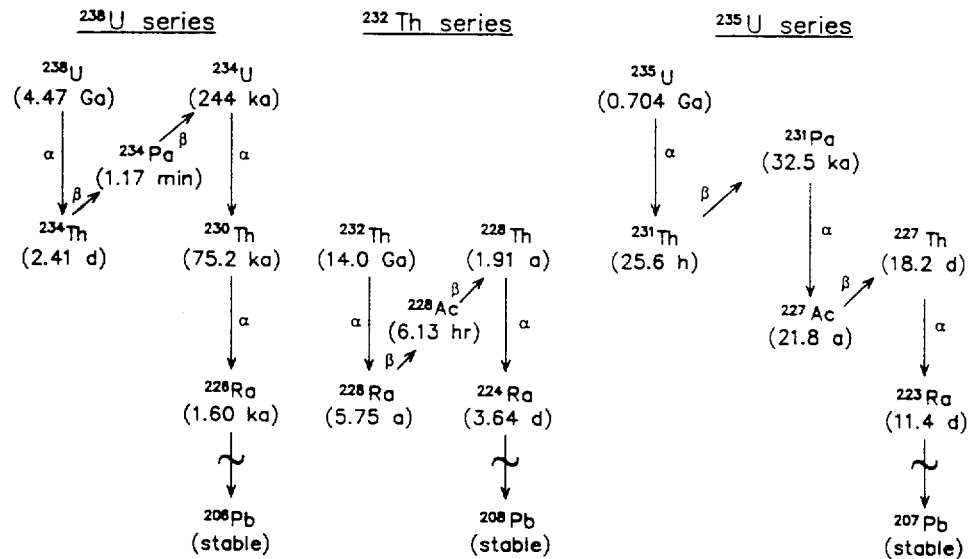


Figure 2. Decay series of naturally occurring uranium and thorium nuclides.

depositional environments, and they display a variety of textures and structures. Most of the dense, pure carbonates are suitable for reliable U-series dating.

Speleothems (carbonates precipitated in caves) are usually good material for U-series dating. Results are utilized in various ways. Ages can establish the local cave chronology and rates of deposition (Thompson and others, 1975). Speleothem growth in an arid climate may indicate pluvial periods, and lack of growth may indicate dry climatic conditions (Harmon and Curl, 1978). The absence of speleothem growth in alpine caves indicates periods of prolonged cold, preventing the movement of ground water (Harmon and others, 1977 and Lively, 1983). Combinations of speleothem dating with stable isotopic analyses are used in paleoclimatic studies in both temperate and glacial zones (Mills, this volume; Schwartz and others, 1976; Thompson and others, 1976; Harmon and others, 1978a; and Harmon and others, 1978b).

Calcitic veins are dense, low-temperature precipitates from calcium carbonate-saturated ground water that fill or line fractures. Some of these veins provide a continuous record for the past 2 m.y., and they can be dated reliably by the ^{230}Th deficiency and ^{234}U excess methods (Winograd and Doty, 1980). Reduced deuterium contents in fluid inclusions of U-series-dated calcitic veins from the southern Great Basin indicate major uplift of the Sierra Nevada during the Quaternary (Winograd and others, 1985). Dates on calcitic veins in the Amargosa Desert, Nevada, indicate a lowering of the paleo-ground-water table at that area by about 0.04 m/1000 yr, probably due to an increase in aridity during the Pleistocene (Winograd and Szabo, 1985), and these dates provide other implications for the climatic record (Winograd and others, 1988). Uranium-series dating of calcitic

veins occurring in ash-flow tuffs at Yucca Mountain, Nevada, suggests episodic fluid movements and fracture filling during the past 400,000 yr (Szabo and Kyser, 1985).

Travertines (dense and clean varieties of spring-deposited carbonates) are also suitable for U-series dating. They often occur as extensive horizontal or sloping layers. Travertines may cap fluvial terrace deposits, thus providing limiting ages for periods of deposition and terrace cutting (Schwartz and Gascoyne, 1984). Extensive erosion during the Pleistocene developed pediments in central Montana. Dating travertines associated with one pediment surface indicates that the surface is older than about 320,000 yr (Szabo and Lindsey, 1986). Evidence for paleospring activities is represented by travertine deposits in Grand Canyon National Park, Arizona dated at about 170, 110, and 80 ka (Szabo and others, 1986).

The porous variety of spring-deposited calcium carbonate (calcareous tufa), usually contains detrital materials, and their open structure permits secondary mobilization or addition of the U-series nuclides. Separation and analysis of both the acid-soluble carbonates and acid-insoluble residues of carefully selected samples may yield useful limiting dates for various Quaternary processes (Szabo and others, 1981a).

Clean and dense parts of lacustrine carbonates may yield reasonable dates by U-series analysis (Kaufman and Broecker, 1965). Lacustrine carbonates, however, usually contain various amounts of detrital materials, thus requiring large age corrections due to initial ^{230}Th contamination (Kaufman, 1971).

Secondary carbonate, concretions, rinds, and components that may be either pedogenic or nonpedogenic and are referred to as caliches or calcretes are potentially datable by U-series meth-

ods. These deposits usually contain large amounts of detrital residues, therefore, extensive age corrections are required for the uranium and thorium derived from the noncarbonate fraction. Selected dense calcretes from the Nevada Test Site region yielded useful limiting ages for recent faulting (Knauss, 1981; Szabo and others, 1981a). By multiple analysis of both the carbonate and the detrital fractions of caliche cement samples, Ku and others (1979) determined periods of carbonate cementation in alluvial deposits of the Mohave Desert, California.

Carbonate-rinds, nodules, and rhizocretions are pedogenic or ground-water-precipitated carbonates that coat rock surfaces, form in sediments, or form root-like structures. If dense and relatively clean, these materials can be successfully dated by U-series methods. Carbonate-rinds on boulders from fan deposits near Arco, Idaho, have been dated. Rind carbonates accumulated between about 10,000 and 100,000 yr ago, and apparently remained a closed system with respect to uranium and thorium migration (Szabo and Rosholt, 1982). Carbonate-rind dates indicate an age of about 200,000 yr for the Yermo fan deposit at Calico, California (Bischoff and others, 1981).

Corals have consistently yielded reliable age results, provided they are composed of unrecrystallized aragonite and are free of void-filling contaminants. Coral flourishes in the tropics, but certain solitary species occur even in temperate regions. Up to the present, only four California and one Oregon Pacific coast localities yielded enough coral material for U-series dating. The California localities are: Nestor Terrace, San Diego (Ku and Kern, 1974); Cayucos, San Luis Obispo County; San Nicolas Island (listed in Ku and Kern, 1974); and San Clemente Island (Muhs and Szabo, 1982). The Oregon coral is from the Whiskey Run Terrace, Bandon (Kennedy and others, 1982). The dating results of corals have been applied for calculating local uplift rates and for calibrating amino-acid ratios from mollusks, which in turn were used for regional correlations and relative dating (Wehmiller and others, 1977; Kennedy and others, 1982; and Muhs, 1985).

Over 55 fossil corals have been dated from marine deposits (some in place) along the southeastern U.S. Atlantic Coastal Plain (Szabo, 1985). Ages of these corals have been used for paleoclimatic reconstruction (Cronin and others, 1981) and for lithostratigraphic and biostratigraphic differentiation (Colquhoun, this volume; Mixon and others, 1982; and McCartan and others, 1982). Fossiliferous deposits along the northern part of the Atlantic Coastal Plain contain scarce corals; dated fragments from the Pleistocene Sankasty Sand, southeastern Massachusetts, indicate a last interglacial age (about 130,000 yr) for the deposition of this marine unit (Oldale and others, 1982). Of the conterminous United States, reef-building corals occur only in southern Florida. Dates from fossil corals from the Pleistocene Key Largo Limestone and reef deposits of the Bahamas indicate that reef formation occurred about 135 ka in the southern Florida area, while sea level was several meters above its present level (Osmond and others, 1965; Neumann and Moore, 1975; and Harmon and others, 1978b).

Mollusks, abundant in many marine, fluvial and lacustrine sediments, are potentially datable by U-series methods. Unlike corals, however, major amounts of uranium enter the molluscan shells after the death of the animals, and they often remain susceptible to gradual or episodic post-depositional assimilation of uranium so that some pre-Pleistocene samples give erroneous finite dates (Kaufman and others, 1971). Furthermore, shells may be subject to recoil gain of ^{231}Pa , ^{230}Th , and ^{234}U (Szabo and Rosholt, 1969); to partial loss of ^{230}Th and/or ^{231}Pa (Szabo and Gard, 1975; and Szabo and others, 1981b); and to initial ^{230}Th contamination, as determined by measured ^{232}Th (Osmond and others, 1970). In the absence of other U-series datable materials, and in conjunction with other correlative techniques, mollusk dates generally are only approximate, usually minimum, ages for depositional events (Szabo and Rosholt, 1969; Szabo and Vedder, 1971; Bradley and Addicott, 1968—redated by Szabo, 1980a; Wehmiller and others, 1977; and Mixon and others, 1982). Fossil echinoids from California also show open-system conditions similar to mollusks (Muhs and Kennedy, 1985).

Secondary deposits other than carbonates

Detritus-free evaporites may yield useful U-series dates for the time of sedimentation. Dates on bulk salt samples (mostly halite, trona, and gaylussite) in Searles Lake, California, have been reported recently (Peng and others, 1978; and Bischoff and others, 1985), where the lake sediment consists of sequences of mud (pluvial) and salt (arid) layers. Results indicate semidry and intermediate climate with moderate salinities during the period from about 200 to 300 ka, followed by a generally wet climate and greater water depth with low salinities during about the last 100,000 yr.

Under favorable conditions, other evaporites such as sulfates are also datable. Anhydrite samples from Stanton's Cave, Grand Canyon National Park, Arizona, yielded apparently reliable U-series dates between 16 and 59 ka (Rosholt and others, 1987a). Dating of gypsum spring deposits near Carlsbad, New Mexico, was attempted (Szabo and others, 1980), but the results show that these surface-exposed samples contain detrital contaminants, and did not remain an ideal closed system with respect to uranium and daughter elements.

Knauss (1981) reported that some pure secondary silica, opal deposits, contain uranium, but negligible amounts of thorium, and that the samples appear to constitute a closed system with respect to uranium isotopes and their respective radioactive daughters. Laminated opal from the Yucca Mountain region, Nevada (Szabo and O'Malley, 1985), and opal-filling fractures in ash-flow tuffs of Yucca Mountain, Nevada (Szabo and Kyser, 1985), have been dated but there is at present no independent age control to test the reliability of the results. In theory, clean secondary accumulations of iron and manganese hydroxides and oxides can be dated by U-series. Desert varnishes, dark coatings of ferromanganese oxides on exposed rock surfaces in arid climate regions, have been proposed as suitable materials for dating

(Knauss and Ku, 1980), but again, no independent age control is as yet available.

Fossil bones take up uranium after the death of the animal, and do so presumably until all active organic matter within the bone has decomposed. Comparison of U-series and ^{14}C dates of bones younger than 30,000 yr indicates that most secondary uranium assimilation occurs within a few thousand years after burial, but in some cases the progressive uranium uptake by these fossils can be considerably longer (Szabo, 1980b). Some of the older U-series-dated bone samples from alluvial deposits of Colorado (Szabo, 1980b), from the middle unit of the Riverbank alluvium near Sacramento, California (Hansen and Begg, 1970), and from gypsum deposits, Carlsbad, New Mexico (Szabo and others, 1980), have provided useful, although probably minimum-age estimates for the deposition of sediments containing the fossils. Severe weathering can cause uranium loss, resulting in U-series ages that are older than the actual burial age of the bone (Bada and others, 1984). Other materials, such as wood (Szabo, 1972), peat (Vogel and Kronfeld, 1980; Zielinski and others, 1986), and organic matter adhering to sand (Szabo, 1982) have been attempted for U-series dating, but most of these studies resulted in minimum-age estimates only, due to the open-system behavior of uranium.

Volcanic rocks

Young volcanic rocks can be dated by U-series methods in certain favorable circumstances. The requirements are: (1) that secular equilibrium was maintained between ^{238}U , ^{234}U , and ^{230}Th during the process of partial melting and during uprising and eruption of the magma, (2) that no contamination occurred by remelting of the older crust, and (3) that the volcanic rock remained a chemically closed system after solidification. During crystallization of the volcanic rocks, all individual mineral phases are assumed to have the same $^{230}\text{Th}/^{232}\text{Th}$ activity ratios, but their $^{238}\text{U}/^{232}\text{Th}$ would differ according to the relative partition coefficients of uranium and thorium in the different mineral phases. In all mineral phases, the ^{230}Th then approaches reestablishment of radioactive equilibrium relative to the amount of uranium in that particular phase. In an ideal case, a plot of $^{230}\text{Th}/^{232}\text{Th}$ against $^{238}\text{U}/^{232}\text{Th}$ defines a line, the slope of which will vary as a function of time (Harmon and Rosholt, 1982). This method has been utilized to date rhyolites from Mono Crater, California (Taddeucci and others, 1967), and Long Valley, California (Baranowski and Harmon, 1978).

URANIUM-TREND DATING

For successful conventional uranium-series dating, a closed system is required to exist throughout the history of a sample, meaning that there has been no postdepositional migration of ^{238}U or of its daughter products, ^{234}U and ^{230}Th . In contrast, open-system dating techniques require no such restrictions on postdepositional migration of these radioisotopes within and be-

tween deposits. Results of many studies of U-series disequilibria indicate that uranium commonly exhibits open-system behavior in many near-surface deposits (Ivanovich and Harmon, 1982). Because materials suitable for closed-system dating often are lacking in Quaternary deposits, an open-system dating method is needed. The model for uranium-trend dating was developed by Rosholt (1985) and applied to a variety of Quaternary deposits, including alluvium, eolian sediments, glacial deposits, zeolitized volcanic ash, and marine terrace deposits (Muhs and others, 1989). This open-system, empirical model requires a calibration based on deposits of known age; results of such calibrations are included in Rosholt and others (1985b).

For U-trend dating of sediments, the distribution of uranium-series members during and after sedimentation must have been controlled by their open-system behavior. Sediments and soils are penetrated continuously or episodically with ground water or soil water that contains at least small amounts of dissolved uranium, some of which may include exchange of locally leached and/or adsorbed uranium. As this waterborne uranium decays, it produces a trail of radioactive daughter products that are readily adsorbed in solid matrix materials such as clay and silt. If the trail of daughter products, ^{234}U and ^{230}Th , is distributed through the deposit in a consistent pattern, then uranium-trend dating is possible. The large number of geochemical variables in an open system precludes the definition of a rigorous mathematical model for uranium migration. Instead, an empirical model is used to define the parameters that can reasonably explain the patterns of isotopic distribution. This model requires independent time calibration with known-age deposits and careful evaluation of the stratigraphic relationships of the deposits to be dated; however, they do not have to occur in the same geographic area as the calibration deposits (Rosholt and others, 1985b).

Analyses of the abundances of ^{238}U , ^{234}U , ^{230}Th , and ^{232}Th in a single sample do not establish a meaningful time-related relationship of isotopic distribution in an open-system environment. However, analyses of several samples, each of which has only slightly different physical properties and only slightly different chemical compositions within a unit, may provide a consistent pattern in the distribution of these isotopes (Rosholt, 1985). Analyses of 5 to 8 samples per unit from several alluvial, colluvial, glacial, and eolian deposits have shown that these types of deposits, ranging from clay-silt to gravel units, have isotopic distributions that appear to fit an open-system model (Rosholt and others, 1985a and 1985b). To obtain a U-trend date, several samples are collected from a vertical section of each separate stratigraphic unit. The number of samples required to establish a reliable linear trend in the data depends on the variation in ratios of uranium and thorium that define the trend line.

It is preferable to collect samples from a channel cut through deposits exposed in a trench wall or a relatively fresh, well-exposed outcrop; existence of soil development is not a necessary requirement, nor is sampling of the entire stratigraphic unit always necessary. Pebbles and other larger fragments are removed

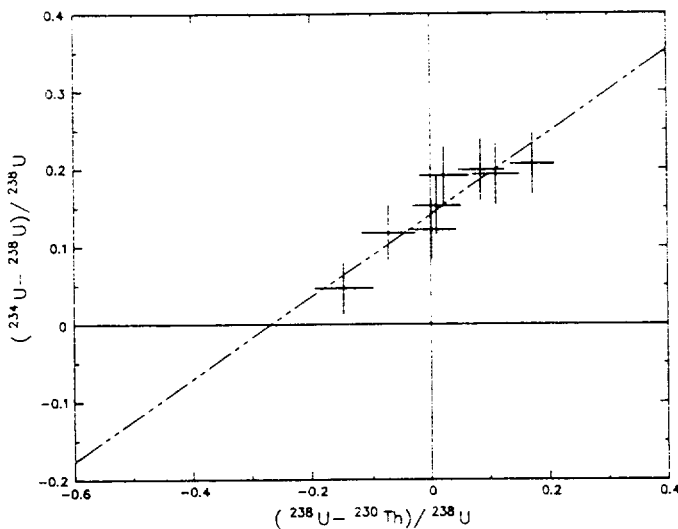


Figure 3. Uranium-trend plot of alluvium (160 ka) at Charlie Brown Quarry, Shoshone, California. All samples are plotted in terms of activity ratios; zero coordinates represent radioactive equilibrium in isotopic ratios (reproduced from Rosholt and others, 1985a).

by sieving and the remaining less-than-2-mm size fraction is pulverized to less-than-0.2-mm size, homogenized, and retained for analysis. Chemical procedures used for separating uranium and thorium for alpha spectrometry measurements are those described by Rosholt (1984 and 1985). For defining uranium-trend slopes, the results of these analyses are plotted in the form of $(^{234}\text{U}-^{238}\text{U})/^{238}\text{U}$ against $(^{238}\text{U}-^{230}\text{Th})/^{238}\text{U}$. Ideally, this yields a linear relationship, as shown in Figure 3, in which the slope is a function of the age of the deposit based on the calibration.

Applications for dating Quaternary deposits

In a report for the Nevada Test Site (Rosholt and others, 1985a), 31 of 37 depositional units analyzed were datable by the U-trend method. These results have median age estimates that indicate four separate time frames of deposition during the late and middle Pleistocene in this geographic area: 40 ± 15 ka, 170 ± 40 ka, 270 ± 50 ka, and 440 ± 60 ka. The results are reasonably consistent with other dates (Swadley and others, 1984) and with estimates based on geomorphic evidence. Analyses of deposits from a trench near Beatty, Nevada, suggest that a sequence of several fluvial deposits was laid down by the Amargosa River at the base of the Beatty scarp during the last 500,000 yr (Rosholt and others, 1988). Deposition of silts, sands, and gravel were dated at 75 ± 10 ka, 155 ± 30 ka, and 500 ± 100 ka.

Nine units from deposits in New Mexico have yielded ages ranging from about 20 ka to about 700 ka (Rosholt and others,

unpublished data). The deposits include alluvium, colluvium, eolian sand, and gypsum; some of the alluvial deposits now have well-developed carbonate horizons. The U-trend dates for two of these middle Pleistocene calcretes appear to be too young, based on geologic considerations, because of the effect of late stages of carbonate accumulation. The remaining deposits give reasonable ages based on stratigraphic relationships. Uranium-trend systematics of deposits in New Mexico and in Nevada indicate that resolution of chronology is better for calcareous deposits than for noncalcareous deposits such as glacial till and loess. However, very strong calcium carbonate development, such as in calcretes, tends to yield ages closer to the mean age of carbonate enrichment rather than the ages of deposition of the host sediments. Alluvial deposits, which tend to be more poorly sorted and of mixed mineralogy, usually yield a better spread of the data on the uranium-trend plot than do eolian, quartz-rich sand deposits.

Studies of unconsolidated Quaternary deposits in Grand Canyon National Park along the Colorado River near Nankoweep Creek and in the vicinity of Basalt Canyon and Tanner Creek reveal a history of relatively young downcutting and deposition in the lowest 100 m of the canyon (Patton this volume; Machette and others, 1986). This interpretation is based on U-trend ages of the deposits and on the stratigraphic relations between deposits. Ages were obtained on Pleistocene deposits that form prominent terraces from 20 m to 50 m above the present river level; four ages were determined, ranging from 40 ± 24 ka to 150 ± 30 ka, with increasing age for higher level terraces. A rockfall debris 60 m above the river on the Nankoweep delta was dated at 210 ± 25 ka. Farther from the river, alluvial deposits in high valleys (400 to 500 m above the river) at Chuar Valley and Surprise Valley were dated at 300 ± 100 ka and 250 ± 30 ka, respectively (Rosholt and others, 1986).

In Fisher Valley, Utah (Colman and others, 1986), U-trend ages were reported on basin-fill sediments. A Lava Creek Ash horizon was dated at 530 ± 70 ka; ages of 240 ± 35 ka and 210 ± 40 ka were obtained for the top of the basin-fill sediments; and 9 ± 11 ka was obtained for Holocene eolian sand. These results for the oldest and youngest units are in fair agreement with ages determined by tephrochronology (610 ka) and radiocarbon (8 and 9 ka) methods, respectively (Patton and others, this volume).

In the San Joaquin Valley, the U-trend method was used to determine ages on sediments ranging from about 30 to 600 ka (J. N. Rosholt, unpublished data); these included Pleistocene deposits of the upper and lower members of the Modesto Formation, the upper and middle units of the Riverbank Formation, and the upper unit of the Turlock Lake Formation. Of 13 depositional units analyzed, 5 were not datable because the U-trend method does not appear to work for soils with missing horizons or for soils that have developed in parent materials of more than one age. On the California coast, marine terrace deposits near San Pedro were dated by U-trend method at 150 ± 50 ka, 230 ± 60 ka, and >700 ka (Muhs and others, 1989). These dates are in agreement with conventional U-series and amino acid age determinations.

DISCUSSION

A variety of middle and late Pleistocene depositional, erosional, climatic, and volcanic events can be dated, and rates of change can be determined, by applying U-series methods. To obtain reliable results, however, one needs to find the high-quality, homogenous samples that have formed in a short period in relation to their age and represent a discrete geologic event. Unfortunately, nature rarely provides such ideal samples; therefore, investigators have devised different correction techniques to account for the presence of impurities. The closed-system condition (no migration or addition of nuclides) is always required in conventional U-series dating, but it is seldom ascertained. Because of uranium mobility, often the uptake of uranium is dated, not the deposit itself, and in these cases dates should be interpreted as minimum-age estimates.

Uranium-trend dating results show that it is a suitable method of estimating the age of some Quaternary deposits. The most reliable ages appear to be in the time range of 60,000 to 600,000 yr, which, at best, may be accurate within ± 10 percent for a deposit whose samples provide a linear pattern of isotopic variation. The U-trend ages have large relative errors near the lower (10 ka) and upper (800 ka) limits of the method; deposits younger than 20 ka have errors near or greater than ± 100 percent, and deposits older than 600 ka have errors greater than ± 20 percent.

Conventional U-series and U-trend dating have yielded useful results for various Quaternary dating problems. Due to the imperfections, the reliability and accuracy of the dates are not uniform, however. Therefore it is a good practice to test the dating results against the stratigraphic constraints of the particular geologic application.

PALEOMAGNETIC DATING

Joseph C. Liddicoat

Two characteristics of the Earth's magnetic field have application for dating stratigraphy—reversals of polarity and systematic changes in the paleomagnetic vector. The benefits and limitations of each are controlled by several factors, and among them is the time interval. Whereas the reversal time scale (Harland and others, 1982) covers all of the Quaternary (and beyond), records of short- and long-term behavior (called secular variation) of the field apply only to the post-Wisconsin and Holocene. Also restricting are the location and areal extent of the study; there are no bounds on magnetostratigraphic studies, but secular variation is confined mainly to regions several thousand kilometers across. In this discussion, we will not deal with the specifics of paleomagnetism or the Earth's magnetic field, which are in McElhinny (1973) and Merrill and McElhinny (1983), but will highlight those elements that bear on stratigraphic correlation and dating.

A reversal of polarity is easy to conceptualize as a stratigraphic marker because it occurs simultaneously around the world. Four boundaries are well known for the Quaternary, and their age is established primarily by K/Ar dating of volcanic rocks: termination of the Olduvai Normal Subchron (1.67 Ma), limits of the Jaramillo Normal Subchron (0.97 Ma and 0.90 Ma), and onset of the Brunhes Normal Chron (0.73 Ma; Mankinen and Dalrymple, 1979). Additional reversals have been encountered and dated in Quaternary volcanic rocks, and they likewise serve as distinct horizons wherever identified. The best data are for the Cobb Mountain Normal Subchron in California (1.19 ± 0.2 Ma; Mankinen and others, 1978), the Emperor Reversed Subchron in Idaho (0.46 ± 0.05 Ma; Ryan, 1972; Champion and others, 1981), and the Laschamp Reversed Subchron in France (Bonhommet and Zahringer, 1969) that is assigned the age of about 0.04 Ma (Heller and Peterson, 1982). Another brief reversal is the Blake Reversed Subchron at about 0.12 Ma (Denham and others, 1977) that was discovered in cored sediment from the Blake Plateau in the western North Atlantic (Smith and Foster, 1969), but is not found in all sections believed to span that interval. The same applies to several other short episodes of reversed polarity in the Brunhes Normal Chron that are not universally recognized for a variety of reasons; examples are the Gothenburg in Sweden (Mörner and others, 1971) and Biwa in Japan (Kawai and others, 1972). As a result, they are not in all compilations of the reversal time scale, including the one adapted for the Decade of North American Geology (Palmer, 1983).

If the magnetostratigraphy is complete to the base of the Quaternary (as in a core of lacustrine or deep-sea sediment), dating the stratigraphy using only the reversal time scale can be done with a high level of confidence. However, where there are hiatuses in the section, a safe assumption is that rocks possessing reversed polarity acquired that magnetization before 0.73 Ma. A similar rationale cannot be used for rocks of normal polarity because they might be remagnetized by the present (normal) field. Fortunately, field and laboratory (demagnetization) experiments can usually establish whether the magnetization is primary or secondary in origin. In a section where the polarity is normal exclusively, improvement of the dating beyond assignment to the Brunhes Normal Chron is left to correlating secular variation of the paleomagnetic field. It is a subject that has received considerable attention in recent years both in stratigraphic studies and in investigations of the dynamics of the Earth's core.

Because secular variation is the result of a complex interaction between the dipole and non-dipole fields, it is highly variable when considered worldwide. Still, where systematic changes in declination, inclination, and intensity are calibrated by radiometric dates, the curves are potentially useful for correlating and dating stratigraphy on a regional scale. Among the places where successful application has been made using wet lake sediments are the midwestern United States, Canada, Great Britain, Europe, and Australia. The curves for those and additional regions are in Creer and others (1983).

Changes in the paleomagnetic vector and field strength are also preserved as thermal remanent magnetization in baked clay at archeological sites. Because of the very good age control on samples (usually by radiocarbon) and stringent requirements on archeomagnetic data, reliable curves for much of the Holocene are available for the southwestern United States, Britain, Europe, the Middle East, and Australia (Wolfman, 1983). The curves not only have utility in stratigraphic studies, but help to confirm the secular variation measured in lake sediments as recorded by the process of detrital remanent magnetization.

The value of detailed curves of secular variation would be enhanced if there is a large departure from typical field behavior that does not constitute a reversal; such directions are called an excursion (Cox and others, 1975). In practice, excursions are difficult to locate in the stratigraphic record because they have a duration of only a few thousand years at most. A case in point is the Moho Lake Excursion (Denham and Cox, 1971; Liddicoat and Coe, 1979) that occurred about 26 ka (Liddicoat and others, 1982) in exposed dry lake sediments in east-central California. Within the structural basin containing pluvial Lake Russell (of which Moho Lake is the remnant), the excursion can be positively traced over a distance of 20 km using a distinctive tephra layer as a marker (Denham, 1974). Only recently, and after several unsuccessful attempts at other localities (Verosub, 1982), was the excursion discovered in sediment from another pluvial lake. The closest one, Lake Lahontan in southwestern Nevada, is 200 km away (Liddicoat and others, 1982), and the other, Summer Lake, is 300 km farther to the north in southern Oregon (Negrini and others, 1984). In each instance, it was not the excursion that was first identified, but the associated tephra layer or another one close in age (Davis, 1985). Thus, the utility of an excursion alone as a method for placing an age on stratigraphy in a large geographical area (such as the Great Basin of the western United States) remains to be demonstrated. Other excursions in the Pleistocene have been reported, but they have not been verified at multiple sites (Banerjee and others, 1979; Verosub, 1982) and as yet do not warrant serious consideration as stratigraphic markers.

Rock-magnetic information, such as susceptibility, and other laboratory experiments designed to identify the physical properties and composition of the carrier of magnetization are akin to records of secular variation in wet lake sediment. The approach is relatively quick and circumvents the problems associated with paleomagnetic studies of cores in which there might be errors in orientation or there has been disturbance to the sediment during recovery and subsequent sampling. The early work in North America began in the Midwest (Banerjee, 1981) and followed a successful application of the technique in Great Britain (Blomendal and others, 1979). Rock-magnetic studies are thus becoming an important part of detailed investigations of wet lake sediments, and complement the other methods for dating and correlating stratigraphy within late Pleistocene and Holocene lakes or in a drainage basin (Thompson and others, 1975; 1980).

THERMOLUMINESCENCE DATING

Steven L. Forman and Michael N. Machette

INTRODUCTION

The development of thermoluminescence (TL) dating techniques during the past two decades came about through TL studies of pottery from archaeological sites (Flemming, 1979; Aitken, 1974, 1985). During the past ten years these techniques have been applied successfully to dating of Quaternary sediments (see review articles by Dreimanis and others, 1978; Wintle and Huntley, 1982; Singhvi and Mejdahl, 1985). The basic principles of the technique for dating Quaternary sediment are similar to those used in dating archaeological materials. However, heating of pottery removes any TL signal that may have accumulated in the minerals, whereas in sediments the inherited TL in minerals is assumed to be zeroed by exposure to sunlight (light bleaching) prior to deposition. This important difference in zeroing mechanisms prompted development of new laboratory procedures for dating sediments (i.e., see Wintle and Huntley, 1980). For TL dating of sediments, environments of deposition are evaluated in terms of their effectiveness in removing previously acquired TL from minerals. Samples are taken from sediment that has not been exposed to sunlight since it was deposited.

As a dating technique, TL does not depend on presence of organic or volcanic materials, and it has the distinct advantage of directly dating many kinds of sediment. More importantly, it can provide age determinations at close intervals and at significant positions in a stratigraphic section. The TL method can be applied to sediments ranging from younger than 100 ka to possibly as old as 500 ka. Because of its wide applicability, TL is an extremely important new dating technique for Quaternary deposits. This brief review explains the method, discusses the types of materials that can be dated, and discusses some of the problems involved in different applications of the method. Extensive literature on TL dating is reviewed in Aitken (1985), PACT volumes 3, 6, and 9 (Journal of the European Study Group on Physical, Chemical, and Mathematical Techniques Applies to Archaeology and in Nuclear Tracks and Radiation Measurements (1985, v. 10, nos. 1, 2, 4-6). These sources give more complete reference listings dedicated to this subject.

THERMOLUMINESCENCE DATING OF GEOLOGIC MATERIAL

Thermoluminescence dating of minerals was first attempted by Daniels and others (1953). They measured TL signals from some common minerals, but production of reliable age determinations was difficult. McDougall (1968) summarized much of the early research on thermoluminescence of geologic materials. The potential of dating unheated sediment by TL was first recognized by Morozov (1968) and later described by Shelkopyas (1971),

who obtained ages for sediments in the Soviet Union. In assessing the early Soviet TL dating, Wintle and Huntley (1982) concluded that the obtained TL dates may be in correct chronologic sequence but that they may be in error by a factor of 2 to 10. Bothner and Johnson (1969) reported TL studies from four deep-sea cores rich in nanofossils. They found that the naturally induced TL, thought to be characteristic of foraminiferal calcite (Johnson and Blanchard, 1967), increased down-core to a plateau (saturation) value. Huntley and Johnson (1976) reported a similar increase in equivalent dose with depth in a core of radiolarian-rich sediment. These studies led to Wintle and Huntley's (1979) recognition that the TL in these marine sediments was from detrital grains that adhere to the nanofossils, rather than the nanofossils themselves. Following this fundamental discovery there has been increased interest in and application of thermoluminescence to dating of mineral sediments.

Two new dating techniques related to thermoluminescence are electron-spin resonance (ESR) (Hennig and Grün, 1983) and optical dating (Huntley and others, 1985). ESR dating is based on direct measurement of radiation-induced paramagnetic electrons that have been trapped in crystal defects through geologic time. The technique has been applied to apatite and to organic and inorganic carbonate, and research is underway using silicate minerals. Optical dating involves photo-stimulated luminescence, rather than heat stimulation (thermoluminescence). Electrons accumulated in traps through geological time are freed by laser light, thus transferring electrons to luminescence centers, which transmit visible light.

FUNDAMENTALS OF THERMOLUMINESCENCE DATING

The TL signal emitted by mineral grains is acquired by exposure to ionizing radiation. The radiation causes electrons to be displaced from outer electron shells and trapped in crystal defects. In most environments, the contribution from cosmic rays is small, especially at depths of more than 10 cm in sediment. Therefore the causative radiation in sediment is almost entirely alpha, beta, and gamma particles that are released during the decay of radioactive nuclei of ^{40}K , ^{238}U , and ^{232}Th contained in the sediment. In order to obtain a reliable date from a given sample of mineral sediment, its electron traps initially must have been emptied by exposure to light, and these traps subsequently must have accumulated and retained a post-deposition TL signal. The TL signal is quantified by measuring the light emitted as a sample is heated continuously from about 25° to 500°C at a rate of about 5°C/sec in an oxygen-free atmosphere (see Fig. 4). Minerals such as feldspar, quartz, and calcium carbonate have diagnostic TL-response (glow) curves at different temperature ranges.

To evaluate the amount of radiation received by the sample in its geologic environment, the sample's sensitivity to radiation must be determined. This sensitivity is assessed in the laboratory by measurement of the TL response to irradiation from a cali-

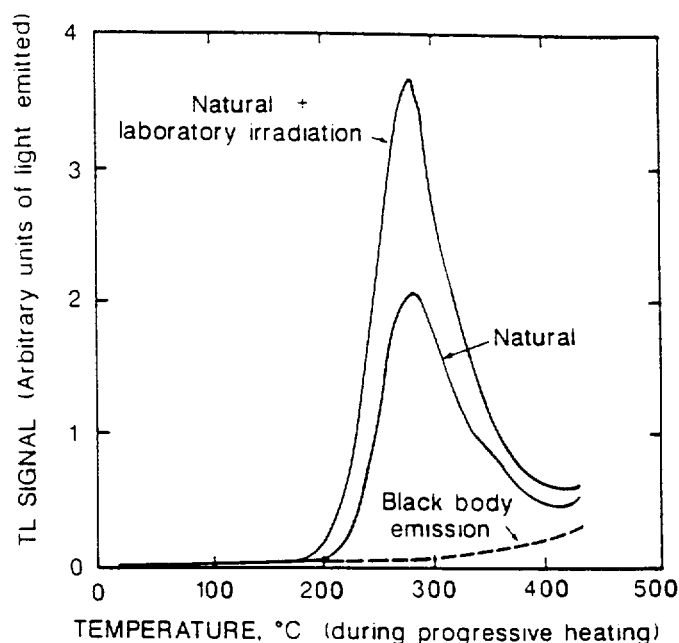


Figure 4. Natural TL glow curve and laboratory TL glow curve caused by an additional 360 gray of radiation. Material is a fine-grained poly-mineralic sediment. Samples were preheated at 150°C for 16 hours prior to glowing to enhance the TL signal above 200°C.

brated source of beta or gamma rays. Assuming that the laboratory irradiation simulates natural conditions and that TL does not decay more in nature (under long-term conditions) than in the laboratory (short-term conditions), the equivalent dose (ED) can be determined. Equivalent dose is the amount of laboratory radiation that produces a TL response "equivalent" to that of the natural sediment.

Three methods have been developed to assess ED (Fig. 5).

1. Regeneration method (Wintle and Prószyńska, 1983). The natural TL in sediment is measured and then aliquots of the sediment are bleached in the laboratory to their experimentally determined pre-depositional TL level. These aliquots then are re-exposed to increasing doses of radiation, and the level of natural TL is matched to the regenerated TL curve. ED is determined as shown on Figure 5A. This method is used predominantly on sediments that have been zeroed (light bleached) of TL prior to their deposition. These sediments are mainly wind-transported materials, such as loess and eolian sand.

2. Total bleach method (Singhvi and others, 1982). Without prior laboratory bleaching, the natural sediment is irradiated at progressive levels, and the rate of TL acquisition is defined by a sloping line shown in Figure 5B. ED is the intercept of this sloping line with the TL level induced by total light bleaching (horizontal dashed line). This method commonly is applied to eolian sediments to check for sensitivity changes relative to the

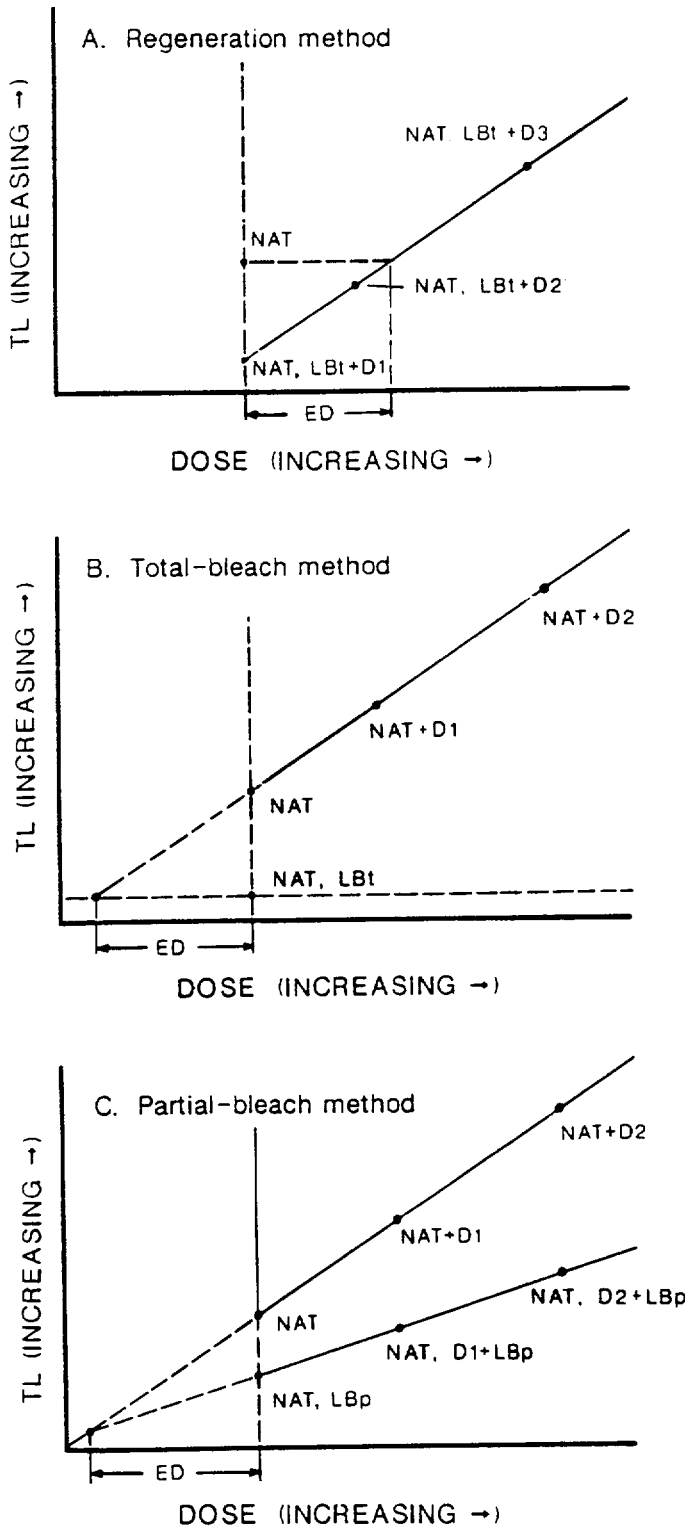


Figure 5. Three methods used to determine equivalent dose (ED) in TL dating of sediment: A) regeneration method, B) total bleach method, and C) partial bleach method. Abbreviations indicate the following: NAT, natural TL of sediment; LB, light-bleach procedure performed on sediment (LBp, partial bleach; LBt, total bleach) and D, additional incremental doses of radiation to sediment (D_1 , D_2 , D_{12}). Modified from Singhvi and Mejdahl (1985).

regeneration method and to ascertain if the growth in the TL signal is linear with increasing radiation.

3. **Partial bleach method** (Wintle and Huntley, 1980). ED is defined by the intersection of two sloping lines, as shown in Figure 5C: (1) the regression line defined by TL resulting from progressive doses of laboratory radiation on natural sediment, and (2) the regression line determined from partially light-bleached sediment that previously has been exposed to progressive doses of laboratory radiation. A level of partial bleaching that has been determined experimentally on the basis of the sediment's environment of deposition is applied. This technique commonly is used for water-lain sediments (alluvial, lacustrine, and debris-flow deposits) that may not have been fully light bleached prior to deposition (i.e., the inherited TL signal is only partially zeroed).

Depending on the type of material being analyzed, TL is measured on specific grain sizes and (or) mineral fractions. Most workers prefer the 3 to 11 μm micrometer fraction of polymineralic materials or the 100 to 300 μm fraction of quartz or feldspar grains. The radiation contributed by alpha, beta, and gamma particles is assessed most easily for these minerals and grain sizes. The 3 to 11 μm grains are exposed to the full effect of alpha, beta, and gamma radiation, whereas the 100 to 300 μm grains are incompletely penetrated by alpha and beta particles. However, there will be no apparent effect from alpha particles and there will be a reduced contribution of TL from beta particles if the outer surface of the grains are removed by acid etching. The effect of beta radiation in large mineral grains is not well understood, but it does depend on grain size (Mejdahl, 1979). Additionally, radiation generated internally may be an important contribution in the larger grains.

Wintle (1973) showed that sediments that were stored after irradiation had lost TL compared with those samples measured shortly after irradiation. This loss of TL was termed "anomalous fading" because the observed stability of the TL signal is much less than that predicted from kinetic considerations. The phenomenon is not present in all minerals, although feldspars—especially those of volcanic origin—seem to be particularly susceptible to fading (Wintle, 1973; 1977). If corrections are not made for anomalous fading, then both the ED and the TL age will be underestimated. Lamothe (1984), Berger (1984, 1985a), and Templer (1985) developed procedures to circumvent the effects of anomalous fading.

Once an acceptable value of ED has been determined, the sample's age is calculated from the following relation:

$$\text{TL Age} = \frac{\text{Equivalent Dose (ED)}}{\text{Dose Rate (DR)}}$$

where DR is the annual dose rate (grays/yr) in the material's natural environment. DR is calculated from the types and amounts of radioactive elements in the sample and their rates of production of gamma, beta, and alpha particles. The gamma component can be measured directly by placing field dosimeters

in the sediment (for as much as a year), by using a gamma spectrometer, or by elemental analysis of the sediment. The alpha and beta contributions usually are determined by measuring the alpha activity of the uranium and thorium decay chains and the total potassium content of the sample. Alpha particles are 5 to 20 percent as effective as beta and gamma particles in producing TL because of localized saturation in the alpha track (Zimmerman, 1972). The calculated dose rate (DR) commonly is corrected for absorption of alpha, beta, and gamma radiation by water in the sediment. This correction factor is the greatest potential source of error in a TL age determination for sediment because of possible variations in pore-water content during and after burial (i.e., as a result of periodic drying and wetting). An additional problem may be caused by disequilibrium of the uranium-decay chain, especially if a significant amount of radon has diffused through the sediment. For example, uranium-series disequilibrium occurs during deposition of deep-sea sediments and cave speleothems, and analysis of these materials requires using a model of time-dependent dose rates (Wintle, 1978; Wintle and Huntley, 1980). Post-depositional weathering, accumulations of secondary minerals in soils (silica, calcium carbonate, and clay), and ground-water movement also can change the amounts and types of radioactive elements in the sampled material.

APPLICATION OF THERMOLUMINESCENCE TO DATING

Only recently has TL been used as in Quaternary studies in North America. Much of the pioneering work on TL dating of sediment was on the loesses of Europe (i.e., Wintle and others, 1984). Loesses and loess-like deposits are widespread, they have paleoclimatic significance, and they have been difficult to date by methods other than radiocarbon. Eolian sediments are ideal for TL dating because they satisfy the basic criterion of exposure to sunlight during deposition.

In the United States, the preliminary studies by Johnson and others (1984) on loess from southern Mississippi indicate that the TL signal may have been accumulated linearly during the past 130,000 yr. TL ages from the Peoria Loess (late Wisconsin, latest Pleistocene) are in agreement with radiocarbon ages from the same deposits. Similar results (but having considerable scatter and showing chronologic reversals) were obtained from the Peoria Loess in Iowa (Norton and Bradford, 1985). However, three of their TL ages, from the older Farmdale Loess and Loveland Loess, are in conflict with ages inferred from stratigraphic and climatic relations. The significance of the TL dates from the older loesses is difficult to evaluate because there are only a few analyses and the basic laboratory data were not presented.

Wintle and Westgate (1986) made a detailed study of the mineralogy and thermoluminescence properties of loess interbedded with the Old Crow tephra (volcanic ash) near Fairbanks, Alaska. The TL signal in the fine fraction of the loess was prima-

rily from feldspar, which did not exhibit anomalous fading. Four determinations on loess yielded an average TL age of 86 ± 8 ka, which is consistent with geologic constraints on the tephra's age.

Significant advances have been made on TL dating of water-laid sediments. Mineral grains transported by and deposited in water are exposed to a less intense and more restricted spectrum of light than are mineral grains deposited in eolian sediments. Huntley (1985) summarized methods for dating incompletely light-bleached sediments of marine, fluvial, and lacustrine sediments. Berger's (1984, 1985a) TL studies of glacial-lacustrine silt units showed that those sediments were incompletely bleached prior to deposition. He also showed that in rapidly deposited water-lain sediments from British Columbia, Canada, feldspars were bleached preferentially over quartz. Also, the pre-depositional (inherited) TL signal of glacial silt was not significantly reset before deposition in lakes, but mudflow silts were sufficiently bleached to be dated. By using an artificial light spectrum that simulated attenuated light bleaching in the lacustrine environment, Berger (1984) obtained TL ages of 36 and 66 ka for the glacial-lacustrine silt units, in agreement with age controls based on regional stratigraphic correlations.

A similar procedure of partial light bleaching was used to date sediments of the St. Pierre interstade in southern Quebec (Lamothe, 1984). Sediments of the interstade exhibited significant anomalous fading, but delayed measurement of the post-irradiation TL signal minimized the fading; the determined TL age of 61.1 ± 9.2 ka is consistent with the enrichment radiocarbon age for the unit. TL dates for lacustrine silt units related to the past three major lake cycles in the Bonneville Basin in Utah were used to establish a local history of faulting (McCalpin, 1986). In this study, the moisture history of the sediment was reconstructed and its effects on dose rate (DR) were considered in the age determinations. The TL ages of 13 to 138 ka are compatible with accepted ages of the lacustrine units that are based on amino acid racemization ratios from shells, soil development, and the regional history of the Bonneville basin.

The TL technique also has proven useful in dating soils. Huntley and others (1983) reported TL ages for buried soils from two late Holocene archaeological sites in British Columbia. The A horizons yielded ages that agreed with radiocarbon dates from the soil parent material. Wintle and Catt (1985) studied a surface soil and two buried soils developed in Holocene deposits; they determined that the degree of light bleaching in a soil is related chiefly to the depth and degree of pedoturbation (mixing). In these soils, surface A horizons commonly are zeroed, and TL in the upper part of B horizons may be partly zeroed, depending on the extent and depth of mixing. The upper horizons of a buried soil in loess yielded apparent TL ages of 4.6 ± 0.4 ka and 7.4 ± 0.7 ka, in general agreement with a radiocarbon age from the same material. However, the lower part of the soil yielded TL ages that were younger than expected, indicating that weathering may affect TL acquisition in the loess.

TL has been applied to the dating of soluble minerals that

accumulate in sediments. The precipitation and crystallization of soluble minerals, such as calcium carbonate, gypsum, and halite, sets the TL clock of each individual crystal into motion (Zeller and others, 1955). TL has been applied with limited success to the dating of calcite stalagmites (Wintle, 1978; Hennig and others, 1980; Debenham and Aitken, 1984). Recently, the TL properties of pedogenic calcium carbonate were studied from calcic soils of known age in the Rio Grande Valley of New Mexico (May and Machette, 1984). The TL signal increased systematically in soils ranging in age from about 15 ka to at least 400 ka, but the processes of TL acquisition and dose rate history of these soils are complex and still poorly understood. Nonetheless, the method is potentially useful for dating secondary precipitates in soils and sediments.

Significant advances in the analytical techniques of TL now permit the dating of volcanic ashes (Berger and Huntley, 1983; Berger, 1985b). Due to the high temperatures involved in the eruption and deposition of volcanic ash, the ash is emplaced without inherited TL. The glass fraction from ash exhibits negligible anomalous fading and it may retain a stable TL signal for as much as 500 ka.

SUMMARY

In North America, the application of TL dating to geologic materials has gained popularity since Wintle and Huntley's (1979) study of deep marine sediments. TL has been applied to a variety of terrestrial deposits; during the past five years, intensive research on TL dating of eolian and water-laid sediments has produced new techniques that provide near-routine dating capabilities. Recently, research has expanded to chemical precipitates, volcanic ashes, and buried soils; preliminary results from these studies are promising. However, since the TL technique is still in its infancy, it should be considered experimental and should be applied judiciously. The measurement of TL and the processes of TL acquisition by natural materials are complex and not fully understood at present. Additionally, the mechanisms of bleaching by sunlight are not understood, including the physical mechanisms for different levels of bleaching. Significant problems remain in determining past dose rates, particularly where diagenetic processes have changed initial concentrations of radioactive elements.

Although the TL technique has restrictions and limitations (as do most dating techniques), the greatest asset of thermoluminescence is that it directly dates a wide variety of types and ages of sediment. Thus, the method can provide detailed chronologic information about past geologic events that cannot be dated by other methods. Study of deposits with independent dating control and clear stratigraphic relations may result in refinement of the method and may provide important information related to the effect of light bleaching in different sedimentary environments, the mobility of radioactive elements, and the moisture history of sediments.

AMINO ACID GEOCHRONOLOGY OF FOSSIL MOLLUSKS

D. R. Muhs

INTRODUCTION

In the last two decades, considerable progress has been made in using ratios of the protein amino acids in fossils, such as shell and bone, to estimate the fossil's relative or numerical age. The basis of amino acid geochronology is the observation that the protein of living organisms contains only amino acids of the L configuration. Upon the death of an organism, amino acids of the L configuration convert to amino acids with D configuration, a process referred to as racemization. Racemization is a reversible reaction that results in increased D/L ratios in a fossil through time until a D/L equilibrium ratio (1.00 to 1.30, depending on the amino acid) is reached. Thus, in a simplified view, a higher D/L ratio in a fossil indicates a relatively greater age.

Several lines of evidence suggest that amino acid ratios do not increase linearly over time; in other words, they do not follow simple, first-order reversible kinetics. Analyses of reasonably well-dated deep-sea sediments (Wehmiller and Hare, 1971; King and Neville, 1977) indicate that foraminifera experience a rapid linear change at first, followed by a much slower linear rate of change, with an uncertain area in between (Fig. 6). Fossil mollusks have been thought to follow similar, nonlinear kinetic pathways, but sufficient data to prove this are still lacking (Wehmiller, 1982). Pyrolysis experiments at elevated temperatures on modern mollusks clearly indicate that nonlinear kinetics are followed in the racemization reaction. However, some pyrolysis experiments indicate that the break in slope may occur at higher D/L ratios than is indicated by analyses of deep-sea foraminifera (Masters and Bada, 1977; Kriausakul and Mitterer, 1978). In any case, it is generally agreed that the causes of the change in rate of racemization are related to two factors: (1) racemization occurs at strikingly different rates depending on the position of the amino acid in the peptide chain (internal, terminal, or free) and (2) the changing abundances of different molecular weight components in the fossils (Wehmiller, 1984a).

Amino acid geochronology has been used in the U.S. in a wide variety of contexts in Quaternary stratigraphy, tectonics, paleoclimate, sea-level history, and archaeology. This section will only highlight some recent results on mollusks in the conterminous U.S. More detailed reviews are found in Williams and Smith (1977), Hare and others (1980), Wehmiller (1982, 1984a), Miller (1985), and Bada (1985).

FACTORS AFFECTING AMINO ACID RATIOS

Several variables are known to affect amino acid racemization rates and/or observed ratios in fossils including temperature (both the mean annual temperature and the amplitude of the

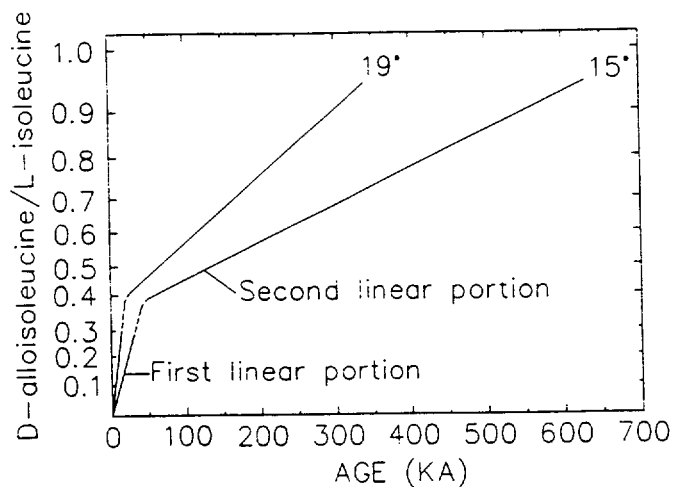


Figure 6: Possible pathways of racemization based on extrapolation of deep-sea foraminifera kinetics to higher temperatures, derived from data in Wehmiller and Belknap (1978). Particularly uncertain areas are indicated by dashed lines.

annual temperature cycle), genus, type of amino acid, and diagenetic processes (Wehmiller, 1982). Temperature history is one of the most critical factors, because higher temperatures greatly increase racemization rates. However, because of repeated climatic changes, it generally is difficult to estimate diagenetic temperature histories. Wehmiller (1982) gives a method for estimating what he calls the Effective Quaternary Temperature (EQT) of a sample from paleoclimatic data. The EQT is defined as the integrated kinetic effect of all temperatures to which a sample has been exposed during its burial history. Refinement of EQTs for various localities by Wehmiller's method will be an important advancement in amino acid studies.

An important and often overlooked factor is the effect of burial depth on temperature. Wehmiller (1977) found that average racemization rate constants varied by more than four times within a depth interval of 1.5 m in a Holocene shell midden in California, due to differences in the amplitude of the annual temperature cycle. Similar results have been reported by McCoy (1987) in the Great Basin. Often, information about depth of sampling is not given in amino acid studies, but it is clear from Wehmiller and McCoy's data that depth of burial has a considerable effect on amino acid ratios in shells from the same deposit.

The rate of racemization is not constant among different genera or among different amino acids in the same molluscan genus. Lajoie and others (1980) have reported a large number of amino acid ratios for different, co-existing genera of west coast marine mollusks from the same stratigraphic unit. Their data indicate that some genera racemize much more quickly than others (as much as 40 to 50 percent), but there is no significant

difference in rates of racemization between species of the same genus. Miller and Hare (1980) also report significant differences in amino acid ratios between different genera of nonmarine mollusks. Apparently, however, there are also reversals of this generalization in the later stages of diagenesis: in some older deposits, amino acid ratios of a given genus are greater than those of another genus, whereas the opposite relationship holds for the same two genera in younger deposits (Lajoie and others, 1980). These investigators also found that there are differences in rates of racemization among different amino acids in the same genus, with proline being most rapid and valine the slowest. Brigham (1983) conducted experiments with valves of a single species from a single deposit in order to investigate intrashell variability. Her results indicate that amino acid ratios did not vary significantly between five anatomically different shell parts; however, results from the central or hinge parts of valves had less variability about their mean values. She also found that the absolute concentrations of various amino acids did vary significantly between shell parts.

In addition to natural sources of variability in amino acid ratios, there are also differences in reported amino acid ratios due to the type of laboratory analysis used. At present, there are four analytical methods in routine use, three using gas chromatographic (GC) techniques (Kvenvolden and others, 1972; Frank and others, 1977; Hoopes and others, 1978) and one using ion-exchange liquid chromatography (LC) (Hare, 1975). The LC method is most commonly used, but the only amino acid ratio obtained is D-alloisoleucine/L-isoleucine. The GC methods are more expensive and are less commonly used, but yield D/L ratios for several amino acids, including alanine, valine, leucine, proline, aspartic acid, glutamic acid, and phenylalanine. Unfortunately, alloisoleucine and isoleucine are usually not well resolved on GC systems, so it is often not possible to compare results from GC and LC systems. Most investigators report amino acid ratios of total extractions, i.e., those including both protein-bound amino acids and those freed by natural hydrolysis. However, the pool of free amino acids contains amino acids from terminal positions where the rate of racemization is high (Kriauksakul and Mitterer, 1978), so some investigators analyze separate extractions of free amino acids as well as total extractions. In cold regions such as arctic North America, amino acid ratios in the free fraction are useful because the overall rate of racemization is low (Nelson, 1982; Miller, 1985). Interlaboratory comparisons indicate that there are differences in results on control samples (Wehmiller, 1984b). Coefficients of variation range from 3 to 18 percent, depending on the amino acid and are best for alanine, glutamic acid, and aspartic acid and worst for isoleucine, proline, and valine. Instrumental rather than wet-chemical preparation procedures are apparently responsible for most of the variability.

AMINOSTRATIGRAPHY AND RELATIVE AGES

The simplest application of amino acid ratios in geochronological studies is relative age determination and lateral correla-

tion, or aminostratigraphy (Miller and Hare, 1980). The main assumption in this approach is that the localities studied have had similar temperature histories. Stratigraphic units that have mollusks with amino acid ratios that cluster around a certain value can be identified as aminozones (Nelson, 1982).

The aminostratigraphic approach has been used with considerable success on the west coast of the U.S. by Wehmiller and others (1977), Lajoie and others (1979), and Kennedy and others (1982). Similarity of D/L leucine ratios in fossil bivalves allows correlation of discontinuous exposures of the lowest emergent marine terrace in southern California. At other localities on the west coast, small but significant differences in D/L ratios between the lowest terraces and terraces 10 to 30 m higher indicate two distinct high stands of sea that are closely spaced in time, such as high stands of ~120 ka versus high stands of ~105 ka or ~80 ka. Such results were obtained for terrace pairs in California near San Diego, Santa Barbara, and Point Año Nuevo, and on Whidbey Island, Washington. Similar results were obtained for low-elevation terrace pairs on the southern California Channel Islands by Muhs (1983, 1985). Wehmiller and others (1977) and Lajoie and others (1979) found unusually low D/L ratios in fossils collected from low terraces near Goleta and Ventura, California, and Cape Blanco, Oregon. These terraces are estimated to be on the order of 30,000 to 50,000 yr old rather than 80,000 to 120,000 yr old as is the case with low terraces found elsewhere on the Pacific coast of North America. The significance of these results is two fold: (1) the time-honored concept that the lowest emergent terrace along the Pacific coast is everywhere equivalent in age is clearly in error, and (2) significantly higher uplift rates are implied for localities where young terraces are found.

The major aminostratigraphic studies in the U.S. using freshwater mollusks have been conducted by W. D. McCoy and co-workers in the Great Basin. In the Lake Bonneville Basin, McCoy (1987) and Scott and others (1983) recognize four major aminozones related to major lake cycles. The oldest deposit is >600 ka, and the youngest is ~11 to 30 ka. In the Lahontan Basin, McCoy (1981) recognizes five major lake cycles and has distinguished three of them with amino acid ratios. Comparing amino acid ratios in shells from the last two major lake cycles in the Bonneville and Lahontan basins, McCoy (1981) suggests the cycles can be correlated.

In the midcontinent of the U.S., terrestrial gastropods in glacial tills or sediment associated with till appear to be suitable for aminostratigraphic correlation. Miller and others (1987) analyzed terrestrial gastropods from glaciated parts of Indiana and found four distinct aminozones ranging in age from late Wisconsin (~20 ka) to >730 ka. Midcontinent tills, loesses, and other sediments have considerable potential for aminostratigraphy because terrestrial gastropods are common there.

AMINOSTRATIGRAPHY USING LATITUDINAL TEMPERATURE GRADIENTS

A refinement to the aminostratigraphic approach used above was presented by Kennedy and others (1982), Wehmiller

and Belknap (1982), Wehmiller (1982), and Hearty and others (1986), who combined local aminostratigraphic data with regional temperature gradients to develop regional amino acid isochrons. The idea is based on the assumption that, while paleotemperatures along a north-south trending coastline may have differed from those of the present, regional temperature gradients have always been in the same direction. Thus, in deposits of similar age, one should expect to find systematically lower D/L ratios in fossils as one moves north into cooler latitudes. Kennedy and others (1982) used this approach for lateral terrace correlation on the Pacific coast of the U.S. (Fig. 7). They plotted D/L ratios in fossil *Saxidomus* as a function of latitude and connected geographically proximal points into isochrons. Age control for Pleistocene deposits was provided by U-series ages of coral at a few localities. Their correlations are supported by faunal aspects: terraces thought to be 80 to 105 kyr old are characterized by cool-water faunas, whereas terraces thought to be ~120 kyr old are characterized by warm-water faunas.

A similar latitudinal gradient approach to aminostratigraphy was developed for U.S. Atlantic coast marine deposits by Wehmiller and Belknap (1982). They generated latitudinal isochron plots of D/L leucine ratios in fossil *Mercenaria* and their results indicate at least six major periods of marine sedimentation. Thus, their data suggest more depositional episodes than the biostratigraphic criteria of Cronin (1980) and the multiple criteria of McCartan and others (1982). One interpretation of these conflicting results is that amino acid ratios may be more sensitive age-indicators than biostratigraphic or other criteria. For some localities, however, uranium-series age estimates conflict with amino acid results (Wehmiller and Belknap, 1982; Szabo, 1985). Wehmiller and Belknap (1982) suggest that the problem may be related to uranium-series-dated samples that have relatively low $^{230}\text{Th}/^{232}\text{Th}$ ratios. Correction for the samples with low $^{230}\text{Th}/^{232}\text{Th}$ ratios does not eliminate the conflict, however (Szabo, 1985). Also, Wehmiller and Belknap (1982) used different uranium-series age estimates of corals to calibrate their isochrons; thus the issue of agreement versus disagreement of uranium-series and amino acid age estimates depends on which deposits are selected for age comparison and which dated deposits are used for calibration.

NUMERICAL AGES FROM KINETIC MODELS

An important goal of amino acid geochronology is the development of numerical ages from amino acid ratios. Such age estimates require not only knowledge of sample temperature history but also an understanding of racemization kinetics. Some studies have assumed that racemization follows simple linear kinetics and numerical ages have been generated using independent age control on one or more deposits for calibration. For example, Mitterer (1975) assumed an age of ~124 ka for the Coffee Mill Hammock Formation in Florida and used this age estimate and some radiocarbon-dated Holocene deposits as calibration points to generate linear kinetic model ages for four older units. Al-

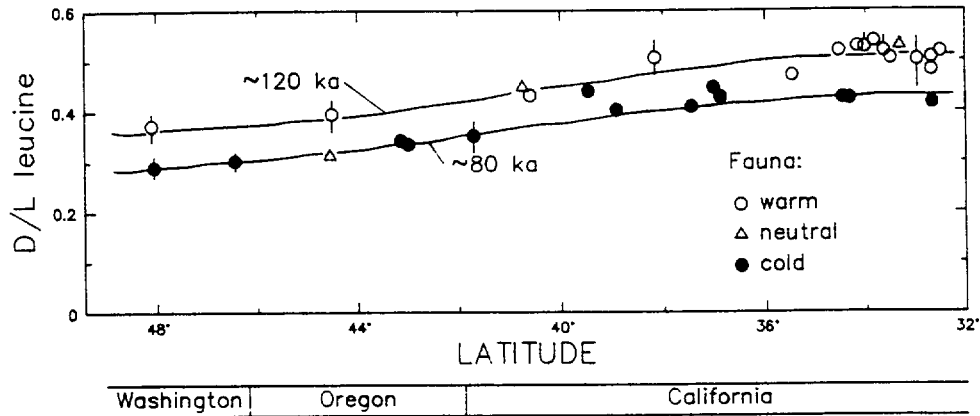


Figure 7. Latitudinal isochron plots of D/L ratios (leucine) in *Saxidomus* from the Pacific coast of the U.S. from marine terraces of the last interglacial complex. Modified from Kennedy and others (1982).

though his age estimates seemed to be reasonable based on similar dates derived from other coastlines and the deep-sea record, his results were criticized by Wehmiller and Belknap (1978), who showed that Mitterer's age estimates would require temperature histories that were incompatible with available paleoclimatic data. They showed that a nonlinear kinetic model made more reasonable assumptions about temperature history for the area, and recalculated ages for the Florida units based on Mitterer's amino acid ratios and their nonlinear model. The new age estimates are significantly older than Mitterer's original determinations.

In colder regions where the rate of racemization is low, even old deposits may have D/L ratios that fall on the first linear portion of the racemization pathway of Figure 6. In such situations, it is probably reasonable to calculate numerical ages assuming linear kinetics, and the main uncertainty remaining is temperature history; where this is the case, alternative numerical ages can be calculated using a variety of temperature history models. Nelson and Van Arsdale (1986) used such an approach for fossil gastropods found in alluvium in central Utah and used the derived ages to determine fault slip rates. A similar approach was used by Miller (1985) to develop a chronology for marine deposition in Arctic Canada.

Nonlinear kinetic models for amino acid racemization have been developed by a number of investigators. Using the assumption that foraminifera provide a reasonable analog to mollusks and extrapolating foraminifera racemization pathways to higher temperatures, nonlinear kinetic models have been used to generate numerical age estimates for marine mollusks on both the east and west coasts of the U.S. by Wehmiller and others (1977), Wehmiller and Belknap (1978, 1982), Lajoie and others (1979), Belknap and Wehmiller (1980), Wehmiller (1981), Muhs and Rosholt (1984), and Muhs (1983, 1985). Calibration for most of these studies was from deposits with coral that have U-series ages of ~120 ka. In all studies, an assumption was made that marine fossils older than ~120 ka have experienced temperature

histories similar to ~120 ka samples. On San Nicolas Island, California, nonlinear kinetic model age estimates calculated for the same terraces by Wehmiller and Belknap (1978) and Muhs (1985) disagree significantly. The problem may be related to the fact that different genera, differing numbers of samples, and different amino acids were analyzed in the two studies, but the results imply that nonlinear kinetic modeling as presented by Wehmiller and others (1977) is perhaps not universally applicable. An alternative approach that has been used by some workers is to calculate numerical ages based on linear kinetics, but to treat these as minimum-age estimates (Masters and Bada, 1977; Karrow and Bada, 1980; Muhs, 1985). Whereas the analysis presented by Wehmiller and Belknap (1978) argues convincingly against linear kinetics applied to numerical age estimates, probably there are still too few calibration points to define accurately a racemization pathway for mollusks.

ADVANTAGES OF AMINO ACID GEOCHRONOLOGY

Several factors make amino acid geochronology a particularly useful technique in Quaternary studies. One advantage is that mollusks suitable for such work are common in Quaternary deposits. A second advantage is that very small sample sizes are required, normally only 100 to 400 mg (Miller and Hare, 1980), but sometimes as little as 5 mg (Wehmiller, 1984a). This gives the investigator the possibility of analyzing the same shell for both amino acid ratios and accelerator ^{14}C dating. In addition, because individual shells can be analyzed, amino acid ratios can identify mixed populations, or deposits that contain shells of more than one age. Evidence for reworking of shells into younger deposits based on amino acid ratios has been documented by Nelson (1982). Finally, in most environments, racemization rates are low enough that amino acid ratios can be used for relative age determinations of shells that are well beyond the range of radiocarbon dating.

GSA V14 No 6

GSA V14 No 6

ABSTRACTS with PROGRAMS 1982



35th Annual Meeting
ROCKY MOUNTAIN SECTION
The Geological Society of America

SAC
T & MSS
RESOURCE CENTER

May 7-8, 1982
Montana State University
Bozeman, Montana

changes in species composition through the end of the Pleistocene and the beginning of the Holocene similar to that seen in other late Pleistocene faunas in northern Wyoming. These changes indicate the following sequence of environmental changes may have been widespread over the Northwestern High Plains during this time period: During the full Glacial (pre-15,000 RCYBP), some type of tundra conditions existed (possibly similar to that proposed for the Beringian area). This changed to a more grassland-like situation between 14,000 and 11,000 RCYBP. After 11,000 RCYBP, the extinction of the megafauna and the loss of the northern tundra and boreal forest micromammals from the Wyoming mammalian fauna indicates the environment was beginning to approach that found in the area today. Essentially modern conditions were attained sometime after 9,000 RCYBP.

ALTERATION AND VEIN MINERALIZATION, SCHWARTZWALDER URANIUM MINE, JEFFERSON COUNTY, COLORADO

WALLACE, Alan R., U. S. Geological Survey, Denver, CO 80225; and KARLSON, Richard C., Cotter Corporation, Golden, CO 80401
Carbonate-rich hydrothermal fluids produced extensive wallrock alteration and vein mineralization at the Schwartzwaldner mine. Renewed movement along pre-existing fractures during early Laramide uplift created conduits, especially in brittle gneisses and quartzites. Two stages of wallrock alteration occurred prior to uranium deposition: early carbonate + sericite, and later adularia + hematite. During this alteration, host rocks lost Si, Al, Fe, and gained K; Ca and CO₂ remained constant in calc-silicate gneisses but increased in garnet gneisses; and Na increased in garnet gneisses and decreased in calc-silicate gneiss. No ore-stage alteration is evident.

Veins formed in five stages: (1) deposition of Fe-rich carbonates, quartz, and sulfides; (2) major uranium deposition; (3) brecciation and deposition of a fine-grained carbonate matrix; (4) uranium remobilization and deposition with carbonates, sulfides, and arsenides; and (5) shearing and deposition of carbonates and sulfides. Repeated faulting complexly brecciated ore and gangue minerals.

The alteration and vein sequence indicates that fluids became progressively more alkaline and oxygenated prior to uranium deposition in stage 2. Vein minerals and fluid inclusions suggest that uranium was transported as a carbonate complex at temperatures higher than 150°C. Deposition of uranium in stage 2, and remobilization in stage 4, probably were controlled by fluctuations in P(CO₂) and P(O₂), and possibly by aqueous sulfur species. The physical properties of the wallrocks were an important control for creating sites of ore deposition, but chemical properties were apparently of minimal importance.

PATTERNS OF THRUST FAULTING IN WESTERN MONTANA AND EAST-CENTRAL IDAHO

WALLACE, C. A., RUPPEL, E. T., HARRISON, J. E., AND REYNOLDS, M. W., U. S. Geological Survey, P. O. Box 25046, Denver Federal Center, Denver, CO 80225

Between the Canadian border and the Snake River Plain, major thrust-fault systems moved thick and laterally extensive plates of rock eastward during the Mesozoic and early Tertiary. Thrust faulting took place mainly in the Cretaceous, but may have commenced as early as Jurassic and locally terminated as late as Eocene time. Thrusts generally become younger to the east. Differences in stratigraphic successions, in lithofacies, and in structural style distinguish the major plates.

Thrust plates contain Proterozoic rocks in the western part of the area and Paleozoic and Mesozoic rocks in the east. North of the Lewis and Clark line is the Rocky Mountain fold and thrust belt, which is mainly within rocks of the Belt Supergroup; east of the belt is the Montana disturbed belt, which is the frontal zone where Proterozoic and Paleozoic rocks have been thrust eastward over Mesozoic rocks of the foreland. South of the Lewis and Clark line, a similar pattern involves the Sapphire plate, the Helena salient, and again a fold and thrust belt on the east. South of the Willow Creek lineament, the thrust zones step to the west. The Medicine Lodge plate, on the west, includes Proterozoic and Paleozoic rocks, and is structurally above the Grasshopper plate, farther east, which contains younger Proterozoic and Paleozoic rocks. These major thrust plates are fringed on the east by a frontal zone of thrust-faulted Paleozoic and Mesozoic rocks. At the north edge of the Snake River Plain, the Wild Horse and Pioneer plates contain Proterozoic and Paleozoic rocks, whereas the frontal zone thrusts have transported Paleozoic and Mesozoic rocks.

ROCK GLACIERS OF THE TOBACCO ROOT RANGE, SOUTHWESTERN MONTANA

WARD, Philip N., Department of Geology, Indiana University, Bloomington, IN 47401; and HALL, Robert D., Department of Geology, Indiana University-Purdue University, Indianapolis, IN 46202

Twelve rock glaciers in eleven cirques in the Tobacco Root Range in southwestern Montana have been mapped to determine their morphology, including overall shape, long-axis orientation, and distal slope angle. In addition, their relative ages have been studied through lichenometry, clast weathering, and examination of the soil profiles. The latter study includes particle-size and geochemical analyses. Shapes range from lobate to spatulate. The slope of a rock

glacier may be related to the amount of source material, which, in turn, may be a function of the orientation of foliation planes in the cirque walls. All of the rock glaciers appear to be stable and inactive as evidenced by a substantial lichen cover. However, fresh collapse features may indicate the presence of some remaining interstitial ice. Two advances of the rock glaciers have taken place in several of the cirques, with the lobe of the second advance superimposed on the first. However, other cirques contain smaller rock glaciers, apparently associated with only one of the advances.

MECHANICAL CONTROLS ON THE FORMATION OF NORTH AMERICAN INTRACRATONIC BASINS DURING THE PALEOZOIC

WASHINGTON, Paul A., Department of Geology and Geography, Weber State College, Ogden, UT 84408

Sedimentary basins which formed within the interior of the North American craton during the Paleozoic can be correlated with orogenic events along the borders of the continent. Subsidence within any given basin occurred only during relatively short intervals, coinciding with major orogenic events, separated by long periods of stability. Each orogenic event is associated with a distinctive pattern of active basins.

Compressive events are accompanied by either rectangular or linear arrays of basins. The rectangular arrays are similar to interference sine-wave pattern predicted by plate buckling theory. The linear arrangements of basins resemble the patterns expected within wide ductile shear zones. Major strike-slip movement along the cratonic margins produces similar linear basin arrays. The Paleozoic intracratonic basins of North America, therefore, appear to have formed totally in response to tectonic events along the borders of the continent.

CONODONT COLOR VS. STRAIN: AN ADDITIONAL FACTOR

WASHINGTON, Paul A., and MCCARTNEY, Kevin P., Department of Geology and Geography, Weber State College, Ogden, UT 84408

Just as previous studies have shown that conodont color is a function of peak metamorphic temperature, there is also a correlation between strain and conodont color. By studying the color of conodonts collected from single limestone outcrops exhibiting large variations in strain, it is found that as strain increases, the conodont color index also increases.

In order to minimize variations in temperature, samples were taken where large variations in strain could be observed in less than 10 meters. Strain values were determined for these same localities using both fossil distortion and the calcite twin gauge. Most localities were within the Mississippian Gardison limestone near Ogden, Utah.

The relationship found by this study complicates the application of conodont color to regional temperature studies. In fact, the results of the original study of conodont colors in the Appalachians can be reinterpreted to show just as strong a correlation with strain values.

FOSSIL PATTERNED GROUND AND ROCK GLACIERS IN THE RUBY MOUNTAINS, NEVADA

Wayne, William J., Department of Geology, University of Nebraska, Lincoln, NE 68588.

Distribution of fossil rock glaciers and patterned ground, which are forms produced in permafrost areas, can help in the establishment and interpretation of past climatic conditions. Rock glaciers developed in many of the cirques of the Ruby-East Humboldt Range in Nevada during the late Wisconsinian deglaciation; some were active again at least once during Holocene time. Sorted stripes and circles are abundant on slopes and flats above the tops of the valley glaciers in the range; none are active today, however. Most of the 22 fossil rock glaciers recognized through airphoto study are small lobate forms, but one fills its valley in the manner of a debris-covered glacier, and 5 began as rockfalls that buried and insulated glacial ice until the adjacent clean ice had disappeared during the late phases of the Angel Lake (=Pinedale) Age. Three of these 5 show a Holocene lobate redevelopment, as do three of the lobate rock glaciers. At least 4 of the small lobate rock glaciers seem to be wholly neoglacial.

Of the 22 rock glaciers in the range, 16 are oriented between N30°W and N45°E; 4 of the remaining 6 are oriented generally to the east, 2 toward the west. Their altitudes range from 2440 m to 3080 m. All four that are lower than 2700 m formed as debris-covered glacier ice. Lobate rock glaciers, which form as a permafrost feature, suggest that the mean annual 0°C isotherm in the range was no higher than 2400 m during late Angel Lake time and only slightly higher during at least one of the Holocene neoglacial periods. The estimated present mean annual temperature at 2400 m is approximately 5.2°C. Sorted circles of Angel Lake age at 3000 m near the north end of the range tend to confirm the paleotemperature estimate. Lack of precipitation, rather than significant warming, probably caused Angel Lake deglaciation and absence of neoglaciation.

LATE QUATERNARY GLACIATIONS OF THE TALKEETNA MOUNTAINS, ALASKA

WELSCH, Dennis, and GOODWIN, Robert, Woodward-Clyde Consultants, Santa Ana, Calif., 92705, and TEN BRINK, Norman, Geology Dept., Grand Valley State, Allendale, Mich. 49401

Pre-Wisconsinian (Illinoian?) glaciers from the Talkeetna Mountains and the Alaska Range merged to form piedmont glaciers that inundated the Talkeetna Mountains up to 5000 ft. During the early Wisconsin Clear

MIDDLE QUATERNARY SAND RAMPS IN THE SOUTHERN GREAT BASIN, CALIFORNIA AND NEVADA

No 70228

WHITNEY, John W., SWADLEY, W. C. and SHROBA, Ralph R., U.S. Geological Survey, Federal Center MS 913, Denver, CO 80225

Sand ramps are unique, little-studied landforms in the southern Great Basin that occupy positions similar to those of alluvial fans. They are underlain by multiple deposits of eolian sand, significant portions of which have been reworked by hillslope runoff and mixed colluvial gravel. In places, sand was blown against hills and mountains during dry and windy Pleistocene climatic episodes as long ago as 0.75 m.y. Preliminary mineralogic study suggests that sandy areas on the adjacent basin floors were the primary sources.

In 1954, H.T.U. Smith described sand ramps as sand aprons and suggested that they had formed during the dry, middle Holocene Altithermal interval. Our investigations, however, show that the sand ramps are composed of sheets of gravelly sand and interbedded buried soils as old as middle Quaternary. As many as ten buried soils are exposed in deep gullies cut into the sand ramps. At four localities in the northern Amargosa Desert, two identifiable volcanic-ash beds provide limiting ages for the sand ramps, interbedded soils, and faults that disrupt the sand sheets. An ash bed of Bishop Tuff, dated at 0.74 m.y., is near the base of the sand ramp at each locality. At Busted Butte, Nevada, an unidentified rhyolitic ash bed is about 4 m above the Bishop ash bed. Also at Busted Butte, but in a different exposure, basaltic ash that is correlated with 0.24-m.y.-old basalt is present near the surface of the sand ramp. Gullies in the sand ramps probably formed during the late Quaternary. Late Quaternary sand is concentrated at the toe of the sand ramp by infrequent storm runoff.

The sand ramps consist of the oldest Quaternary "eolian" deposits in the southwestern U.S. and contain a wealth of Quaternary paleoclimatic, pedologic, and tectonic information.

BROAD INFLUENCES OF TOPOGRAPHY AND PLANETARY ROTATION IN ESTABLISHING THE EOLIAN PATTERN IN THE WESTERN DESERT OF EGYPT AND NEIGHBORING COUNTRIES

No 76853

WHITNEY, Marion T., Central Michigan University, Mt. Pleasant, Michigan 48859

Eolian forms, erosional and depositional, in western Egypt and neighboring countries are principally linear and oriented essentially with the unidirectional wind—northwesterly in the Horse Latitudes, north-easterly in the Tropic of Cancer, making a huge clockwise gyre of near trends. The primary influence in establishing this eolian pattern is response of atmosphere to the rotation of the planet. The secondary influence, causing some deviation in trend and modification of linear form, is due to aerodynamic response of atmosphere to topography such as broad swells over plateaus, abrupt changes at escarpments and division and closure of streamlines around local hills or regional massifs.

The Limestone Plateau and lesser highlands, rising from sea level constitute broad swells, serving like giant airfoils, forcing wind to rise and form trains of vortices that create long corridors, flanked by limestone yardangs in the eastern part of the plateau.

Dune form changes over the broad swells. From whalebacks in lowlands, long seif dunes finger out over the swell, then alter to barchan dune trains near southward-facing escarpments where sudden updraft complicates the aerodynamics. Southward, barchan trains merge into sand plains, but the linear form persists as alternating light and dark streaks, caused by division and closure of streamlines around sandstone hills, blackened with desert varnish. Acceleration in the division erodes the varnish and pebbles. Closure of the streamlines segregates the dark materials for hundreds of kilometers in the lee of the hills.

TECTONIC GEOMORPHOLOGY ON THE COASTAL PLAIN OF SOUTHWEST COLOMBIA

No 57633

WHITTECAR, G. Richard, BABUIN, Michael L., BARRINGER, Richard A., and DARBY, Dennis A., Department of Geological Sciences, Old Dominion University, Norfolk, VA 23508

Landforms and patterns of fluvial sedimentation within the lower Rio Patia drainage basin reflect the influence of Quaternary tectonism. Dissected alluvial fans along the toe of the Cordillera Occidental contain very coarse-grained gravels deposited by high-gradient braided streams. Radiocarbon dates and the degree of soil development indicate the fan-forming uplift(?) occurred during the Pleistocene. Fracture pattern analyses of rectified stream segments incised into the Quaternary alluvium suggest strong structural control by major Andean faults. Anticlinal uplift near the coast during the Holocene(?) produced areas of radial drainage, altered the courses of large streams by piracy, and induced slow aggradation of upstream levees. These levees dammed lacustrine lakes in small tributary valleys. Anomalous trends in levee sedimentation suggest that upstream propagation of the effects of uplift occurs by slope reduction and by hydraulic ponding of tributaries during floods. Stream profiles developed prior to this Holocene uplift control the lateral extent of the hydraulic ponding effects.

EVIDENCE FOR A LOWER CRUSTAL ORIGIN OF HIGH-AL ORTHOPYROXENE MEGACRYSTS IN PROTEROZOIC ANORTHOSESITES

No 73193

WIEBE, R. A., Geology Dept., Franklin and Marshall College, Lancaster PA 17604-3003

Nodules and xenocrysts dominated by high-Al orthopyroxene (HAO) occur in strongly chilled Proterozoic basaltic dikes which cut the Nain anorthosite complex, Labrador. HAO (En 73-68, Al₂O₃ = 6.5-4.5) lacks exsolution; it occurs both as anhedral xenocrysts up to 10 cm in diameter and with euhedral plagioclase (An₅₅) in optitic nodules. Rarely, olivine occurs with HAO and Al-spinel with plagioclase. Scarce Fe-rich nodules contain: (1) opx + pig, (2) aug + pig, and (3) coarsely exsolved ulvöspinel. Pyroxene pairs yield T's of 1250 to 1170°C, whereas coexisting lamellae in exsolved ulvöspinel yield T's between 1145 and 1120°C, with f₀₂ near the WM buffer. If all nodules came from a similar depth, the rare occurrence of olivine with plagioclase suggests a maximum pressure of about 11 kb. The high subsolidus T's of the nodules contrasts with the low T of the host anorthosites at the time of dike emplacement and hence indicates a deep source for the nodules.

HAO is nearly identical in composition to the high-Al orthopyroxene megacrysts with exsolved plagioclase (HAOM) found in most Proterozoic anorthosites. Many nodules of plagioclase and HAO also have textures comparable to optitic occurrences of HAOM in anorthosite. Rafting of cotectic nodules from the lower crust could explain occurrences of HAOM in shallow-level anorthosites.

The nodules and xenocrysts are samples of lower crustal cumulates. Their compositions suggest that they were produced by magmas similar to those that were parental to the anorthosites. They lend support to models which derive anorthosites by fractional crystallization of basaltic magma.

EARLY MESOZOIC RECONSTRUCTIONS, TECTONICS AND PALEO-GEOGRAPHY OF CARIBBEAN-GULF OF MEXICO-ATLANTIC AREA

No 75582

R. W. Wiener and I. O. Norton, Exxon Production Research Company, P. O. Box 2189, Houston, TX 77252-2189

Five plate reconstructions with paleogeography show the evolution of the Gulf of Mexico-Caribbean-Atlantic from Late Triassic through Late Jurassic time. The reconstructions are constrained by oceanic geophysical data, by the distribution of Paleozoic tectonic belts and early Mesozoic sedimentary and igneous rocks, and by restoration of post-Jurassic faulting.

Late Triassic rifting formed grabens in which continental sediments and tholeiitic volcanics accumulated. Overlying salt was deposited from ingress of Tethyan waters into circum-Atlantic grabens. Oceanic crust formed in the Atlantic about 165 m.y. ago, followed by a spreading-center jump about 160 m.y. ago. The NA/SA-Africa plate boundary was a zone of intracontinental faulting from the left-lateral Bahama fracture zone to a zone of normal and strike-slip faulting in the Gulf, to the left-lateral Mojave-Sonora megashear. In western North America subduction of Pacific crust and calc-alkaline igneous activity occurred throughout the Jurassic, associated with sea-floor spreading in the Atlantic and westward motion of North America.

Sea-floor spreading began in the proto-Caribbean in the middle Jurassic, while only rifting occurred in the Gulf of Mexico, where the Louann salt was deposited from Pacific waters. In the late Jurassic, steepening of the Pacific subduction zone resulted in back-arc extension in Mexico. At the same time, sea-floor spreading began in the Gulf of Mexico, resulting in marine transgression. In the late Oxfordian, spreading center reorganization occurred in the Gulf. Movement ceased on the Mojave-Sonora megashear and began on the Salina Cruz right-lateral fault. In latest Jurassic spreading ceased in the Gulf, but continued in the proto-Caribbean.

DIAGENETIC FEATURE OF A CRETACEOUS CLASTIC SHORELINE SEQUENCE, NORTHERN GREAT PLAINS PROVINCE

No 69419

WILDE, Edith M., Montana Bureau of Mines and Geology, Montana Tech, Butte, MT 59701

The Fox Hills Formation (youngest formation of the Montana Group) is, geographically, a very extensive, although thin unit which extends from central Canada southward through Montana, the Dakotas and Wyoming. This predominantly silty sandstone and shale unit records the final withdrawal of the epicontinental sea from the western interior of the United States. This typical shoreline sequence crops out along the flanks of the 150 mile (240 km) long Cedar Creek anticline, which extends southeastward from eastern Montana into northwestern South Dakota.

Evidence indicating multiple source areas for these sediments includes the content of probable volcanic grains, metamorphic and sedimentary rock fragments, and quartz and calcite grains with inclusions of matrix materials. Diagenetic features include quartz overgrowths, more extensive alteration of K-spar than plagioclase, clay alteration of rock fragments, and formation of authigenic rims on most grains.

An assemblage of chlorite, montmorillonite, calcite and minor dolomite is characteristic of distributary channel and river-mouth bar facies. Illite, kaolinite and montmorillonite with minor calcite are more common in beach, crevasse splay and subtidal environments.

Differences in clay assemblages indicate the primary influence of depositional environments on clay formation. The presence of montmorillonite and probable volcanic grains in most depositional environments may indicate that montmorillonite formed as an in situ weathering product of widespread volcanic sediments.

ABSTRACTS with PROGRAMS 1985

98th Annual Meeting

The Geological Society of America

The Paleontological Society (77th)
The Mineralogical Society of America (66th)
The Society of Economic Geologists (65th)
Cushman Foundation (36th)
Geochemical Society (30th)
National Association of Geology Teachers (26th)
Geoscience Information Society (20th)

**OCTOBER 28-31, 1985 ORLANDO, FLORIDA
ORANGE COUNTY CONVENTION/CIVIC CENTER**

ABSTRACTS WITH PROGRAMS, VOL. 17, NO. 7, 1985 ANNUAL MEETING

ISSN 0016-7592

ABSTRACTS with PROGRAMS 1988



84th Annual Meeting

CORDILLERAN SECTION

The Geological Society of America

with the
Paleontological Society of America
Pacific Coast Section

**March 29-31, 1988
The Las Vegas Hilton Hotel
Las Vegas, Nevada**

Volume 20, Number 3, February 1988
ISSN 0016-7592

°C, 9 (±1) kb for kyanite-staurolite schists. These quantitative results are consistent with estimates based on mineral assemblages in Skagit ultramafic rocks. Additional evidence for high pressure is the presence of coexisting staurolite and hornblende in amphibolites. Garnets in both sillimanite gneisses and kyanite-staurolite schists were homogenized by extensive intracrystalline diffusion, indicating high (> 650 °C) temperatures.

Peak metamorphic pressures were under kyanite grade conditions. Matrix sill grew from ky during decompression in pelitic rocks in which $T > 700$ °C. Decompression was nearly isothermal ($dp/dT \sim 70$ bars/°C). Evidence for decompression includes the following: (1) armored relics of ky, st, and rutile in garnet in sill gneisses, (2) symplectite rims around Ca-rich garnets, (3) Ca decrease at garnet rims, and (4) anthophyllite + forsterite in ultramafic rocks.

Anatectic P-T conditions were attained during the Skagit metamorphism. Previous studies have proposed subsolidus processes for the migmatization of the Skagit Gneiss. Fluid inclusion data may provide additional evidence for partial melting: primary, dense CO₂ fluid inclusions in quartz in the migmatites may have formed when H₂O from an H₂O-CO₂ metamorphic fluid was partitioned into the melt phase during anatexis. At the P-T conditions determined, the infiltration of fluid would initiate partial melting along the path of the fluid.

№ 3949

DECIPHERING QUATERNARY ALLUVIAL HISTORY IN LAS VEGAS WASH, NEVADA BY RADIOCARBON AND ROCK-VARNISH DATING

WHITNEY, J.W., U.S. Geological Survey, Federal Center MS 913, Denver, CO 80225; HARRINGTON, C.D., Earth and Space Sciences Division, Los Alamos National Laboratory, Los Alamos, NM 87545; and GLANCY, P.A., U.S. Geological Survey, 705 North Plaza St., Carson City, NV 89701

Recent downcutting in Las Vegas Wash has exposed over 10 m of fine-grained alluvial fill that radiocarbon-dated charcoal and organic mats indicates was deposited mostly during the last 3000 years. Remnants of earlier alluvial fills are preserved within the narrow canyon of the lower wash and suggest that the alluvial history of the wash was dominated by several major episodes of aggradation and subsequent downcutting.

Dating the older alluvial surfaces and deposits is difficult because dense calcium carbonate, volcanic ash, vertebrate fossils, and other datable materials are absent or rare. Rock varnish, however, is present on all surfaces and was used to distinguish fills of different ages by comparison of varnish cation ratios (K+Ca/Ti), and to estimate times when these surfaces stabilized. Varnish sampling was difficult on broad, low-gradient surfaces because sheet flooding has worked many surface cobbles. Large non-reworked boulders were selected for analysis wherever possible.

Two alluvial surfaces dominate the topography of Las Vegas Wash. They are approximately the same height above the modern stream, but varnish on their surfaces yield significantly different cation ratios. Preliminary analyses suggest the older alluvial surface stabilized about 1.2 Ma, whereas the surface of the younger fill, which may correlate to the Chemsheuvi Formation in the Colorado River Valley, stabilized about 0.34 Ma. Rock-varnish dating indicates that the two major alluvial surfaces in Las Vegas Wash formed during the early and middle Pleistocene.

№ 24350

THE BIOTROME-FORMING ORGANISM *PALAEOAPLYSINA* FROM THE LOWER PERMIAN MCCLLOUD LIMESTONE OF NORTHERN CALIFORNIA

Wilson, Edward C., Natural History Museum of Los Angeles County, 900 Exposition Blvd., Los Angeles, CA 90007 and WATKINS, Rodney, Department of Geology, California State University, Chico, CA 95929

Palaeoaplysina Krotov, 1888 is a biotrome-forming organism known from the Pennsylvanian and Lower Permian of western Russia, the Arctic, Idaho, and California. It is a calcareous fossil, consisting of broad tabular plates that are cellular and pierced by numerous canals which open as fine pores on one surface of the plates. Although the genus has been referred to the Porifera, Coelenterata, and algae, its systematic position remains uncertain. *Palaeoaplysina* is locally abundant in fusulinid zones A and D (Wolfcampian) of the McCloud Limestone where it forms biotromal horizons up to 4 meters thick. It also occurs as a minor constituent in the formation in siliceous boundstones and as rare plates in packstones and wackestones that are dominated by non-colonial taxa. Unabraded plate fragments up to 20 cm long are oriented subparallel to bedding and are self-supporting but unattached. The pore-bearing surfaces of the plates generally face upwards. Well-preserved specimens show irregularly polygonal cells 0.07 to 0.4 mm in diameter, gradually increasing in cell size from the porous to the non-porous surface of the plates. *Palaeoaplysina* forms as much as 51 percent of the sediment volume and is associated with common phylloid algae and less abundant crinoid debris, bryozoans, brachiopods, gastropods, solitary rugose sponges and fusulinids. An encrusting fauna of *Spirorbis* is common on the phylloid plates but rare on *Palaeoaplysina*.

№ 3327

HYDROLOGIC SETTING OF YUCCA MOUNTAIN, NEVADA

WILSON, William E., U.S. Geological Survey, P.O. Box 25046, M/S 421 Denver Federal Center, Denver, CO 80225

Yucca Mountain is in the Alkali Flat-Furnace Creek Ranch groundwater subs basin. Saturated-zone flow occurs in alluvium, volcanic tuff, and carbonate rocks, and generally is from north to south. Modeling indicates that about 45 percent of recharge may occur through Fortymile Wash, about 5 kilometers east of Yucca Mountain. Discharge occurs as evapotranspiration (65 percent) and spring flow (35 percent). Beneath Yucca Mountain, the potentiometric surface is steep in the northern and western parts and is almost horizontal in the eastern and southern parts.

The unsaturated zone beneath Yucca Mountain is 500 to 750 meters thick. The hydrogeologic units consist of alternating layers of welded and nonwelded tuff. In comparison to the nonwelded tuffs, the welded tuffs characteristically have greater fracture density, much smaller matrix saturated hydraulic conductivity, and smaller matrix porosity. The Ghost Dance fault transects the site and may be a conduit for flow. Unsaturated-zone flux beneath the proposed repository zone is estimated to be about 0.5 millimeter per year. At depths greater than the proposed nuclear-waste repository, unsaturated-zone flow probably is predominantly in the matrix, but factors controlling fracture and matrix flow are not well understood.

The potential effects of future climatic changes on hydrologic conditions are being evaluated by modeling, interpreting paleohydrologic evidence, and studying sites that are modern analogs of Quaternary hydrologic conditions.

№ 24393

EARLY PROTEROZOIC CHRONOLOGY OF THE EASTERN MOJAVE DESERT

WOODEN, J.L., MILLER, D.M., HOWARD, K.A., MS 937, U.S. Geological Survey, 345 Middlefield Rd., Menlo Park, CA 94025

Pb and Nd isotopic data show that the early Proterozoic rocks of the SW U.S. can be divided into two major crustal terranes - Mojave and Arizona - along a N-S boundary in western Arizona. This distinction is supported by geochronologic data (U-Pb zircon) for the E. Mojave Desert that indicate a different pre-1710 Ma history for each terrane. The oldest basement recognized in the Mojave is metasupracrustal rocks that contain zircons with complex U-Pb systematics (as the result of episodic Pb loss at 1700 Ma) and variable Pb-Pb ages (1700 - 1975 Ma, N. New York; 1800 - 1920 Ma, E. Ivanpah; 2100 - 2300 Ma, Turtle Mtns.). The origin of this older crustal component is uncertain (detrital; older in situ crust; other?); however, its presence partly explains the distinct isotopic signature of the Mojave, and similar rocks are not presently recognized in C. AZ. Metaplutonic rocks about 1760 Ma old (approx. age of older plutonics in C. AZ) intruded this basement in the E. Ivanpah Mtns. and possibly in the N. New York Mtns. Although much of the SW U.S. experienced an event at 1700-1710 Ma ago (a time of crustal suturing?), high-grade metamorphism (low P) and strong deformation occurred in the E. Mojave in contrast to the shallower and weaker events in AZ. The intensity of this event in the Mojave masks its earlier history; but the protoliths for widespread, siliceous and K-rich, granitic gneisses appear to have been emplaced shortly before the high-grade event (1708, 1710 Ma, N. New York; 1710 Ma, N. Providence; 1713 Ma, McCullough; 1726 Ma, Piute Mtns.). The post-1700 Ma history of the E. Mojave is similar to that of AZ. There was minor plutonism in the E. Mojave at about 1695 Ma ago (a stronger event in AZ) which was followed by a major intrusive event between 1683 and 1672 Ma ago (poorly known in AZ). This later event includes some of the major megacrystic granites of the Mojave such as the Fenner "gneiss". Later plutonism at 1660 and 1640-1630 Ma ago in the Mojave is volumetrically less significant, but matches intrusive events in southern AZ.

№ 2169

OBSERVATIONS ON A TECTONIC MAP OF THE DEATH VALLEY REGION, CALIFORNIA-NEVADA

WRIGHT, L.A., Dept. of Geosciences, Pennsylvania State University, University Park, PA 16802

A recently compiled tectonic map of Death Valley and vicinity, south of latitude 37°00', includes a chronology of Cenozoic rock units based on ⁴⁰K/^{Ar} age determinations. The map shows features, heretofore unrecorded or more clearly delineated than on available geologic maps, providing evidence that: (1) most or all of the 12 Ma and younger rock units of the Central Death Valley igneous field lie, in the manner of a rhombochiasm, between the en echelon terminations of the NW-trending, right-lateral Furnace Creek and Sheephead fault zones; (2) the Black Mt. block is cut by numerous NNE-striking faults younger than 5 Ma; (3) palinspastic restoration of these young displacements delineates a major branch of the Sheephead fault zone that once curved N to NE to become a gently SE-dipping normal fault (the Sheephead detachment) of regional extent and active from pre-10 Ma to ~5 Ma; (4) the Amargosa chaos is attributable to collapse of the shallow, western part of the upper plate above a NW-moving lower plate; (5) the highly faulted Virgin Spring phase of the chaos records mainly pre-10 Ma extension, whereas the less faulted Calico phase records extension and accompanying listric normal faulting contemporaneous with and following most of the volcanic activity (10 Ma to 5 Ma); (6) basic volcanism has alternated with intermediate and acidic volcanism, beginning as early as ~11 Ma and occurring most extensively within the 4 Ma to 5 Ma interval when much of

Stream capture followed deposition of Q_2 , eliminating upvalley sediment contributions to the Yucca Wash alluvial fan. As a result, sufficiently old strain gauges (Q_1 and Q_2) are preserved across northern Midway Valley to assess possible north-trending faults. Surficial units near prospective surface facilities include Q_1 to Q_3 . Stratigraphic relationships suggest that younger units (Q_2 to Q_3) are thin (1 to 2 m) and overlie older units more suitable for assessment of low slip rate faults.

To assist the identification of possible Quaternary faults, photolineaments were mapped in Midway Valley. Photolineaments of possible tectonic origin were identified in colluvial/alluvial units along the Paintbrush Canyon and Bow Ridge faults; however, no displacement of surficial surfaces has been recognized across lineaments in other parts of the valley. Photolineaments near potential surface facilities have been identified as possible "targets" for future site-specific trenching activities.

This work was performed for the U. S. Department of Energy, Yucca Mountain Site Characterization Office, under contract DE-AC04-76DP00789.

03:30 p.m. O'Neill, J. M.

No 1384

STRIKE-SLIP FAULTING AND OROCLINAL BENDING AT YUCCA MOUNTAIN, NEVADA: EVIDENCE FROM PHOTOLOGIC AND KINEMATIC ANALYSIS

O'NEILL, J. M., WHITNEY, J. W., and HUDSON, M. R., U.S. Geological Survey, M.S. 913, Federal Center, Denver, CO 80225

The main structural grain at Yucca Mountain, as seen from low-sun angle aerial photographs, is a pronounced north-trending linear fabric defined by parallel, east-dip-sloping fault blocks. Fault-block ridges are bounded on the west by normal faults that appear as isolated, colinear scarps in alluvium and as offset bedrock units. All ridge-bounding faults in this area are structurally connected to adjacent subparallel faults, most commonly by short north-west-trending fault splays. The generally north-trending high-angle faults primarily display down-to-the-west normal offset but also have a minor, auxiliary component of left-lateral slip. Left-lateral slip is indicated by (1) an echelon fault splays that are structurally linked, commonly by north-west-trending pull-apart zones, (2) slickenlines, and (3) apparent offset of stream channels. These pull-apart zones range from tens of meters to more than 3 kilometers wide. The smallest pull-apart zones are well developed along the Windy Wash and Solitario Canyon faults on the west side of Yucca Mountain. The largest of these features is interpreted to structurally link the Bow Ridge and Solitario Canyon faults in the north-central part of Yucca Mountain, directly south of Yucca Wash; the pronounced north-west-trending drainage system in this northern part of Yucca Mountain appears to be controlled by tension fractures related to the left-lateral component of movement on these north-trending faults. Midway Valley, directly east of the large pull-apart zone, may also owe its origin, in part, to a pull-apart mechanism.

Paleomagnetic data collected from Miocene ash-flow sheets indicate that Yucca Mountain has undergone clockwise vertical-axis rotation as large as 10° . This rotation increases to the south and began about 13 Ma. The left-lateral component of slip along Yucca Mountain faults is interpreted to reflect displacements between rigid fault blocks within a structural domain undergoing clockwise, "domino style" rotation. Evidence of left-lateral slip in Quaternary deposits suggests that clockwise rotation is an ongoing process.

03:45 p.m. Whitney, John W.

No 1399

QUATERNARY MOVEMENT ON THE PAINTBRUSH CANYON-STAGECOACH ROAD FAULT SYSTEM, YUCCA MOUNTAIN, NEVADA

WHITNEY, John W. and MUHS, Daniel R., U.S. Geological Survey, Box 25046, M/S 913, Denver, CO 80225

The north- to northeast-trending Paintbrush Canyon-Stagecoach Road fault system is a primary fault system for which maximum vibratory ground motion and surface displacement will be calculated for the design of the potential underground repository at Yucca Mountain and adjacent surface facilities in Midway Valley. The fault system is 33 km long, near the east edge of Yucca Mountain, and well exposed along five segments. The three southern segments show Quaternary fault activity over distances of 3-4 km on each segment, and Quaternary movement is suspected, but not proven, on the northern segments. Slickenlines exposed on Tertiary-age fault breccia on the three southern segments demonstrate a component of left-lateral slip with rakes as great as 47° . Deflected and offset stream channels that cross the Fran Ridge and Stagecoach Road fault segments suggest that left-lateral oblique movement has continued during the Quaternary.

Faults and fractures are exposed to a depth of about 20 m in deep arroyos cut into sand ramps on the west flanks of Busted Butte and Fran Ridge. At least four, probably five, soils are present in the sand ramps; all are offset, but not all soils are exposed in each arroyo. An apparent maximum dip-slip displacement of 4.1 m was measured on the deepest soil exposed at Busted Butte. This soil has a maximum age of about 700,000 yr, for it overlies an eolian sand unit that contains the 738,000-yr-old Bishop Ash. Assuming oblique fault movement of about 45° during the last 700,000 yr for a preliminary fault assessment, the total oblique slip would be 5.8 m since the beginning of the middle Pleistocene, or a slip rate of 8.3 mm/ka (0.0083 mm/year).

Five episodes of fault movement have offset four soils at Busted Butte. The latest episode of faulting at Busted Butte probably occurred during the late Quaternary. Results of uranium-series dating (a closed-system method) of $CaCO_3$ in the buried soils indicates that some samples have experienced open-system conditions. Consequently, the U-series method may not be reliable on soils in sand ramps at Yucca Mountain.

04:00 p.m. Gibson, J. Duane

No 7648

RECENT DEVELOPMENTS AFFECTING PRECLOSURE SEISMIC HAZARD ASSESSMENT FOR THE POTENTIAL NUCLEAR WASTE REPOSITORY AT YUCCA MOUNTAIN, NEVADA.

GIBSON, J. Duane, Sandia National Laboratories, P. O. Box 5800, Organization 6315, Albuquerque, NM 87185-5800.

Considerable work has been performed by many organizations in the last decade that is relevant to seismic hazard assessment for the potential high-level nuclear waste repository at Yucca Mountain in southwestern Nevada. Recent developments include: (1) decreased confidence in the assignment of numerical ages of the Quaternary units, which could affect timing of fault movement, and (2) improved estimation of expected ground motion and rupture hazards by deterministic and probabilistic methods. Results from various studies are evaluated for the approximately 100-year-long preclosure period of constructing, operating, and decommissioning the repository.

Determining the timing and rate of seismic activity is dependent on accurate dating of displaced stratigraphic and geomorphic features. Several dating techniques, such as Uranium-series, Uranium-trend, thermoluminescence, and rock varnish, have been utilized at Yucca Mountain. In some cases, different dating techniques provide markedly different ages for the same unit. As found in the case of the Lathrop Wells volcanic cone, ages of Quaternary units determined by different methods may vary by as much as an order of magnitude. Inconsistencies in the apparent age of Quaternary units result in increased uncertainty in slip rate, recurrence interval, and age of last movement for faults, all critical inputs to seismic hazard analysis.

Numerous deterministic and probabilistic seismic hazard studies have been performed at Yucca Mountain. A recent deterministic study predicted the most likely peak ground acceleration as 0.4 g, resulting from rupture of the Bare Mountain Fault, which is 14 kilometers west of Yucca Mountain. In contrasting probabilistic studies, calculated annual probabilities for exceeding a peak ground acceleration of 0.4 g range from 10⁻¹ to less than 10⁻⁴. The ground rupture hazard of exceeding 10 centimeters vertical displacement at the surface facilities has been estimated at less than 10⁻⁸. All of these hazard analyses contain large uncertainties, owing to the limited site-specific data. These uncertainties are countered and the seismic hazards mitigated, at least in part, by the safety factors incorporated into the design of the surface facilities. New geologic data, especially from paleoseismic studies, must be collected and factored into seismic hazard analyses so that results can be validated and uncertainties reduced.

This work was performed for the U. S. Department of Energy, Yucca Mountain Site Characterization Office, under contract DE-AC04-76DP00789.

04:15 p.m. Spengler, R. W.

No 1390

A LOW-ANGLE BRECCIA ZONE OF HYDROLOGIC SIGNIFICANCE AT YUCCA MOUNTAIN, NEVADA

SPENGLER, R. W., and ROSENBAUM, J. G., U. S. Geological Survey, P.O. Box 25046, MS 913, Denver Federal Center, Denver, CO, 80225

A recently analyzed gently dipping subsurface zone of brecciation at Yucca Mountain, Nevada may provide a significant transport pathway for radionuclide migration. If laterally extensive, the breccia zone may link permeable north- to northeast-trending high-angle fault and fracture zones within the southeastern part of the Yucca Mountain site area. Previously reported 10- to 50-m-thick permeable zones, contributing more than 20 percent of the water production in test wells UE-25 B#1 and USW H-4, correlate with the occurrence of individual or sets of fractures that cut nonwelded to partially welded zones within the upper to middle parts of the Prow Pass, Bullfrog, and Tram Members of the Crater Flat Tuff. These fractures commonly dip steeply (70° - 90°), strike between N. 10° W. and N. 55° E., are commonly slickensided, and appear to represent the subsurface expression of an exposed northeast-trending belt of high-angle, west-dipping, closely spaced, normal faults along the eastern margin of the potential repository.

More than 20 percent of the water production in test wells UE-25 C#1 and UE-25 C#3, located about 2 km southeast of the potential repository, is from flow points within a distinctive, closed-framework, unsorted breccia that cuts the upper nonwelded to partially welded zone of the Tram Member. The 40- to 60-m-thick breccia is monolithic, composed of variably oriented clasts as large as 20 cm of nonwelded to partially welded, cryptocrystalline to granophytic, ash-flow tuff of the Tram Member. Clasts are locally silicified and hematite-rich and are commonly separated by a thin matrix of mosaic quartz, calcite, and hematite. The top of conspicuous brecciation and alteration, recognized at a depth of about 850 m in the three test wells of the C-hole complex, positioned 30-77 m apart, dips about 15° to the northwest, in contrast to the 17° east to northeast dip of overlying members of the Crater Flat Tuff. Abundant subparallel hematite-coated fractures, commonly dipping between 20° and 60° , show evidence of shearing. Consistency of paleomagnetic data derived from individual clasts of variable orientations suggests that brecciation occurred prior to the complete cooling of the rock mass, favoring a mixed pyroclastic-epiclastic genesis. The geometry of the zone, cross-cutting stratification, and of subparallel shear fractures supports a tectonic origin. Regardless of mode of development, the gently dipping breccia represents a unique site-scale hydrogeologic feature worthy of further subsurface characterization.

04:30 p.m. Rautman, C. A.

No 7584

MICROSTRATIGRAPHIC UNITS AND SPATIAL CORRELATION OF HYDROLOGIC PROPERTIES IN TUFF, YUCCA MOUNTAIN, NEVADA

RAUTMAN, C. A., Sandia National Labs., Albuquerque, NM 87185; FLINT, A. L., CHORNACK, M. P., U. S. Geological Survey, P. O. Box 327, Mercury, NV 89023; McGRAW, M., Pacific Northwest Laboratories, P. O. Box 999, Richland, WA 99352

Hydrologic modeling of the potential high-level nuclear waste repository site at Yucca Mountain, Nevada, will require the assignment of hydrologic rock properties to computational cells in a numerical representation of the geologic setting. The specific rock properties assigned should reflect the natural variability of the rock units under investigation as well as the spatial continuity exhibited by those units.

Recent outcrop studies conducted jointly by the U. S. Geological Survey and Sandia National Laboratories have obtained closely spaced (1-5 m) measurements of a number of important hydrologic properties. Preliminary evaluation of these data, which represent both vertical transects through a major portion of the unsaturated stratigraphic interval at Yucca Mountain and

MON
pm

GEOLOGICAL SOCIETY OF AMERICA

ABSTRACTS WITH PROGRAMS



1991 ANNUAL MEETING

SAN DIEGO, CALIFORNIA • OCTOBER 21-24, 1991
SAN DIEGO CONVENTION CENTER

ASSOCIATED SOCIETIES

Association of Geoscientists for International Development
Association for Women Geoscientists
Cushman Foundation*
Geochemical Society*
Geoscience Information Society*
Mineralogical Society of America*
National Association of Geology Teachers*
National Earth Science Teachers Association
Paleontological Society*
Sigma Gamma Epsilon
Society of Economic Geologists*
Society of Vertebrate Paleontologists

* Representatives serve on the 1991 Joint Technical Program Committee



The Geological Society of America

ABSTRACTS WITH PROGRAMS, VOL. 23, NO. 5, 1991 ANNUAL MEETING, ISSN 0016-7292
